



PHD

**Machine learning methods for the analysis of precipitation patterns
(Alternative Format Thesis)**

Barnes, Andrew

Award date:
2022

Awarding institution:
University of Bath

[Link to publication](#)

Alternative formats

If you require this document in an alternative format, please contact:
openaccess@bath.ac.uk

Copyright of this thesis rests with the author. Access is subject to the above licence, if given. If no licence is specified above, original content in this thesis is licensed under the terms of the Creative Commons Attribution-NonCommercial 4.0 International (CC BY-NC-ND 4.0) Licence (<https://creativecommons.org/licenses/by-nc-nd/4.0/>). Any third-party copyright material present remains the property of its respective owner(s) and is licensed under its existing terms.

Take down policy

If you consider content within Bath's Research Portal to be in breach of UK law, please contact: openaccess@bath.ac.uk with the details. Your claim will be investigated and, where appropriate, the item will be removed from public view as soon as possible.



PHD

**Machine learning methods for the analysis of precipitation patterns
(Alternative Format Thesis)**

Barnes, Andrew

Award date:
2022

Awarding institution:
University of Bath

[Link to publication](#)

Alternative formats

If you require this document in an alternative format, please contact:
openaccess@bath.ac.uk

Copyright of this thesis rests with the author. Access is subject to the above licence, if given. If no licence is specified above, original content in this thesis is licensed under the terms of the Creative Commons Attribution-NonCommercial 4.0 International (CC BY-NC-ND 4.0) Licence (<https://creativecommons.org/licenses/by-nc-nd/4.0/>). Any third-party copyright material present remains the property of its respective owner(s) and is licensed under its existing terms.

Take down policy

If you consider content within Bath's Research Portal to be in breach of UK law, please contact: openaccess@bath.ac.uk with the details. Your claim will be investigated and, where appropriate, the item will be removed from public view as soon as possible.

Machine learning methods for the analysis of precipitation patterns

Andrew Paul Barnes

A thesis submitted for the degree of Doctor of Philosophy

University of Bath

Department of Architecture and Civil Engineering
Faculty of Engineering and Design

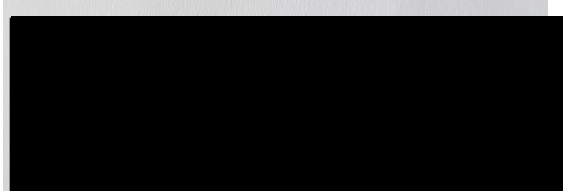
September, 2021

Copyright

Attention is drawn to the fact that copyright of this thesis/portfolio rests with the author and copyright of any previously published materials included may rest with third parties. A copy of this thesis/portfolio has been supplied on condition that anyone who consults it understands that they must not copy it or use material from it except as licenced, permitted by law or with the consent of the author or other copyright owners, as applicable.

DECLARATION OF ANY PREVIOUS SUBMISSION OF THE WORK

The material presented here for examination for the award of a higher degree by research has not been incorporated into a submission for another degree.

**DECLARATION OF AUTHORSHIP**

I am the author of this thesis, and the work described therein was carried out by myself personally. Where work was conducted in collaboration appropriate notice is given to the reader.



Summary

Extreme rainfall is becoming more common and is resulting in an increasing number of extreme flood events. Exploring why extreme rainfall events occur and how forecasts of such events can be improved is becoming key to improving society's preparedness and response to such events. This thesis evaluates and expands the capability of machine learning methods to aid both our understanding and forecasting of heavy rainfall events.

First, atmospheric trajectories were generated and clustered to identify the key moisture pathways relating to extreme rainfall events. This showed the applicability of new clustering methodologies to the identification of extreme rainfall circulation mechanisms. Following this, cluster analysis was then used to carry out an indepth analysis of the synoptic-scale meteorological conditions relating to extreme rainfall events in the UK. This resulted in the identification of a causal relationship between mean sea-level pressure and 2m air temperature patterns and extreme rainfall distributions. This highlights the importance of mean sea-level pressure anomaly polarisation across the North Atlantic, including strong and significant relationships between the synoptic patterns associated with extreme rainfall events and large-scale climatic indices such as the North Atlantic Oscillation and Atlantic Multidecedal Oscillation.

A neural network based sensitivity analysis technique was employed to identify which synoptic regions across the North Atlantic are important for understanding the difference between extreme and regular rainfall events in Great Britain. Following this a new model was developed using the gained knowledge to forecast regional, monthly rainfall values using forecasted synoptic meteorological images. This new image based forecasting model was shown to outperform the current state-of-the-art forecasting models; for example, at a one-month lead-time the image based model outperforms the ECMWF's mathematical model by 6mm. However, when comparing the models on the most extreme rainfall events the new image-based model produces errors 28mm lower than the ECMWF's model. Further to this, sensitivity analysis of the image-based model reveals a strong relationship between a low mean sea-level pressure anomaly followed by a high mean sea-level pressure anomaly in the North Atlantic results in greatly increased rainfall forecasts. A similar analysis of the temperature inputs highlights a key polarisation between warm and cool air to the south west of Great Britain and France can also lead to heightened rainfall.

Finally, a series of new forecasting techniques were developed which use a sequences of synoptic images in the form of a meteorological video to forecast regional, monthly rainfall. This video-based model when combined with the MetOffice's state of the art

forecasting model can improve rainfall forecasts across Great Britain. Highlighting this video-based forecasting method

Throughout this thesis state-of-the-art machine learning techniques were expanded and evaluated in the interpretation and forecasting of extreme rainfall events. The results highlight the capability of machine learning methods to not only match but also improve our current understanding of rainfall based forecasting and analysis. This thesis also leads the way in opening new avenues of potential work including the investigation of the cost-benefit analysis of using these new, data intensive models. Further to this, new and exciting questions remain as to the sensitivity of this work to alternative meteorological variables such as integrated water vapour and wind vectors.

Acknowledgements

Firstly, I would like to thank both Dr. Thomas Kjeldsen and Dr. Nick McCullen for their incredible support and supervision throughout my time at Bath. I believe we made a fantastic team and it has been a pleasure working with both of them. Specifically, I would like to thank Dr. McCullen for his encouragement to break through barriers and to not shy away from my sometimes ludicrous ideas when solving problems. Luckily this is where I would like to thank Dr. Kjeldsen who was able to (somehow) keep me in line and provided the support, encouragement and guidance I needed to become the independent researcher I am today.

I would like to also thank the UK Centre of Ecology and Hydrology for allowing me to spend three months working within their excellent water resources department; and although it would be impossible for me to thank everyone who supported me there I would like to add my special thanks to Dr. Cecilia Svensson for her supervision, expertise and support, I learnt a tremendous amount during our time working together.

I am also grateful to the WISE CDT and EPSRC for offering me this incredible opportunity and for providing me the opportunity to develop a wonderful network of people and for offering ample opportunities to share my research with both industry and academia.

I would also like to take this opportunity to thank the crew in Coffee #1 (Tory, Matt, Katie and Stacey) who have provided ample coffee and have always managed to make me smile while I was writing this thesis.

Finally, I would like to thank my wonderful friends who have been by my side for this journey in it's entirety. My special thanks go to Stephanie, Jess, Matt, and Dave for being here when I've needed them the most. I also cannot thank my friends without mentioning the wonderful Bobbie-Leigh who has been my pillar of sanity and has listened willingly to my PhD based waffle for over 4 years. You are an incredible friend and you have made this journey bearable, even in the most turbulent times. Thank you.

Contents

1	Introduction	17
1.1	Heavy Rainfall Events	17
1.1.1	Primary Rainfall Mechanisms	17
1.1.2	Secondary Rainfall Mechanisms	18
1.2	Current Techniques	19
1.2.1	Event composites	20
1.2.2	Meteorological Composites	23
1.2.3	Forecasting	24
1.2.4	Opportunities	25
1.3	Research Aims and Objectives	26
1.4	Thesis Structure	27
2	Identifying the origins of extreme rainfall using storm track classification	29
2.1	Preamble	30
2.2	Identifying the origins of extreme rainfall using storm track classification	31
2.2.1	Authorship Statement	31
2.2.2	Abstract	32
2.2.3	Introduction	33
2.2.4	Methods	35
2.2.5	Results	41
2.2.6	Conclusions	48
2.2.7	Acknowledgements	50
2.3	Atmospheric origins of extreme rainfall in the UK	51
2.3.1	Authorship Statement	51
2.3.2	Abstract	52
2.3.3	Introduction	53

2.3.4	Storm Track Extraction	53
2.3.5	Pathway Classification	55
2.3.6	Results	56
2.3.7	Conclusions	60
2.4	Postscript	62
3	North Atlantic air pressure and temperature conditions associated with heavy rainfall in Great Britain	63
3.1	Preamble	64
3.1.1	Authorship Statement	65
3.1.2	Abstract	66
3.2	Introduction	67
3.3	Data	69
3.3.1	Historical Heavy Rainfall Events	70
3.3.2	Meteorological Data	71
3.4	Meteorological Clustering	72
3.4.1	Feature Set Pre-Processing	72
3.4.2	Pattern Clustering	73
3.4.3	Statistical Analysis	73
3.5	Results	74
3.5.1	Summer Classes	74
3.5.2	Winter Classes	80
3.6	Discussion	84
3.6.1	Summer	86
3.6.2	Winter	87
3.6.3	Methodology	87
3.7	Summary and Conclusions	88
3.8	Acknowledgements	89
3.9	Postscript	90
4	Identifying and interpreting extreme rainfall events using image classification	91
4.1	Preamble	92
4.1.1	Authorship Statement	93
4.1.2	Abstract	94
4.2	Introduction	95
4.3	Data	97
4.3.1	Rainfall Events	97

4.3.2	Meteorological Patterns	98
4.4	Classification	99
4.4.1	Neural Network Architecture	99
4.4.2	Classifier Training	100
4.5	Results	101
4.5.1	Model Accuracy	101
4.5.2	Spatial Sensitivity	104
4.5.3	4.3 Limitations	105
4.6	Conclusions	106
4.7	Acknowledgements	107
4.8	Postscript	108
5	Forecasting sub-seasonal rainfall in Great Britain using convolutional-neural networks	110
5.1	Preamble	111
5.1.1	Authorship Statement	112
5.1.2	Abstract	113
5.2	Introduction	114
5.3	Data	116
5.3.1	Regional Precipitation	116
5.3.2	Meteorological Data	118
5.3.3	Data Separation	118
5.4	Forecasting Method	119
5.4.1	Network Structure	119
5.4.2	Training	123
5.5	Validation Results	123
5.5.1	Model Comparisons	123
5.5.2	Sensitivity Analysis	127
5.6	Conclusions	129
5.7	Acknowledgements	131
5.8	Postscript	131
6	Video based forecasting of regional, sub-seasonal rainfall	133
6.1	Preamble	134
6.1.1	Authorship Statement	135
6.1.2	Abstract	136
6.2	Introduction	137
6.3	Data	138

6.3.1	Rainfall	139
6.3.2	Meteorological Data	139
6.3.3	Training, testing and validation	140
6.4	Forecasting Method	141
6.4.1	CNN Variants	141
6.4.2	Ensemble Forecasting	142
6.5	Results	142
6.6	Conclusions	146
6.7	Acknowledgements	147
6.8	Postscript	147
7	Conclusions	149
7.1	Thesis Summary	150
7.2	Results	151
7.3	Future Opportunities	156
	References	157
	Appendices	171

List of Figures

1-1	Graphical representation of the hierarchy of rainfall analysis methods. .	20
2-1	Locations of gauging stations used to extract annual maximum rainfall events, black line indicates the catchment boundary for the Duoro river.	36
2-2	Empirical cumulative distribution for all rainfall data both before normalisation (left) and after (right).	36
2-3	Five backwards trajectories from a single AMAX event starting from the northern most point.	38
2-4	A sample SOM architecture with 98 input nodes representing the 49 latitude and longitude points of a trajectory. All input nodes are connected via weighted edges to the four output nodes (classifications). These output nodes are arranged into a neighbourhood grid before training which results in classifications being similar to their neighbours. For example, classes 2 and 3 contain trajectories which are closer to class 1 than those contained in class 4.	39
2-5	This figure shows both the quantisation (top) and topological (bottom) errors for each of the three classifiers.	41
2-6	A sample of trajectories for each cluster in the primary 4-SOM classifier (PR-4). The classifications plot shows 50 randomly selected trajectories for each class (coloured grey) with a mean trajectory across all relevant trajectories coloured in black. The proportion of trajectories within each class is given in Table 2.2.	42
2-7	A sample of trajectories for each cluster in the 9-SOM primary classifier (PR-9). The classifications plot shows 50 randomly selected trajectories for each class (coloured grey) with a mean trajectory across all relevant trajectories coloured in black. The proportion of trajectories within each class is given in Table 2.3.	43

2-8	A sample of trajectories for each cluster in the 3D 9-SOM classified (3D-9). The classifications plot shows 50 randomly selected trajectories for each class (coloured grey) with a mean trajectory across all relevant trajectories coloured in black. The proportion of trajectories within each class is given in Table 2.4.	44
2-9	A sample of trajectories for each class in the summer 9-SOM classified (SUM-9). The classifications plot shows 50 randomly selected trajectories for each class (coloured grey) with a mean trajectory across all relevant trajectories coloured in black. The proportion of trajectories within each class is given in Table 2.5.	45
2-10	A sample of trajectories for each cluster in the winter 9-SOM classifier (WIN-9). The classifications plot shows 50 randomly selected trajectories for each class (coloured grey) with a mean trajectory across all relevant trajectories coloured in black. The proportion of trajectories within each class is given in Table 2.6.	46
2-11	Rainfall distributions for each cluster in PR-4 (left) and PR-9 (right). In each case the line's number corresponds to the class of storm track represented.	47
2-12	Rainfall distributions for SUM-9 (left) and WIN-9 (right) classifiers. In each case the line's number corresponds to the class of storm track represented.	48
2-13	Location of 42 cities across the UK selected for this study.	54
2-14	Davies-Bouldin Index for each of the three selected clustering methods with a varying number of initiation clusters. Lower values indicate better cluster separation.	56
2-15	Examples of the trajectories classified under each class within the three classifiers used: SOM_4 (a), LNK_5 (b) and KME_6 (c) with the centroids shown in bold.	57
2-16	Proportion of each KME_6 storm classification per hydroclimatic region.	58
2-17	Empirical cumulative distribution function for the frequency of each trajectories within each classification for a given NAO index.	60
3-1	The 125 locations in Great Britain at which series of seasonal rainfall maxima are extracted.	70

3-2	Example of feature set generation for a given heavy rainfall event. This procedure takes the SLP and AT patterns, flattens them into a single dimensional array and finally concatenates them into a final single dimensional array.	72
3-3	Sea level pressure patterns for the four summer classes, showing both the anomaly SLP (a) and raw SLP (b) patterns. The percentages indicate the proportion of events in each class, and the dots provided in (a) denote anomalies significant at the 2% level based on a two-sided Student's t-test.	75
3-4	Sea-level wind speeds for summer classes. The sea-level wind speeds are overlaid on the anomaly temperature patterns for each of the four summer classes, and the opacity illustrates the strength of wind between 2 and 8 m/s. Anomaly 2m air temperature patterns are shown without wind speeds, but with points denoting significance, in supplementary information S1.	76
3-5	500hPa Geopotential Heights for each summer class.	76
3-6	Seasonal frequency of occurrence of heavy rainfall events in the four summer classes as function of time (top row), and detrended seasonal frequencies as a function of detrended NAO index (middle row) and AMO index (bottom row). The figure also shows the correlation coefficient, R, and the significance level (P).	77
3-7	2m air temperature anomalies in the North Atlantic region in the 1, 3, 5, 7 and 9 days prior to the heavy rainfall event occurring, for the four summer classes.	79
3-8	Geographical distribution of heavy rainfall events for each of the four summer classes, for each of 13 administrative regions of Great Britain (regions as in Hollis et al. (2019)). A high opacity indicates a higher proportion of event occurrence.	80
3-9	Sea-Level Pressure patterns for the three winter classes, showing both the anomaly SLP (a) and raw SLP (b) patterns. The percentages indicate the proportion of events in each class and the dots provided in (a) show the anomalies with a 2% significance value using a two-sided Student's t-test.	81
3-10	As Figure 3-6, but for the three winter classes. Anomaly 2m air temperature patterns are shown without wind speeds, but with points denoting significance, in supplementary information S2.	82

3-11	2m air temperature anomalies in the North Atlantic region in the 1, 3, 5, 7 and 9 days prior to the heavy rainfall event occurring, for the three winter classes.	83
3-12	500hPa Geopotential Heights for each summer class.	84
3-13	As figure 3-6, but for the three winter classes.	85
3-14	Geographical distribution of heavy rainfall events for each of the three winter classes for each of 13 administrative regions of Great Britain. A high opacity indicates a higher proportion of event occurrence.	86
4-1	Locations of the regions and points from which rainfall is extracted for both the north west region (b) and south east region (c).	98
4-2	An example neural network structure consisting of three layers where each node is connected via weights (as given by w_x) to the nodes in the layers both before and after.	100
4-3	Loss and accuracies for models classifying between SLPA patterns relating to north west extreme and regular rainfall events.	102
4-4	Loss and accuracies for classifiers classifying between the SLPA patterns relating to south east extreme and regular rainfall events.	103
4-5	Loss and accuracies for models classifying between SLPA patterns relating to extreme events in the north west and south east.	103
4-6	Saliency map showing the spatial contributions of SLPA patterns to classifying extreme and regular rainfall events for both $M_{NW,30}$ (left) and $M_{SE,10}$ (right).	105
4-7	Spatial contributions of SLPA patterns in determining the difference between north west and south east extreme events.	105
5-1	The 13 regions of Great Britain (a) and the corresponding 20km by 20km points (b) used to aggregate monthly rainfall totals (mm).	117
5-2	The three forecast models showing their inputs and outputs.	119
5-3	A convolution applied to a 3-by-3 image using a 2-by-2 kernel. The kernel is moved over the image by one pixel at a time, calculating the value of the subsection by multiplying the kernel by the pixels highlighted.	120
5-4	A max-pooling operation applied to a 3-by-3 image using a patch of size 2-by-2. As the patch moves across the image it extracts the maximum pixel value at each timestep.	121

5-5	A linear layer example following a max pooling layer. This example shows a max pooling layer with output dimensions $[8, 3, 7]$ feeding into a linear layer of size $[1, 100]$. The max-pooling output is first flattened into a 1D vector. Each value in this vector is then connected to every node in the linear layer via a weighted edge which results in a weights matrix of size $[8 \times 3 \times 7, 100]$. The linear layer then uses these weights and the flatened max-pooling vector to calculate the layer's output as described by Equation 5.1.	122
5-6	Architecture of the convolutional neural network model. Each layer is provided with the number of dimensions of its output matrix. For example, the first convolutional layer has an output size of $[16, 30, 60]$, this also indicates the number of filters used in the layer (16). These are followed by max-pooling layers and finally two dense linear layers. . . .	122
5-7	Validation rainfall predictions against benchmark rainfall for both the CNN and ECMWF methods in all three lead times: (a) one month, (b) three months and (c) six months.	124
5-8	Cumulative residual of both methods using a three-month lead time against the actual regional rainfall.	125
5-9	Regional and monthly rainfall areas as a proportion of the average rainfall for the given month or region. This is given for both methods and all three lead times: (a) one month, (b) three months and (c) six months. . . .	127
5-10	Normalized attribution values for increasing rainfall predictions in both NW England (top) and SE England (bottom) for both MSLP (a) and 2m air temperature (b).	129
6-1	The 13 administrative regions of Great Britain.	140
6-2	Three CNN architectures for including a temporal dimension, adapted from Karpathy et al. (2014). Blue boxes indicate convolutional layers, red boxes indicate max-pooling layers, and the yellow boxes indicate fully-connected linear layers.	141
6-3	Two ensemble approaches are presented. First the CNN Ensemble (CNNE) is calculated through taking the mean of all three CNN Results for a given month. Then, the mean of the CNNE and the MOS5 prediction is taken as the post-processing ensemble (PPE).	143
6-4	Predicted rainfall against the benchmark rainfall value for all months in the validation dataset.	143
6-5	Regional RMSEs for each model for the validation dataset.	144

6-6	Ensemble predictions for the validation dataset compared to the benchmark monthly rainfall totals (mm). Left: CNNE, and right: PPE. . . .	145
6-7	The cumulative residual for all forecasting methods including the MetOffice's GloSea5 model.	146
S1	Air temperature anomaly patterns for the four summer classes. Cells marked with a dot denote that the anomaly is significantly different from zero at the 2% significance level based on a two-sided Student's t-test.	171
S2	Air temperature anomaly patterns for the three winter classes. Cells marked with a dot denote that the anomaly is significantly different from zero at the 2% significance level based on a two-sided Student's t-test.	171
S3	Sea-level pressure in the North Atlantic region in the 1, 3, 5, 7 and 9 days prior to the extreme rainfall event occurring, for the four summer classes.	172
S4	Sea-level pressure in the North Atlantic region in the 1, 3, 5, 7 and 9 days prior to the extreme rainfall event occurring, for the three winter classes.	173
S5	Box-and-whisker plots of standardized summer rainfall maxima for all study regions, for each class. The box outlines the upper and lower quartiles with the median as a red line, and the upper (lower) whisker shows the observation that is furthest away from the upper (lower) quartile, but still within 1.5 times the interquartile range.	174
S6	Same as S5, but for winter.	175

List of Tables

2.1	Characteristics of the five classifiers used; here date filtering is inclusive. Number of inputs is defined as the size of each input vector before it is classified, and the number of classes is the number of output nodes available to the SOM.	39
2.2	Proportion of trajectories which are classified under each of the four classes within PR-4.	42
2.3	Proportion of trajectories which are classified under each of the nine classes within PR-9.	43
2.4	Proportion of trajectories which are classified under each of the nine classes within 3D-9.	43
2.5	Proportion of trajectories which are classified under each of the nine classes within SUM-9.	45
2.6	Proportion of trajectories which are classified under each of the nine classification within the 9-SOM winter classifier.	46
2.7	Proportion of trajectories classified under each classification per model.	57
2.8	Percentage of events in each classification with a magnitude > 1	59
4.1	This table indicates the purpose of each model and the datasets which are used. The numbers indicate the class of the given dataset in the given model.	99
5.1	The RMSE scores for both the CNN and ECMWF models covering all three leadtimes given the validation dataset, the top 5% of all events in each region and the complete, overall dataset are given.	125

Chapter 1

Introduction

1.1 Heavy Rainfall Events

Flooding is becoming more frequent (Hu et al. 2018) and the resulting impact it is having across the globe is becoming more severe. The number of global deaths due to flooding is on the rise with severe impact being felt across the world. However, it is not just deaths which are beginning to rise, the World Meteorological Organization highlight that in the first half of 2020 alone more than 9.8 million people were displaced due to hydrometeorological events (World Meteorological Organisation 2021). Most flood events are caused by riverine flooding, the result of heavy rainfall of which the magnitude and frequency is increasing (Donat et al. 2016; Allan, Liu, et al. 2014). This increase in heavy rainfall potential is tightly linked to a warming climate (Donat et al. 2016; Westra, Alexander, and Zwiers 2013; Westra, Fowler, et al. 2014), due to the thermodynamic Clausius-Clapyeron (CC) relation which states a warmer atmosphere can store more water than a cooler one (Utsumi, Seto, et al. 2011; Blenkinsop et al. 2015). Mechanisms such as the CC relation are key to providing sustainable forecasts of heavy rainfall in a changing climate, this thesis expands and evaluates the capability of machine learning methods to identify and use rainfall mechanisms to improve both our understanding and forecasts of heavy rainfall.

1.1.1 Primary Rainfall Mechanisms

Rainfall mechanisms across the globe vary; however, a large portion of global rainfall ($> 41\%$) can be attributed to cyclones (Utsumi, Kim, et al. 2017) characterised by a very low sea-level pressure centre surrounded by strong winds and often form a spiral arrangement. There are two key types of cyclone, tropical cyclones (TC) and extra-

tropical cyclones (ExC). TCs form in tropical waters, with energy being gathered via heat transfer from the ocean (Emanuel 2003). Due to their forming around tropical waters TCs are responsible for a large portion of both extreme and non-extreme rainfall in the Philippines, south-east China, the southern United States and Madagascar (Utsumi, Kim, et al. 2017). In contrast, ExCs develop in and impact the mid-latitudes ($> 30^{\circ}N$, $> 30^{\circ}S$) (Utsumi, Kim, et al. 2017; Gimeno, Vázquez, et al. 2020). ExCs are energized by high temperature contrasts between the cool air masses of the poles and warm oceanic air mass towards the equator. The temperature contrast between the cool and warm airmasses of the mid latitudes is only set to increase in a warming climate with the warm tropical air masses capable of holding and bringing more moisture towards the mid-latitude land masses.

1.1.2 Secondary Rainfall Mechanisms

The secondary impacts of extra-tropical cyclones have also been considered, such as those which happen either before or after the cyclones frontal systems. For example, a common precursor to extra-tropical cyclones are atmospheric rivers (ARs) and recent evidence is highlighting ARs as being key contributors to heavy rainfall events across the world (Gimeno, Vázquez, et al. 2020) with extensive work highlighting their effect in western Europe (Lavers, Allan, et al. 2011; Lavers and Villarini 2013; Lavers and Villarini 2015; Eiras-Barca et al. 2021). The technical definition of ARs is widely debated (Eiras-Barca et al. 2021); however, the American Meteorological Society defines ARs as “A long, narrow, and transient corridor of strong horizontal water vapor transport that is typically associated with a low-level jet stream ahead of the cold front of an extratropical cyclone” (American Meteorological Society 2019). ARs can also influence the development of explosive cyclones. Explosive cyclones are defined by the deepening of their low pressure centers at a rate much faster than ordinary non-explosive cyclones. Because of the sharp gradient towards lower pressures explosive cyclones are often related to stronger winds and heavier precipitation (Tsukijihara, Kawamura, and Kawano 2019; Liberato 2014). Eiras-Barca et al. (2018) assess the role of ARs in the development of explosive cyclones in both the North Atlantic and North Pacific indicating that 80% of explosive cyclones have a related AR whereas only 40% of non-explosive cyclones are linked to ARs. Despite this, there is dispute over whether ARs always tend to result heavy precipitation events or not. For example, Champion et al. (2015) highlight that less than 35% of winter and 15% of summer ARs were associated with relative seasonal extreme rainfall events in the UK. This indicates the presence of an AR alone is not sufficient for heavy precipitation.

Allan et al. (2019) investigated synoptic precursors of extreme short-duration (3-hour) rainfall events in the UK over northwest Europe and the North Atlantic. Their results reveal different conditions associated with intense rainfall events in different parts of the country. For example, intense rainfall events in both the South East of England and western Scotland coincide with negative SLP anomalies in the eastern Atlantic on the day prior to the event. However, for intense rainfall events in the South East of England the centre of this negative SLP anomaly is further south than for events in western Scotland. Their results highlight not only the regional homogeneity of extreme events (e.g. Champion, Blenkinsop, et al. 2019; Svensson and Hannaford 2019) in the UK but also their association with particular synoptic scale atmospheric patterns. Similarly, Ummenhofer et al. (2017) clustered SLP and precipitation patterns over Europe and identified a similar northwest and southeast regional disparity across the British Isles. However, in a study on extreme rainfall in east Africa, Wainwright et al. (2021) show that the presence of a low-pressure anomaly or cyclonic system is again not enough to describe the rainfall quantities. Instead, a combination of magnitude, location and other synoptic factors such as temperature are required to accurately assess the potential impact of a system. The factors described in this section lead to the need for incorporating not only the known rainfall mechanisms such as the CC relation and the presence of cyclonic activity but also the incorporation of unknown meteorological relationships for the future forecasting and understanding of heavy rainfall.

1.2 Current Techniques

Current methods to identify the meteorological drivers for rainfall events can be split into three types: (i) the analysis of meteorological patterns for a subset of rainfall events (event composites), (ii) the analysis of rainfall variation across either a spatial or temporal domain for a subset of meteorological patterns (meteorological composites), and (iii) the sensitivity analysis of rainfall forecasting methods which use meteorological parameters. These three technique varieties are shown in Figure 1-1. Each of these techniques can then be broken down further as shown in Figure 1-1.

Firstly, event composite studies consist of analyses on a subset of events. Such work can either focus on developing an understanding of the meteorological drivers behind distinct events such as Storm Desmond in 2015 (Matthews et al. 2018) and Hurricane Harvey in 2017 (Sarkar, Singh, and Chauhan 2018). Alternatively, event composite studies can base their subsets on information of the events themselves such as location (Westra, Alexander, and Zwiers 2013; Jones, Fowler, et al. 2013; Nalley et al. 2019) or magnitude (Hellström 2005; Brown 2018; Allan, Blenkinsop, et al. 2020; Champion,

Blenkinsop, et al. 2019). Next are meteorological composite methods which use meteorological or process-based subsets; for example, grouping meteorological days based on their synoptic mean sea-level pressure pattern (Neal et al., 2016). From here conclusions regarding the influence the target process has on rainfall variation can be drawn. Popular examples of this analysis type is the use of weather patterns to explain rainfall variation such as the Lamb weather types (Lamb 1950; Lamb 1972; O'Hare and Sweeney 1993) and the more recent MO-30 weather patterns defined by Neal et al. (2016). Finally, the sensitivity of forecasting models can be used to identify the original drivers such as shown by Kumar et al. (2019), Larraondo et al. (2019) and Rasp et al. (2021).

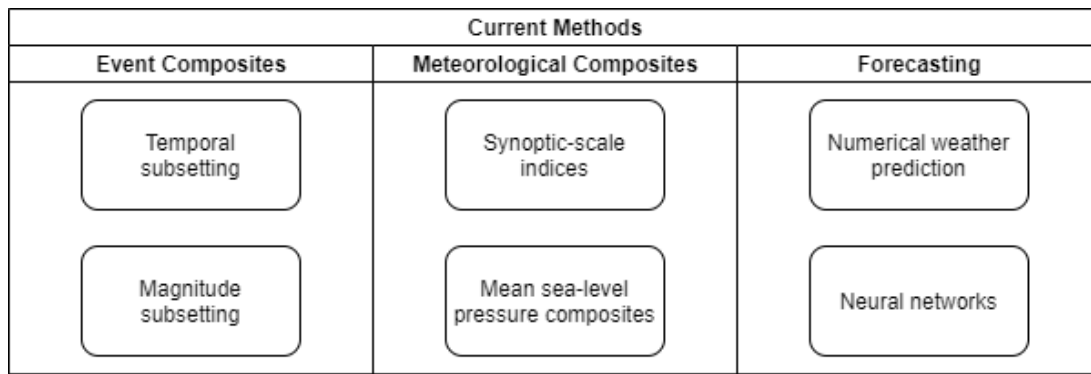


Figure 1-1: Graphical representation of the hierarchy of rainfall analysis methods.

1.2.1 Event composites

Event composite techniques for the analysis of rainfall events are generally based on the definition of a subset of distinct events followed by agglomeration. This section begins by first discussing the three dimensions in which rainfall events can be subset (temporal, magnitude or spatial) followed by which meteorological parameters are commonly used for comparisons and analysis.

Event Subsetting

Event subsetting are methods of rainfall analysis which use aggregates of meteorological conditions for a series of rainfall events to identify and discuss the processes which lead to the resulting rainfall series. The first type of event subsetting is temporal subsetting which can include either the selection a specific event, such as a storm (Matthews et al. 2018) or hurricane (Sarkar, Singh, and Chauhan 2018), or the use of a temporal range could be used to identify the factors relating to rainfall within a time range, such as a aggregating all events within a given season (Huntingford et al. 2014; Wainwright

et al. 2020). An alternative to temporal subsetting is spatial selection which includes the aggregation of rainfall events across a specified region such as countries, continents or another spatial domain. Such studies tend to focus on either the temporal fluctuation in rainfall distributions (Jones, Fowler, et al. 2013) and the resulting spatial correlations with meteorological variables (Ummenhofer et al. 2017) across the predefined region.

Next, magnitude based subsetting methods are considered. Magnitude based subsets are created by splitting rainfall series based on the magnitude of the events. There are primarily two methods for sub-setting extreme rainfall series based on magnitude: a time-based maxima approach or peaks-over threshold. Time-based maxima take the maximum events within a given time band within a series, popular examples include the annual maximum (AMAX) of a daily rainfall series which selected the highest magnitude day from each year within the series (Westra, Alexander, and Zwiers 2013; Jones, Fowler, et al. 2013). However, this can also be applied to a seasonal daily maximum (Jones, Fowler, et al. 2013) or a monthly daily maximum (Brown, 2018). In contrast to selecting a set number of events are peak-over threshold (POT) methods which select any events from a series with magnitudes over a given threshold. Such methods have been employed in the extraction of extreme sub-daily rainfall events (Hellström 2005; Gustafsson, Rayner, and Chen 2010; Allan, Blenkinsop, et al. 2020; Champion, Blenkinsop, et al. 2019) and in the extraction of non-trace rainfall events (Hellström 2005; Jones, Fowler, et al. 2013). Current literature explores the mechanisms by which the meteorological processes result in heavy rainfall; however there have been more recent calls for a more objective approach to this analysis (Kjeldsen et al. 2018).

Maxima based approaches guarantee comparative consistency between different rainfall series; for example, using a maxima approach on two equally long rainfall series from different rainfall stations will result in the same number of events for each station whereas the use of a POT method may not. However, the maxima-based approach does not guarantee the selection of events is comparable between the selected time bands; for example, if using an AMAX approach on a multi-year rainfall series particularly wet and dry years are treated the same, both contributing only a single event. This results in dry years contributing events which may not have a reasonable magnitude to be considered extreme and wet years may not be fully represented if there were multiple large storms throughout the year. There are ways to deal with the short comings of these approaches, such as those used by Champion et al. (2019) and Allan et al. (2019). Champion et al (2019) applies a maximum number of events per rainfall series by taking the largest 30 events from each rainfall series only. Allan et al. (2019) uses an alternative approach which took three events per year of data, this allowed the

study to account for station series with multiple large rainfall events while reducing bias towards rainfall station series.

Meteorological Composites

Following the extraction of events, composite studies use either a composite composite and/or correlation-based techniques to draw relationships between the extracted rainfall series and the meteorological conditions. While many studies will focus on a multitude of meteorological variables (Ummenhofer et al. 2017; Champion, Blenkinsop, et al. 2019; Allan, Blenkinsop, et al. 2020) there are several key features which have proved useful in identifying the meteorological drivers of the respective rainfall events to date: circulation patterns (using mean sea-level pressure, geopotential height and wind vectors), temperature patterns and water vapour patterns.

First, circulation pattern-based analysis is conducted either through the interpretation of synoptic-scale composites of mean sea-level pressure (MSLP) (Ummenhofer et al. 2017; Champion, Blenkinsop, et al. 2019; Allan, Blenkinsop, et al. 2020) and geopotential height (GpH) (Hellström 2005; Champion, Blenkinsop, et al. 2019; Allan, Blenkinsop, et al. 2020) patterns or by correlating the events with change to large scale synoptic indices such as the North Atlantic Oscillation (NAO) (Huntingford et al. 2014; Brown 2018). The NAO indicates the difference in pressure between the generally low pressure centred on Iceland and a generally higher pressure centred on the Azores. Indices such as the NAO influence the MSLP and GpH are often used to generalise large-scale variation in MSLP anomalies. Using either a meteorological variable such as the NAO or a MSLP/GpH composite, the pressure differences are used to explain moisture transport systems, with pressure centres pulling air masses across the globe. However, it is not just concurrent conditions which can be considered; for example, Champion et al. (2019) and Allan et al. (2019) also utilise the preceding circulation variables to identify how rainfall generating patterns develop.

However, circulation patterns alone are not enough to describe rainfall patterns. Temperature patterns relating to rainfall events have also been studied, increase in extreme rainfall intensity with an increase in global temperatures (Westra, Alexander, and Zwiers 2013). The links between rainfall have been linked to three key global temperature oscillations namely the El-Nino-Southern Oscillation (ENSO) (Brown 2018; Nalley et al. 2019), Pacific Decadal Oscillation (PDO) (Nalley et al. 2019) and the Atlantic Multi-decadal Oscillation (AMO) (Brown 2018).

1.2.2 Meteorological Composites

Meteorological composite methods which analyse rainfall distribution across either the spatial or temporal domain of event groups based on their concurrent and prior meteorological conditions. Such methods range from the quantification of precipitation relating to known meteorological processes such as cyclonic activity (Utsumi, Kim, et al. 2017) to those which group time-steps using either local (Lamb 1972; Jenkinson and Collison 1977) or synoptic patterns (Richardson, Fowler, Kilsby, and Neal 2018; Richardson, Fowler, Kilsby, Neal, and Dankers 2020) of mean sea-level pressure.

The first of these analyse the implications of known meteorological processes. To begin, Utsumi et al. (2017) uses three weather systems to calculate their relative contribution to rainfall at both global and regional levels. The weather systems are TCs, frontal and centers of ExCs and finally a ‘others’ category which contains anything not resulting from either a TC or ExC. These systems were detected at 6 hourly intervals using the IBTrACS dataset (Knapp et al. 2010) and a ExC detection method based on Utsumi et al. (2016) using the JRA-25 meteorological dataset (Onogi et al. 2007). Through separating rainfall data using the weather system classifications Utsumi et al. (2017) showed that 4%, 37% and 49% of global precipitation related to TCs, ExCs and other systems, respectively. Related approaches have identified synoptic systems such as ARs with many studies highlighting a relationship between ARs and rainfall across the globe (Champion, Allan, and Lavers 2015; Lavers and Villarini 2013; Lavers and Villarini 2015; Blamey et al. 2018).

Earlier attempts to classify daily synoptic conditions include the Lamb weather types (LWTs) as described by Lamb (1972) which were later automated by Jenkinson & Collison (1977). This scheme uses the grid-point MSLP across the British Isles and assigns each synoptic day to one of 27 classifications describing the circulation pattern present during that day. More recently, Neal et al. (2016) clustered MSLP patterns across a region covering the British Isles and the North Atlantic resulting in 30 patterns (MO-30). Richardson et al. (2017) compared both MO-30 and the LWTs, illustrating a difference in the regional rainfall distributions between the patterns for each classification scheme.

More recent attempts to generalise circulation patterns come in the form of atmospheric trajectory generation. Atmospheric trajectories are the paths taken by parcels of air and can either be forwards or backwards in time and generating them takes a range of meteorological data (MSLP, 2AT, wind vectors and geopotential heights etc.). However, once this data has been gathered a dispersion model such as HYSPLIT (Stein et al. 2015) can be used to generate either the forwards (future) or backwards (preceding)

tracks. Multiple studies clustering the trajectories of both extreme and non-extreme rainfall events leads to the potential to extract different rainfall distributions based on the preceding atmospheric trajectory (Tan, Gan, and Chen 2018; Santos et al. 2018). Moreover, earlier work has attempted to generalise circulation patterns using clustering techniques such as Reusch *et al.* (2007) who used self-organising maps to highlight the coupling of synoptic scale meteorological phenomenon.

Aside from generalising circulation patterns some methods have focussed on the generation of missing rainfall events using clustering. For example, Crane & Hewitson (2014) use a self-organising map technique to combines both station and rainfall characteristics to generate similar rainfall regions. A second self-organizing map is then used to identify the temporal trends within the rainfall regions, this second SOM can then be used to generate missing rainfall data.

1.2.3 Forecasting

Traditional approaches to weather based forecasting rely on mathematical models which can be combined into numerical weather prediction models (NWP) such as the GloSea5 forecasting system (Maclachlan et al. 2015). Other traditional approaches include the role of expert systems which have been shown successful. For example, Wedgbrow *et al.* (2005) use meteorological based expert systems to forecast the correct sign for the flow rate anomalies of the River Thames. Alternative approaches have used the low-frequency predictors of the NAO and sea-surface temperature, showing promising results compared to stochastic approaches (Wilby, Conway, and Jones 2002). More recently however a move towards machine learning based approaches to weather forecasting removes the dependence on pre-defined mathematical models and instead transfers the responsibility over to optimisation procedures such as those used in Neural Networks. A review by Pham et al. (2020) found that neural networks can predict daily and sub-daily rainfall to within 10mm, on a larger sub-seasonal time scale Kumar et al. (2019) showed deep neural networks were capable of predicting regional rainfall; however the resulting errors were high (211.48 - 408.152mm). However, the greatest success in using neural networks was reported by Haidar & Verma (2018), who developed a one-dimensional convolutional neural network (CNN) using climate variables (including, but not limited to, max temperature, min temperature, southern oscillation index, dipole mode index and interdecadal pacific oscillation) to predict monthly rainfall total in eastern Australia. They found that the resulting model showed higher predictive performance than the recently released Australian Community Climate and Earth System (Hudson et al. 2017). Recently, CNNs have been shown as capable at

predicting gridded precipitation; first Larrando et al. (2019) uses Geopotential Height fields across the North Atlantic to predict total 3-hourly precipitation across Western Europe presenting more accurate results than alternative traditional machine learning approaches such as regression.

1.2.4 Opportunities

The processes and methods surrounding heavy rainfall analysis are broad, encompassing highly subjective selection and interpretation of subsets of rainfall events to the interpretation of output from sophisticated numerical weather models. However, there are three key areas in which the methods of analysis can be modernised using recent advances in machine learning methods.

Firstly, the multivariate analysis of meteorological conditions leading up to heavy rainfall events has yet to be interpreted using objective analysis schemes. Current studies (Champion, Blenkinsop, et al. 2019; Allan, Blenkinsop, et al. 2020) use subjective interpretation of multiple variables as discussed above and more recent forecasting works such as Rasp and Thuerey (2021) include multiple time-steps of various parameters to the forecast however offer limited attribution value of the resulting forecast to the initial parameters. This leaves scope to not only investigate the co-variability of different meteorological parameters but also their influence on resulting heavy rainfall distributions and their forecasting potential.

Next, limited objective analysis has been done on the temporal variation of the meteorological conditions. Where recent works consider discrete timesteps such as Champion et al. (2019) and Allan et al. (2019) there is an opportunity to use alternative machine learning techniques to analyse meteorological aggregates such as the atmospheric trajectories used by Tan et al. (2017) and Santos et al. (2018) to develop an objective classification scheme for heavy rainfall events. Furthermore, Rasp and Thuerey (2021) developed a forecasting model using multiple timesteps, but this could be improved using alternative neural network architectures proposed in the domain of video analysis (Karpathy et al. 2014).

Finally, as Rasp and Thuerey (2021) demonstrate, neural network based techniques for forecasting provide ample opportunity for interpretability of the resulting models which can aid in the understanding of how and why heavy rainfall events occur. However, they do not consider the interpretability of variables across different time-steps, where they have offered potential direction there is scope for developing new and localised models for greater interpretability with higher resolution datasets.

1.3 Research Aims and Objectives

The overall aim of this thesis is to evaluate and expand the capability of machine learning methods to aid both our understanding and forecasting potential of heavy rainfall events. Specifically, this thesis aims to address the following hypotheses:

- H1** The moisture pathways leading to heavy rainfall events can be identified using neural-network based clustering and the preceding atmospheric trajectories.
- H2** Combining modern self-organizing maps and regression methods can reveal the interdependence between synoptic-scale atmospheric conditions and heavy rainfall events.
- H3** Synoptic-scale atmospheric conditions be used to train neural-networks to distinguish heavy rainfall events from expected rainfall events.
- H4** Synoptic-scale atmospheric conditions can be combined with new video-based neural-networks to improve sub-seasonal rainfall forecasts.

Each hypothesis is addressed by a series of research objectives as follows:

- H1** The moisture pathways leading to heavy rainfall events can be identified using neural-network based clustering and the preceding atmospheric trajectories.

Objective 1.1 - Develop a novel methodology for clustering trajectory data.

Objective 1.2 - Cluster extreme rainfall events based on their preceding atmospheric trajectories.

Objective 1.3 - Identify variations in the temporal and magnitude distributions of extreme rainfall between each cluster.

- H2** Combining modern self-organizing maps and regression methods can reveal the interdependence between synoptic-scale atmospheric conditions and heavy rainfall events.

Objective 2.1 - Cluster selected synoptic-scale atmospheric conditions for a series of heavy rainfall events.

Objective 2.2 - Evaluate the covariance of the atmospheric conditions within each cluster.

Objective 2.3 - Evaluate the spatial and temporal distributions of each cluster's frequency of occurrence.

H3 Synoptic-scale atmospheric conditions be used to train neural-networks to distinguish heavy rainfall events from expected rainfall events.

Objective 3.1 - Extract both heavy and non-heavy rainfall days from two hydrologically diverse regions.

Objective 3.2 - Develop a neural network based methodology for classifying the events into heavy and non-heavy rainfall events using concurrent atmospheric conditions.

Objective 3.3 - Evaluate the accuracy of the machine learning model and identify the relevant limitations.

H4 Synoptic-scale atmospheric conditions can be combined with new video-based neural-networks to improve sub-seasonal rainfall forecasts.

Objective 4.1 - Extract monthly rainfall values and their relative mean sea level pressure & air temperature profiles for a set of case-study regions.

Objective 4.2 - Develop a machine learning based methodology for forecasting using meteorological patterns.

Objective 4.3 - Evaluate the effectiveness of the new forecasting approach to current sub-seasonal forecasting models.

1.4 Thesis Structure

To answer the research questions provided in section 1.3 this thesis is structured into the following chapters:

Chapter 2 addresses **H1** by detailing the first attempt in this thesis to characterise heavy rainfall events based on the preceding atmospheric conditions, specifically using atmospheric trajectories.

Chapter 3 expands on the work of Chapter 2 by clustering heavy rainfall events based on the inter-dependencies of their concurrent atmospheric conditions. By addressing **H2** this chapter uses the mean-sea level pressure and 2m air temperature anomalies to group heavy rainfall events. The contents of this chapter have been submitted to the International Journal of Climatology.

Chapter 4 develops a new approach to identifying heavy rainfall events by using the concurrent mean-sea level pressure patterns to classify rainfall days as either

heavy or non heavy events. The resulting model is then evaluated against **H3**. The work in this chapter has been submitted to the Journal of Hydroinformatics.

Chapter 5 changes focus from the previous three chapters by forecasting sub-seasonal rainfall based on forecasted atmospheric conditions. In answer to **H4** this chapter develops a machine learning model capable of forecasting monthly, regional rainfall totals. This model is then evaluated against the current ECMWF sub-seasonal forecasting service.

Chapter 6 expands further on Chapter 5 and **H4** by developing a model which incorporates a time dimension into the input data. Instead of using a single image for each month this chapter describes a method of using a series of atmospheric forecasts to forecast each month's regional rainfall. The models developed using this method are then evaluated against forecasts made by the latest MetOffice SEAS5 model.

Chapter 7 then concludes this thesis by summarizing the key findings, providing analysis on the limitations of applied machine learning in this domain and finally highlighting the importance of this work in the future of heavy rainfall analysis.

Chapter 2

Identifying the origins of extreme rainfall using storm track classification

2.1 Preamble


To address **Hypothesis 1**, this chapter reports the results of two experiments which characterise heavy rainfall events based on their preceding atmospheric trajectories using cluster analysis.

This chapter begins by reporting the proof of concept study conducted using extreme rainfall events extracted from a network of rain gauges located in the river Duoro's catchment in north-western Spain. Following the extraction of both annual maximum (AMAX) events and the associated atmospheric trajectories, a set of neural network architectures were developed using the self-organising map framework. These networks were optimised for the clustering of various subsets of the trajectory data and are compared and contrasted in order to address **Objective 1.1** and **Objective 1.2**. The clusters generated by each network were first compared based on their frequency and shape before the extreme rainfall distributions were evaluated in answer to **Objective 1.3**.

The second part of this chapter details a comparison of the self-organising maps method with traditional clustering techniques (k-means and linkage) regarding the clustering of atmospheric trajectories. This comparison of methods further answers **Objective 1.1**. This was done using a case-study of extreme rainfall events observed across Great Britain, extracted from a series of locations across the island from which trajectories were extracted. Each of the clustering methods was used to cluster these trajectories using a varying number of clusters (**Objective 1.2**). The optimal models were then compared based on their centroid shapes and frequency. Finally, the most optimal model was selected to produce both a spatial distribution of the event types across Great Britain and a comparison of the relevance of the North Atlantic Oscillation (NAO) (**Objective 1.3**).

2.2 Identifying the origins of extreme rainfall using storm track classification

2.2.1 Authorship Statement

Status	Published in the Journal of Hydroinformatics.
Details	Barnes, A.P., Santos, M., Carijo, C., Mediero, L., Prosdocimi, I., McCullen, N., Kjeldsen, T.R. Identifying Origins of Extreme Rainfall using Trajectory Classification. (2019) Journal of Hydroinformatics, 22(2).
Authors' contribution	<p>The author of this thesis has primarily (90%) contributed to design and implementation the methodology adopted for the extraction, clustering and analysis of the storm trajectories. The extreme rainfall data used was provided by M.S Santos, C. Garijo and L. Mediero. Each author's exact contributions are as follows:</p> <p>A.P. Barnes: Formulation of ideas (80%), design of methodology (90%), processing and analysis of data (100%), manuscript preparation (85%).</p> <p>M.S. Santos, C. Garijo and L. Mediero: Formulation of ideas (10%), design of methodology (5%), data collection (100%), manuscript preparation (5%).</p> <p>I. Prosdocimi, N. McCullen and T.R. Kjeldsen: Formulation of ideas (10%), design of methodology (5%), manuscript preparation (10%).</p>
Statement from candidate	This paper reports on original research carried out during the first year of the PhD candidature.
Date and Signature	 19-07-2021

2.2.2 Abstract

Identifying patterns in data relating to extreme rainfall is important for classifying and estimating rainfall and flood frequency distributions routinely used in civil engineering design and flood management. This study extracts the key moisture pathways for extreme rainfall events in northern Spain using several novel self-organising map (SOM) models. These models are trained using various subsets of a backwards trajectory data set generated for extreme rainfall events between 1967 and 2016. The results of our analysis show 69.2% of summer rainfall extremes rely on recirculatory moisture pathways concentrated on the Iberian Peninsula where as 57% of winter extremes rely on deep Atlantic pathways to bring moisture from the ocean. These moisture pathways have also shown differences in rainfall magnitude, such as in the summer where peninsular pathways are 8% more likely to deliver the higher magnitude extremes than their Atlantic counterparts.

2.2.3 Introduction

Floods generated by extreme weather events continue to be a global issue causing widespread social and economic damages. Effective flood risk management requires estimates of the frequency and magnitude of future flood characteristics, such as for example the magnitude of the design rainfall and flood events with a return period of 100 or 10000 years. Such estimates are obtained through frequency analysis by fitting statistical extreme value distributions directly to past extreme events. Traditional frequency analysis techniques do not account for differences in the underlying processes causing extreme events. The importance of accounting for different event-generating processes in frequency analysis has been discussed in several studies. Waylen and Woo (1982) separated an annual maximum series of flood peak into events caused by rainfall and snowmelt, respectively, and fitted a mixture distribution consisting of two Gumbel distributions. Hirschboeck (1987) manually divided a flood distribution into eight subcategories each representing floods caused by different atmospheric patterns. This resulted in a set of distributions, each with significantly different structure with some containing multiple peaks, whereas others showed a distinct generalised extreme value distribution (Hirschboeck 1986). Merz & Blöschl, (2003) utilised a process-oriented method by separating the initial flood distribution by generating mechanisms in Austrian catchments, which was then used to show “short rain” floods generally happened in the southern part of the country. Villarini and Smith (2010) found that the upper tail of flood distributions in the Eastern part of the US are influenced by tropical cyclones. Kjeldsen et al. (2018) studied extreme rainfall in South Korea and used information published by the Korean Meteorological Administration to create annual maximum series of one day rainfall caused by typhoons and non-typhoons, respectively.

However, while most studies argue that improved process-understanding will improve the reliability of model predictions, there is still a need to develop objective methods for distinguishing between events generated by different mechanisms (Kjeldsen et al. 2018). In addition, the benefits of process-oriented techniques come at a computational cost; previously constraints regarding the availability of data and computational power have limited our ability to identify these generation mechanisms. Where data has been available it has generally been provided in small sample sizes. This limitation also explains the preference for non-process-based methods which are less computationally expensive (Hirschboeck 1986). Despite this, with increasing amounts of data are becoming available such as through the Hybrid Single Particle Lagrangian Integrated Trajectory Model (HYSPLIT) (Stein et al. 2015) which opens-up new opportunities to take advantage of auxiliary knowledge regarding these extreme events.

This study will focus on the different processes controlling extreme precipitation events in the Douro catchment, located in north-western Spain. Mediero et al. (2014) found a general decrease trend in annual maximum flood series in Spain. In addition, a recent study found that floods towards the north of the Iberian Peninsula are trending towards early winter (Blöschl et al. 2017). Santos et al. (2018) partially explained such decreasing trends by a negative trend in the moisture amount that arrives in Spain, more evident in the case of Continental storms. Without high resolution knowledge of how the underlying processes affect flood distributions current models come with higher process uncertainty.

Current literature explores the large-scale atmospheric processes which influence global rainfall variation. Utsumi et al. (2017) found the main driver for precipitation in central Europe is extratropical cyclones. The author's found a similar result in the Mediterranean but with a higher tendency to be manipulated by extratropical cyclones. Further studies have identified the tropical-subtropical North Atlantic corridor (a corridor stretching from the Gulf of Mexico and the Caribbean Sea to the Mediterranean) to influence moisture fluxes on the Iberian Peninsula (Gimeno, Nieto, et al. 2010; Gimeno, Drumond, et al. 2010; Scoccimarro, Gualdi, and Krichak 2018). Jorba et al. (2004) extracted the high-level trajectories arriving in the Barcelona area by using HYSPLIT, clustering them into 10 different patterns describing the 2D (latitude/longitude) pathways. Such work highlights the tropospheric circulation patterns that influence the Barcelona area by identifying that the main flows come from the Atlantic, 5500m above sea level. However, this study focussed on the upper portion of the atmosphere and therefore is not directly useful for identifying moisture transport systems which are generally found in the lower 2000m (McIntosh 1978). More recently, links have been drawn between low-level trajectory classifications and a temporal trend in their occurrence, by using HYSPLIT to extract trajectories associated with flood events and classifying them using a different clustering method (k-means). The results of this analysis showed the Continental storms appeared to be more common than their Atlantic/Mediterranean counterparts when aligned with extreme flood timings (Santos et al. 2018).

Moisture pathways associated with seasonal extremes have been identified in Canada by following a similar approach, extracting and classifying trajectories for extreme rainfall events at varying altitudes between 0 and 5000m (Tan, Gan, and Chen 2018). The study identifies nine spatially coherent regions using self-organizing maps (SOM), highlighting the key moisture sources related to the seasonal extreme precipitation. Despite this there is limited consideration for varying the number of clusters the algo-

rithm was initialised with and no indication of whether a numerically accurate solution was produced.

Methods for classifying these moisture trajectories can be grouped into two main categories: supervised and unsupervised. Supervised methods for classification rely on having a training data set with both inputs and known outputs. These methods are most useful for identifying similarities and differences between the known classifications. An example of a supervised trajectory classification algorithm is TraClass (Lee et al. 2008), which utilises the known class labels to identify descriptive areas of the trajectories which can be used to differentiate each class. Unsupervised classification methods do not require a training set with known class labels. Instead these methods can be used to identify groups of numerically related input vectors. The most popular unsupervised methods are k-means and SOMs, which have recently been shown to successfully identify trajectory groups (Owens and Hunter 2000; Lee et al. 2008; Tan, Gan, and Chen 2018; Santos et al. 2018).

This paper aims to use self-organising maps both to identify the key moisture pathways which lead to annual maximum (AMAX) rainfall and to highlight the magnitude differences between these classifications. To begin the selected case study and data used is described. Second, the classification methodology and models are introduced. Third, the results of the classification model development are presented before final conclusions are presented.

2.2.4 Methods

Precipitation & Trajectory Data

This analysis focuses on the Douro catchment located in a north-western region of Spain. AMAX series of one-day precipitation were extracted from 310 gauging stations shown in Figure 2-1. The data sets available for each station vary in length with some containing data from 1948 and others only containing data from 1967 to 2016. In total 16,534 one-day rainfall events were extracted. The AMAX data were normalised between 0 and 1 using the equation:

$$NormalisedRainfall_i = \frac{rainfall_i - \min(rainfall_i)}{\max(rainfall_i) - \min(rainfall_i)}, \quad (2.1)$$

where $rainfall_i$ refers to the annual maximum series vector for a given station i .

This provides a more comparable view of the rainfall variation between stations, as

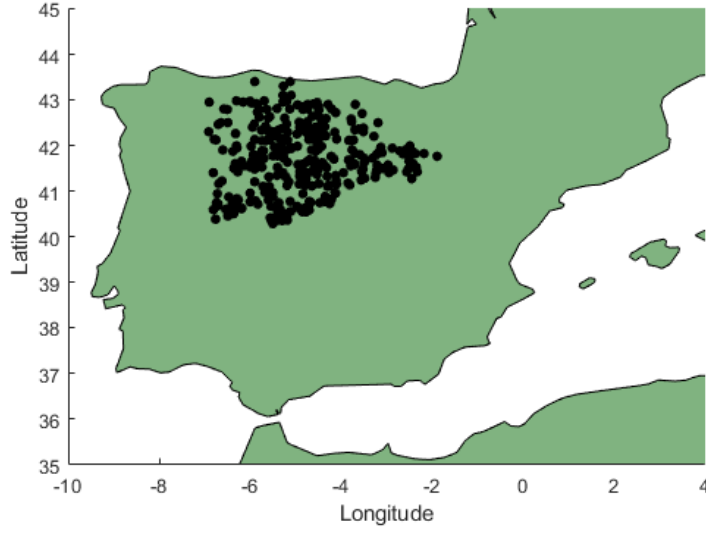


Figure 2-1: Locations of gauging stations used to extract annual maximum rainfall events, black line indicates the catchment boundary for the Duoro river.

rainfall magnitudes depend on height and spatial location, among other variables. Consequently, this normalisation removes differences between stations with high and low rainfall magnitudes, providing a baseline to analyse any magnitude changes without the need to use the station as a dependent variable. The normalisation smooths the empirical cumulative distribution curve of rainfall magnitudes (Figure 2-2).

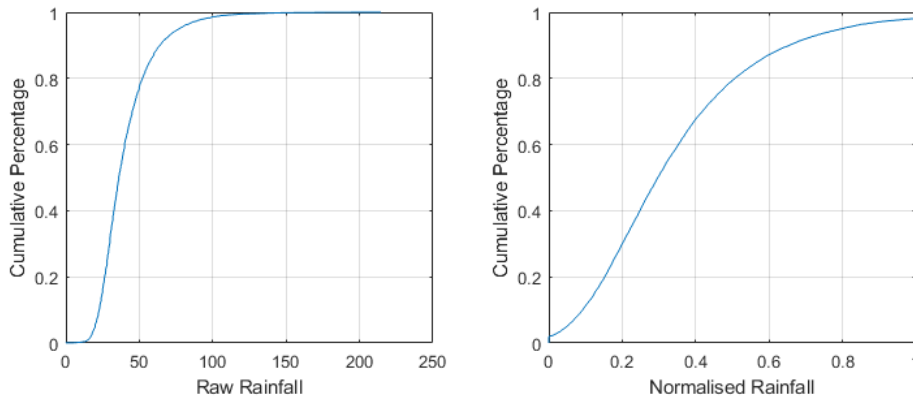


Figure 2-2: Empirical cumulative distribution for all rainfall data both before normalisation (left) and after (right).

For each AMAX event 24 backwards trajectories were generated using the HYSPLIT

system (Stein et al. 2015). In order to generate these trajectories HYSPLIT must be initialised with a start location, start time and run-time which are then used alongside meteorological files to generate a trajectories. We used NCEP/NCAR reanalysis data files (Khalilia and Popescu 2014) as input for the HYSPLIT model. The primary variables used are related to air pressure, velocity, specific humidity and temperature (PRSS, T02M, U10M, V10M, TPP6, HGTS, TEMP, UWND, VWND, WWND and RELH). For a full description of the variables please refer to NOAA (2003). HYSPLIT uses these files to estimate the storm tracks and water budgets for each storm event. The method used by HYSPLIT is a hybrid between a Lagrangian and Eulerian approach which allow the relative calculation of the advection, diffusion and particle concentrations (Draxler and Hess 1997; Draxler and Hess 1998; Stohl and James 2004).

These trajectories were initiated using a set of combinations of altitudes (10, 410, 810, 1210, 1610 and 2010m above sea level) and times (00:00, 06:00, 12:00, 18:00) on the day of the event’s occurrence. The altitudes were selected to coincide with the expectation of moisture pathways generally existing in the lower 2000m of the atmosphere (McIntosh 1978). The length of the backwards trajectories was fixed to 48 hours before the given initiation time and resulted in a total of 331,728 successfully extracted storm tracks, five examples of the output from HYSPLIT are presented in Figure 2-3. Each of these trajectories consists of 49 points identifying the position of the air parcel at each hour interval. Each point has the following information associated with it: Latitude, longitude, altitude, specific humidity and atmospheric pressure. For the purposes of this study only latitude, longitude and altitude are used as the goal is to identify the spatial origin of these events.

Trajectory classification

The SOM approach was adopted to classify these trajectories, due to a significant number of successful hydrological applications (Kaltch, Hjorth, and Berndtsson 2008; Fahimi, Yaseen, and El-shafie 2017; Tan, Gan, and Chen 2018). A self-organised map is a type of neural network architecture used for classifying or reducing the dimensions on input data. It does this through the unsupervised learning of a data set to produce its discretised representation, which is often referred to as a ‘map’. The purpose of which is to describe the relationships between the clusters. An example of a SOM is given in Figure 2-4. SOMs create this map through competitive learning where each output (or class) competes to represent a given input vector (Kohonen and Honkela 2007). For each input vector the closest node is selected and moved closer to the given input vector; a neighbourhood function is then applied such that the neighbours of

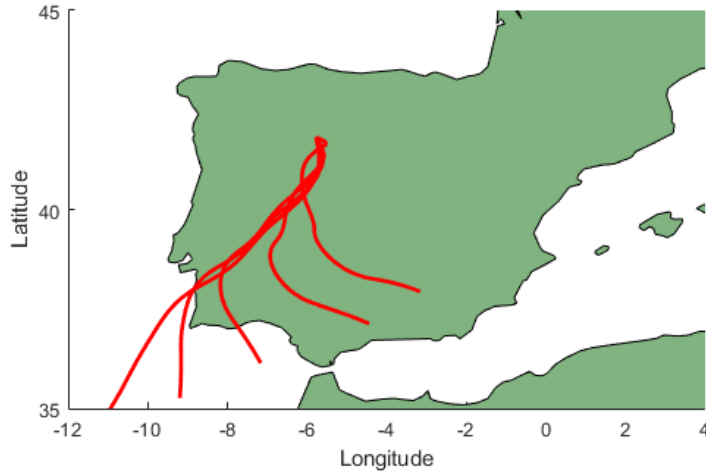


Figure 2-3: Five backwards trajectories from a single AMAX event starting from the northern most point.

the node are also moved although to a lesser extent. This then trickles through the network until the movement is next to none. For a full and detailed description of how the SOM method works please see Kohonen and Honkela (2007).

The key benefit of SOMs is the assurance that inputs which are close in the original high dimensional input space are close in the classified low dimensional space (output), which is not guaranteed by other procedures such as k-means. This works through for each training item (or in our case trajectory) updating both the closest matching output node and its neighbouring nodes. Further to this, although the SOM approach requires a determined number of output nodes or clusters it does not require an assumption on the distribution of the data such as would be required by, for example a Gaussian mixture method (Yang, Kong, and Liu 2004).

Classifier selection

A classification model accepts many inputs and reduces them into a single class. Common approaches to classifying trajectories rely on the development of a single classifier, such as in Tan et al. (2017) who trained a single model and did not consider varying the SOMs parameters such as map size and data sampling. However, such approaches fail to capture the relationship between variables in the dataset and the classifications. Our approach will explore the differences which occur when varying two key parame-

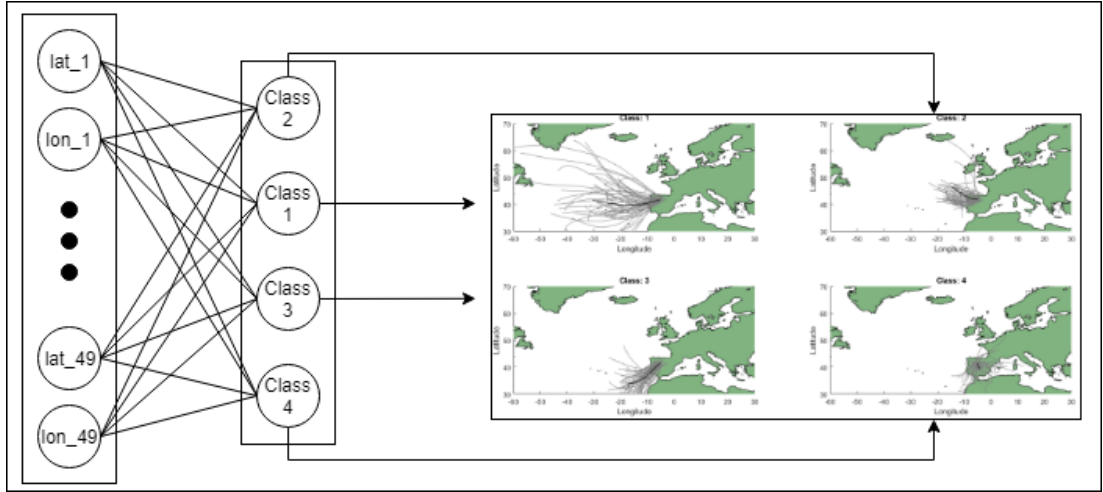


Figure 2-4: A sample SOM architecture with 98 input nodes representing the 49 latitude and longitude points of a trajectory. All input nodes are connected via weighted edges to the four output nodes (classifications). These output nodes are arranged into a neighbourhood grid before training which results in classifications being similar to their neighbours. For example, classes 2 and 3 contain trajectories which are closer to class 1 than those contained in class 4.

Code Name	No. Classes	Altitude	Date Filtering	No. Inputs	No. Trajectories
PR-4	4	No	None	98	331,728
PR-9	9	No	None	98	331,728
3D-9	9	Yes	None	147	331,728
SUM-9	9	No	May-Sep	98	88,776
WIN-9	9	No	Oct-Apr	98	242,952

Table 2.1: Characteristics of the five classifiers used; here date filtering is inclusive. Number of inputs is defined as the size of each input vector before it is classified, and the number of classes is the number of output nodes available to the SOM.

ters, the subset of data used for training and the size of the map. Further to this the separation of the dataset into two training sets for distinct summer/winter classifiers is used to aid in the identification of seasonal variation in the classifications generated. Here we define summer and winter to cover the warm (May-September) and cool (October – April) seasonal variations, following a similar pattern to that used in previous work (Tan, Gan, and Chen 2018). Table 2.1 describes the training data set for the four classifiers chosen and identifies which parts of the input vectors are included as well as any filtering on the trajectories.

Classifier optimisation

To ensure a numerically stable solution is reached each classifier is first trained with 10 different map sizes. A map size refers to the number of nodes in a square grid, for example a 2x2 map size would result in four output classifications and a 3x3 map size results in nine output classifications. These maps indicate how the output nodes (clusters) are arranged. The example given in Figure 2-4 shows four clusters arranged in a 2x2 map with Class 1 having neighbours 2 and 3, Class 3 having neighbours 1 and 4 etc. An alternative approach would be to use a 4x1 map. This structure enables the SOM architecture to identify clusters which may be related, such as classes 1 and 2 from Figure 2-4 are much more similar than classes 1 and 4. A batch processing approach is used for training because it has been shown to be an order of magnitude faster than the alternative linear training approach (Kohonen and Honkela 2007). In addition, two error metrics are calculated for each classifier. The quantisation error calculates the root-mean squared Euclidean distance between each training sample and its best matching node (BMN). The best matching node is defined as the output node with the highest level of activation when a given input is used. The topological error calculates the percentage of training samples which have a first and second BMN which are not adjacent on the output map, ensuring topological consistency (Khalilia and Popescu 2014).

Figure 2-5 shows the errors produced for each of the four classifiers. Each graph gives the squared dimension (map size) of each model on the x-axis, such that a value of two equates to a 2x2 output map which contains four classifications. As is expected in any clustering procedure the quantisation error decreases with the increase in the number of potential classifications as illustrated in all three quantisation error graphs. Despite this there is still clear indication of the numerically superior classifiers as the magnitude of the errors vary significantly.

The large difference in quantisation error could be the curse of dimensionality, an umbrella term for the disadvantages caused by having large input vectors which do not occur when using lower dimensional vectors (Kohonen and Honkela 2007). The 3D classifier uses 147 input variables whereas the other only use 98 and it is known that increasing the number of input variables in already high-dimensional problems can cause a decrease in search performance such as when selecting the BMN (Marimont and Shapiro 1979). These differences are not replicated in the topological errors which tend to increase with an increase in map size. For instance, the primary classifier shows a consistently lower error indicating a better topological fit of the data. Due to the increasing nature of the topological error it is concluded that the smaller maps are

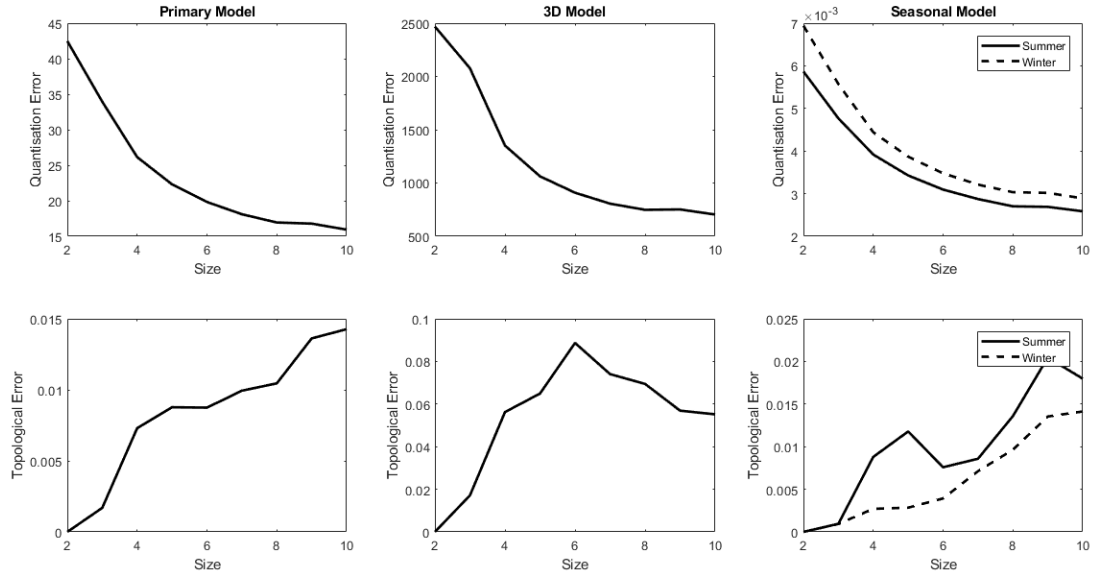


Figure 2-5: This figure shows both the quantisation (top) and topological (bottom) errors for each of the three classifiers.

more numerically accurate. Therefore, this study will utilise a 2x2 map and 3x3 map for the primary and both seasonal models to present any differences between having either a high topological or quantisation error.

2.2.5 Results

This section discusses the resulting classifications for each of the five models presented in Table 1. It highlights the key moisture pathways as well as their prominence in the data set. This section concludes on an analysis of the rainfall magnitudes for each cluster.

Classifications

Beginning with the Primary classifiers, Figure 2-6 shows the classifications generated in the SOM with a 2x2 map size, which is referred to as the Primary 4-SOM classifier (PR-4) indicating it has four output classifications. The results show four patterns: Class 1 contains a mid/western Atlantic originating path, Class 2 includes those coming from the north Atlantic, Class 3 contains the storm tracks coming from the south Atlantic. Class 4 contains the continental or recirculation pathways. The proportion of trajectories falling into each classification is provided in Table 2.2. The two dominant pathways are the recirculation and mid/western Atlantic classes which contain 46.5%

(Class 4) and 35.2% (Class 1) of the sample trajectories respectively. The least common class was the north Atlantic class (Class 2), which only contained 6.7% of the sample; however, this was only slightly lower than the 11.6% of storm tracks classified as south Atlantic storms (Class 3).

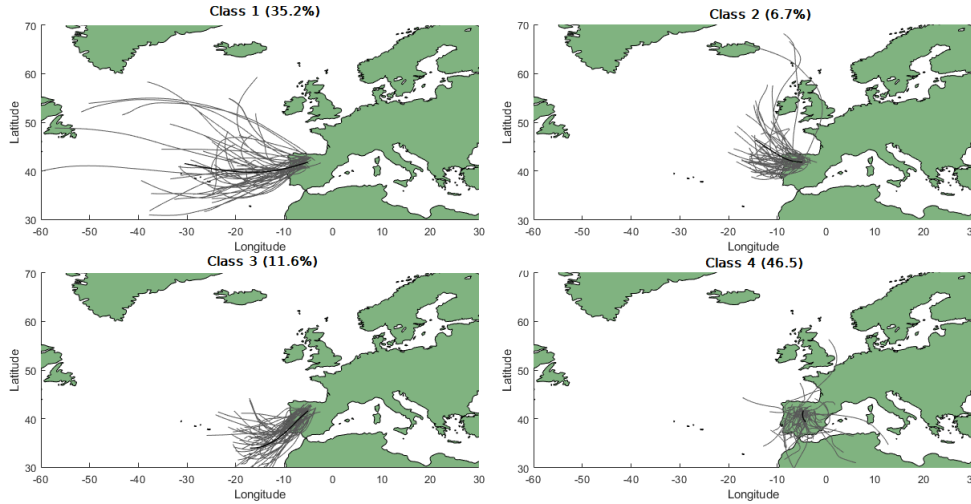


Figure 2-6: A sample of trajectories for each cluster in the primary 4-SOM classifier (PR-4). The classifications plot shows 50 randomly selected trajectories for each class (coloured grey) with a mean trajectory across all relevant trajectories coloured in black. The proportion of trajectories within each class is given in Table 2.2.

	Class			
	1	2	3	4
%	35.2	6.7	11.6	46.5

Table 2.2: Proportion of trajectories which are classified under each of the four classes within PR-4.

Comparing the results of PR-4 with those of a larger map size, reaffirms the key pathways identified. Figure 2-7 shows the classifications produced from the SOM with a 3x3 map size in the Primary classifier (PR-9). Here the classifications appear to be more refined versions of the ones present in PR-4. For example, Classes 7, 4, 1 and 5 appear to be subclasses of the mid/western Atlantic class (Class 1) from PR-4. The same can be seen with the continental class (Class 4) in PR-4 which is broken down into Classes 3 and 6 in the PR-9. Moreover, the north Atlantic classification (Class 2) from PR-4 appears unchanged in the PR-9 (again Class 2). The proportions for each class in PR-9 are expectedly lower due to the greater spread amongst the range of classes as shown in table 2.3. Despite this, the same pattern appears with continental and mid/western Atlantic classes (Class 1 and Class 4) containing the higher proportions of the sample.

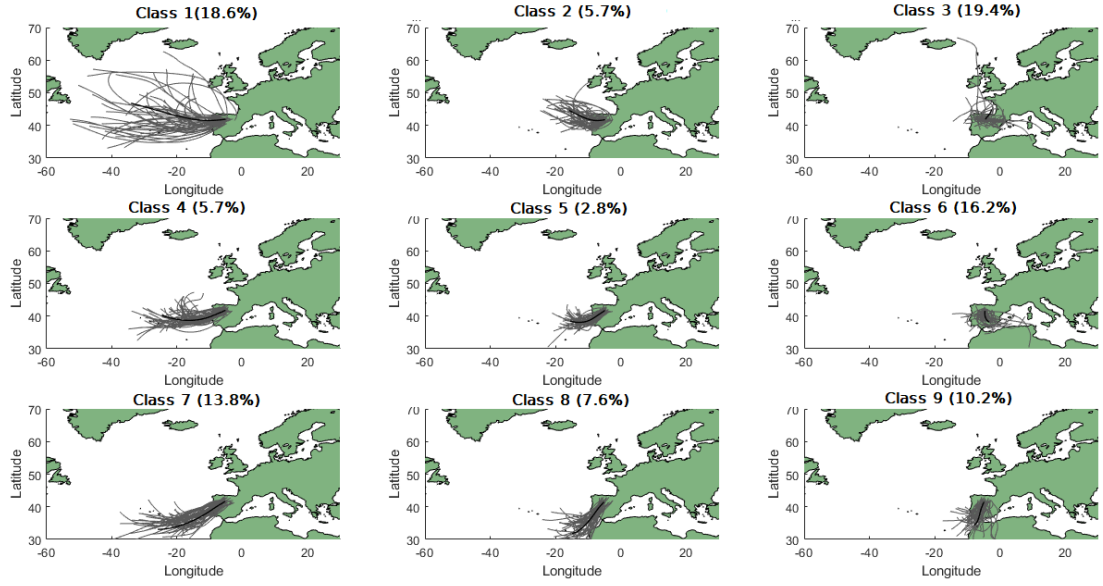


Figure 2-7: A sample of trajectories for each cluster in the 9-SOM primary classifier (PR-9). The classifications plot shows 50 randomly selected trajectories for each class (coloured grey) with a mean trajectory across all relevant trajectories coloured in black. The proportion of trajectories within each class is given in Table 2.3.

	Class								
	1	2	3	4	5	6	7	8	9
%	18.6	5.7	19.4	5.7	2.8	16.2	13.8	7.6	10.2

Table 2.3: Proportion of trajectories which are classified under each of the nine classes within PR-9.

The 3D classifier (3D-9) tended to have the highest numerical errors in comparison to the other classifiers, and on inspection the tracks appear to have a higher visual variance. The two prominent classes shown in Figure 2-8 Classes 1 and 3 differ only in general length and cannot be linked back to classifications in PR-4 or PR-9. However, the spread of trajectories highlighted in table 2.4 shows there is a preference towards classes 1 and 3.

	Class								
	1	2	3	4	5	6	7	8	9
%	35.4	4.9	20.9	7.6	3.0	4.8	6.7	5.7	10.8

Table 2.4: Proportion of trajectories which are classified under each of the nine classes within 3D-9.

Regarding the seasonal classifiers, they produced the lowest errors during the training phase with the winter classifier producing errors slightly higher than the summer clas-

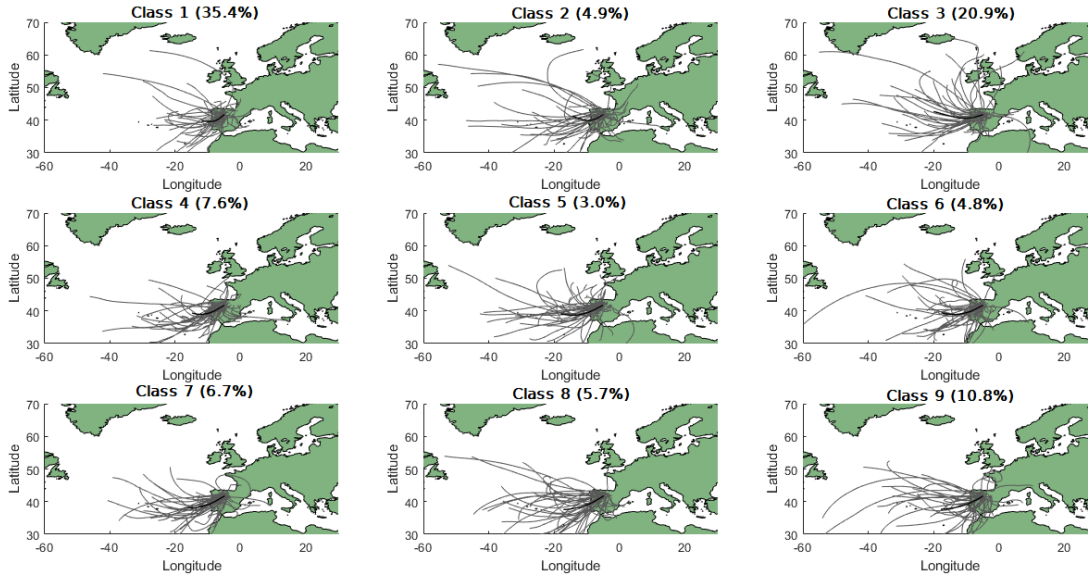


Figure 2-8: A sample of trajectories for each cluster in the 3D 9-SOM classified (3D-9). The classifications plot shows 50 randomly selected trajectories for each class (coloured grey) with a mean trajectory across all relevant trajectories coloured in black. The proportion of trajectories within each class is given in Table 2.4.

sifier. One possible reason for this disparity could be the quantity of the samples used. Winter trajectories accounted for 73.2% of the sample with the remaining 26.8% being summer trajectories. An expected side effect of this is that the seasonal classifiers show consistently lower errors due to the reduced variation in the samples they are trained with.

Figure 2-9 shows the 9-SOM trained on the summer data set (SUM-9), in this classifier there is one Atlantic pathway (Class 1) and two visually smaller Atlantic pathways (Classes 4 and 7). The other classes making up this classifier all visually appear as more refined continental storms, as discussed regarding PR-9 above. However, this classifier also presents three dominant pathways for the summer storms as given by Table 2.5, the mid-Atlantic (Class 1), northern-continental (Class 3) and south eastern Mediterranean tracks (Class 9). These pathways account for 16.8%, 17.5% and 20.7% (55% of the total pathways) of the summer tracks as shown in table 5, reinforcing the conclusion from PR-9 that the dominant summer pathways are continental (or recirculatory) and east-Atlantic originating tracks. These results also compare well with those found by Jorba et al. (2004) who as stated earlier identified recirculatory tracks as the dominant summer pathways; by separating these summer tracks we have further reinforced these results and shown that Atlantic tracks still play a key role in

summer extremes.

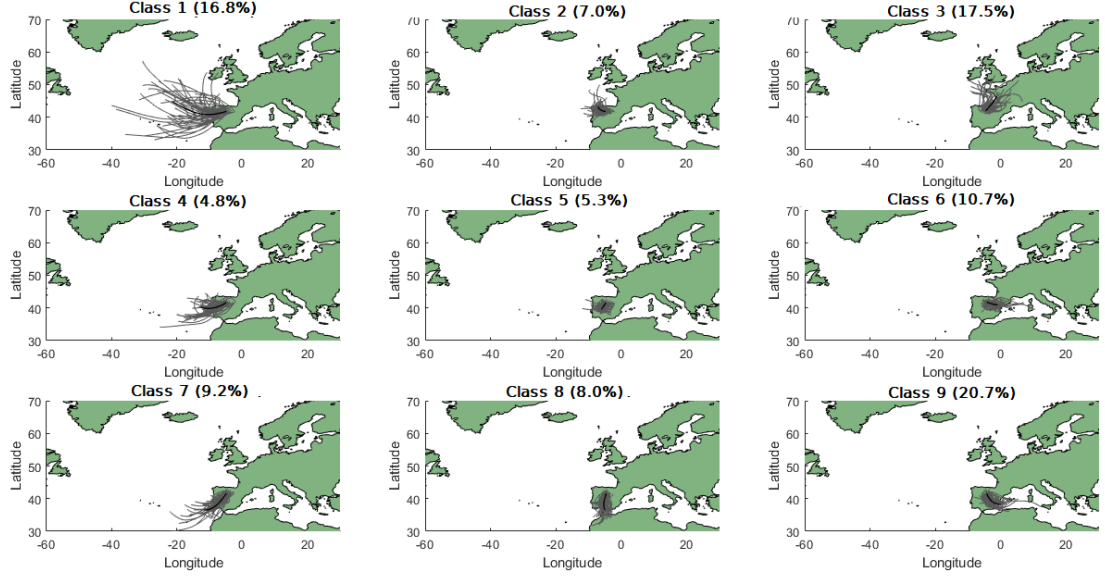


Figure 2-9: A sample of trajectories for each class in the summer 9-SOM classified (SUM-9). The classifications plot shows 50 randomly selected trajectories for each class (coloured grey) with a mean trajectory across all relevant trajectories coloured in black. The proportion of trajectories within each class is given in Table 2.5.

	Class								
	1	2	3	4	5	6	7	8	9
%	16.8	7.0	17.5	4.8	5.3	10.7	9.2	8.0	20.7

Table 2.5: Proportion of trajectories which are classified under each of the nine classes within SUM-9.

The winter 9-SOM classifier (WIN-9) is shown in Figure 2-10 and appears visually similar to PR-9 which can be attributed to the winter storms comprising 73.2% of the sample. Dominant pathways in this classifier consist of deep-Atlantic (Class 1), continental (Class 3) and southern-Atlantic (Class 7) paths; similarly, to SUM-9 these can be identified in earlier results such as Classes 1 and 7 in PR-9 and Class 1 in PR-4. These classes consist of 18.4%, 18.7% and 13.7% (50.8% of the total pathways) of the sample, which are significantly higher than Classes 2, 4 and 5 which only hold 6.3%, 6.8% and 3.6%. Further to this, 38.9% of winter events were classified (classes 1, 4 and 7 in WIN-9) as deep-Atlantic compared to only 16.8% of summer events (class 1 in SUM-9). This shows deep-Atlantic storm trajectories have a seasonal dependence and generate at least twice as many AMAX events during the winter than during the summer.

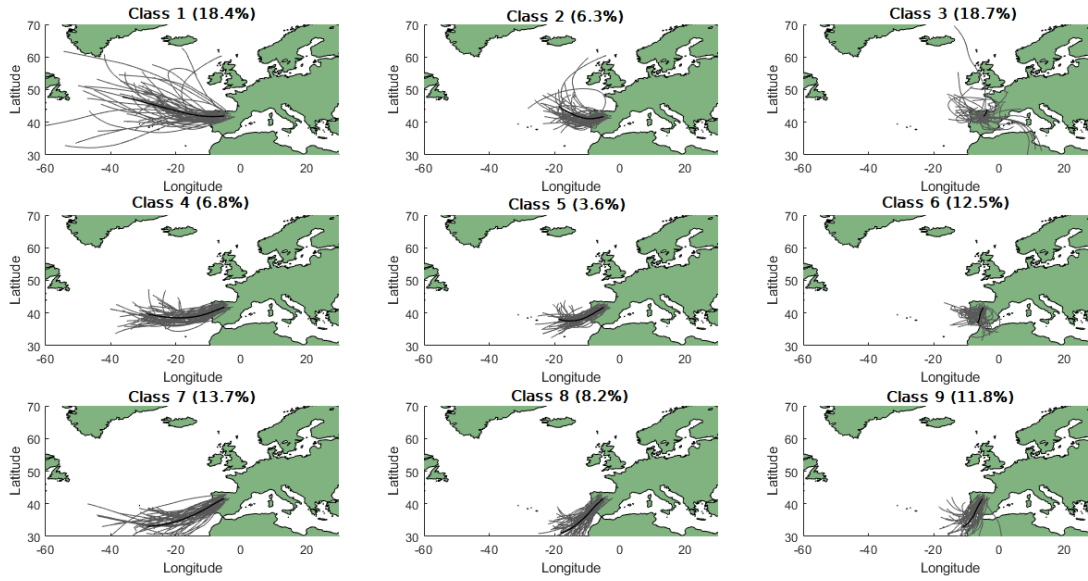


Figure 2-10: A sample of trajectories for each cluster in the winter 9-SOM classifier (WIN-9). The classifications plot shows 50 randomly selected trajectories for each class (coloured grey) with a mean trajectory across all relevant trajectories coloured in black. The proportion of trajectories within each class is given in Table 2.6.

	Class								
	1	2	3	4	5	6	7	8	9
%	18.4	6.3	18.7	6.8	3.6	12.5	13.7	8.2	11.8

Table 2.6: Proportion of trajectories which are classified under each of the nine classification within the 9-SOM winter classifier.

Distributions of rainfall magnitude

A final analysis of the classifiers concerns the distributions of each cluster. Figure 2-11 shows the empirical distributions for each cluster in both PR-4 (left) and PR-9 (right). In both classifiers the classes which are most likely to result in above average magnitude extreme events are from the southern Atlantic. For example, Class 3 from PR-4 and Class 7 from PR-9 have 21.7% and 23.4% relatively of their tracks above this threshold. Both PR-4 and PR-9 also show similar results for the classes which are least likely to produce events above the threshold, with Class 2 (northern-Atlantic) from both the PR-4 and PR-9 only having 18.7% and 18.6% respectively. As these trajectories are similar this further reinforces the case that trajectories from the north Atlantic are less likely to cause the highest/lowest magnitude AMAX values but trajectories from the south Atlantic being more likely to cause these same events. Further to this the proportions given in Tables 2.2 and 2.3 indicate that these north and south Atlantic

trajectories are also the most uncommon.

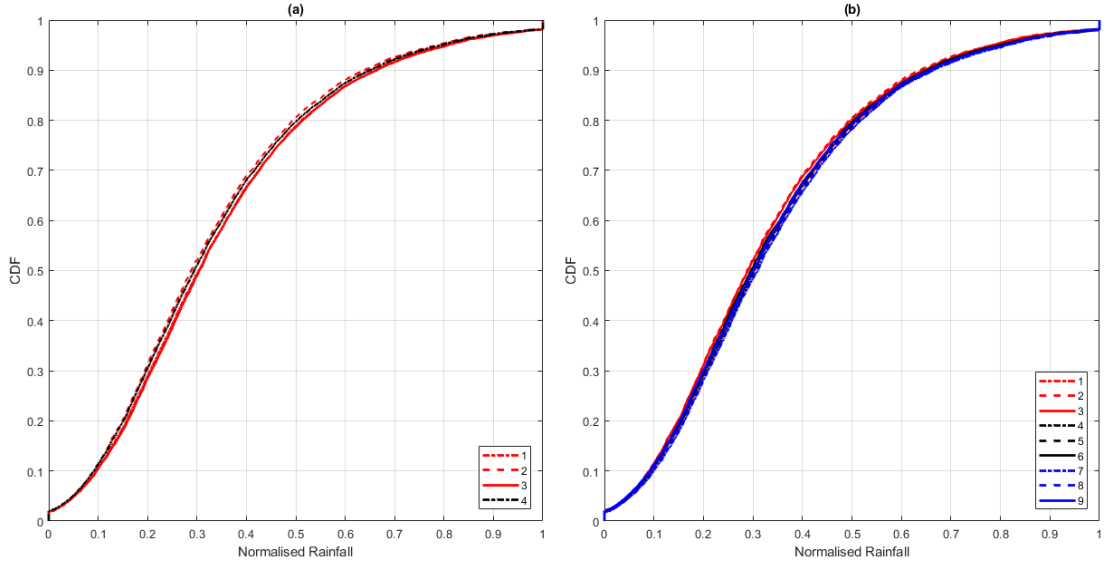


Figure 2-11: Rainfall distributions for each cluster in PR-4 (left) and PR-9 (right). In each case the line's number corresponds to the class of storm track represented.

Figure 2-12 shows the rainfall distributions for the classifications of both the summer (left) and winter (right) classifiers. The summer distributions show a separation into two groups most prominent at a normalised magnitude of 0.35. This separation occurs between the Atlantic tracks (Classes 1, 4 and 7) and the continental tracks (Classes 2, 3, 5, 6 and 8); Class 9 is different in that it doesn't join a group and instead holds a middle ground between the two. Taking a magnitude of 0.5 as a threshold there is a maximum difference of 7.3% in the number of tracks with a magnitude which exceed this threshold between the two groups (Classes 1,2 and 6), the closest difference is 4.5% between Classes 7 and 8. This separation indicates during the summer months it is continental tracks that are more likely to cause higher magnitude events.

In contrast, the winter distributions appear more varied with no dominant group separation as in the summer classifier. Taking the same experiment as above, using a magnitude threshold of 0.5 the lower-Atlantic classes (Class 7 and Class 5) have 23.8% and 24.0% of their samples exceeding this threshold. This indicates the lower-Atlantic storms have a higher likelihood of causing above average magnitude AMAX events in the winter and the continental storms have a higher likelihood of causing these same events in the summer.

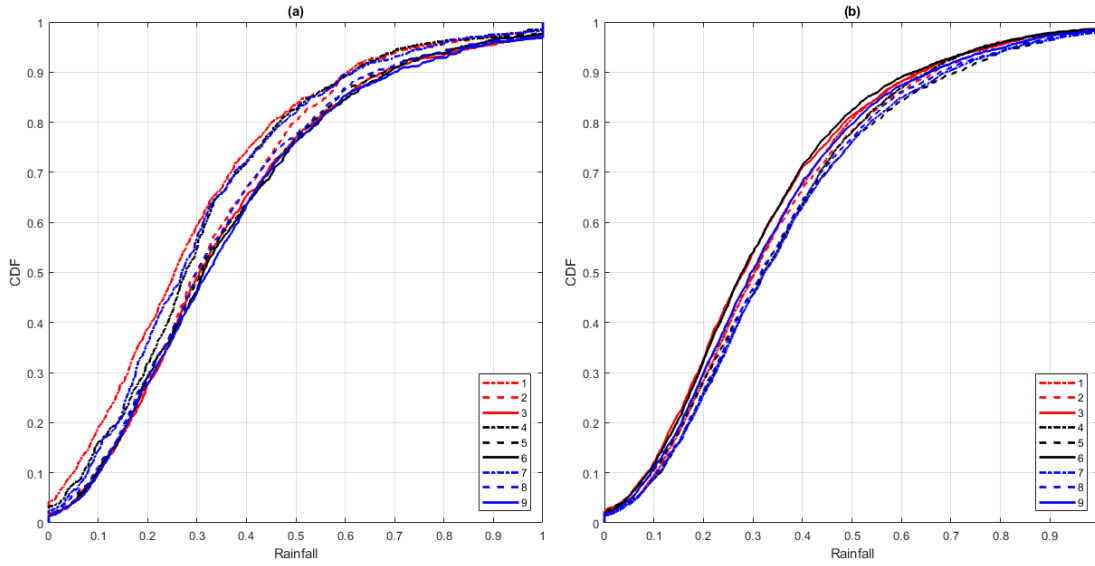


Figure 2-12: Rainfall distributions for SUM-9 (left) and WIN-9 (right) classifiers. In each case the line's number corresponds to the class of storm track represented.

2.2.6 Conclusions

This paper demonstrates the use of self-organising maps for improving the current understanding of rainfall frequency analysis through classification of the moisture pathways leading to an AMAX rainfall event. Five classification models were generated using different subsets of the trajectory data in northern Spain, each provided insight into the applicability of the SOMs and the causes of extreme rainfall in this region. Here we define extreme rainfall events as the annual maximum of one-day precipitation measurements from a series of gauging stations.

1. Clustering on latitude/longitude (2D) trajectories for all rainfall events with four clusters (PR-4) and nine clusters (PR-9).
 - (a) Two prominent classes identified in PR-4 represent 81.7% of the sample trajectories; Class 1 from the mid/Western Atlantic Ocean (35.2%) and Class 4 containing recirculation patterns (46.5%).
 - (b) The prominent classes from PR-4 are verified by PR-9 in which the Atlantic pathways (Classes 1, 4 and 7) account for 38.0% of the sample trajectories.
 - (c) The Southern Atlantic and mid/Western Atlantic pathways classes (Class 1 and 3:PR-4) contained events which had 4.0% more high magnitude extreme events than the shorter Atlantic Class 2 as illustrated in Figure 2-11. A

similar pattern is present in PR-9.

2. Clustering on altitude, latitude & longitude (3D) trajectories for all rainfall events.
 - (a) This model (3D-9) showed the highest numerical errors and produced clusters with little visual difference; this is due to the larger number of input variables required. This is often referred to as the curse of dimensionality.
3. Clustering on longitude & latitude (2D) trajectories for summer events (SUM-9).
 - (a) Three prominent pathways are responsible for 55% of summer extremes, these originate from: the mid-Atlantic (Class 1), northern-Europe (Class 3) and the south-eastern Mediterranean (Class 9).
 - (b) The three Atlantic clusters (Classes 1, 4 and 7) contained at least 4.5% more high magnitude events than the other clusters, in some cases this raised to 7.3%.
4. Clustering on longitude & latitude (2D) trajectories for winter events (WIN-9).
 - (a) The three dominant pathways in this model are similar to the primary models (PR-9 and PR-4) but only represent 50.8% of the trajectories: western-Atlantic (Class 1: 18.4%), continental (Class 3: 18.7%) and southern Atlantic (Class 7: 13.7%).
 - (b) Southern Atlantic classes (Classes 5 and 7) are the most likely pathways to produce above average magnitude extremes at 24.0% and 24% respectively.

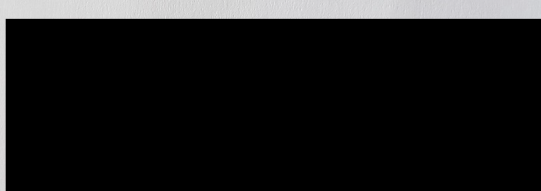
These results show that clustering can provide improved insight into components of rainfall distributions. The SOM approach has proved capable of spatial-clustering of trajectory patterns in 2D; however, we have also shown why care must be taken when considering 3D trajectories to minimise both numerical errors and visual difference. Finally, the results revealed differences in the origins of winter and summer extreme rainfall in the Douro region of northern Spain as detailed above. This work has opened up new questions in the use of alternative input variables to the clustering algorithm; for example, instead of normalising station data a station type could be added as an input variable. Future studies could also investigate the development of a new clustering error metric accounting for both numerical errors and number of clusters to limit the scope of training procedures.

2.2.7 Acknowledgements

The authors gratefully acknowledge the NOAA Air Resources Laboratory (ARL) for the provision of the HYSPLIT transport and dispersion model and the Spanish 'Agencia Estatal de Meteorología' (AEMET) for providing the precipitation data used. The first author acknowledges funding as part of the Water Informatics Science and Engineering Centre for Doctoral Training (WISE CDT) under the National Productivity Investment Fund, grant number EP/R512254/1.

2.3 Atmospheric origins of extreme rainfall in the UK

2.3.1 Authorship Statement

Status	Published in the Proceedings of the IMA's 4th International Flood Risk Conference.
Details	Barnes, A.P., McCullen, N., Kjeldsen, T.R. Atmospheric origins of extreme rainfall in the UK. (2019). Proceedings of the IMA's 4th International Flood Risk Conference.
Authors' contribution	<p>The author of this thesis has primarily (90%) contributed to design and implementation the methodology adopted for the extraction, clustering and analysis of the storm trajectories. Each author's exact contributions are as follows:</p> <p>A.P. Barnes: Formulation of ideas (90%), design of methodology (90%), processing and analysis of data (100%), manuscript preparation (90%).</p> <p>N. McCullen and T.R. Kjeldsen: Formulation of ideas (5%), design of methodology (10%), manuscript preparation (10%).</p>
Statement from candidate	This paper reports on original research carried out during the first year of the PhD candidature. Some minor changes to headings and grammatical corrections have been made.
Date and Signature	 19-07-2021

2.3.2 Abstract

This study extracts and classifies the storm trajectories of extreme rainfall events across the UK using a trajectory dispersion model (HYSPLIT). The trajectories are classified using three unsupervised classification techniques which were compared using a similarity measure. This resulted in the selection and application of the k-means method for identifying six moisture pathways responsible for extreme rainfall. The most frequent subset of these pathways originate from the Atlantic and led to 60.58% of the extreme rainfall events, while the remainder originate from the North Sea. Further to this, we identify the North Sea storms are the more likely to cause above average extreme events especially in Wales. A final comparison is made with the North-Atlantic Oscillation index where storm types which originate from the north and western Atlantic are more frequent during a positive NAO phase where as storms originating near the British Isles are more common in a negative phase.

2.3.3 Introduction

The impacts of extreme weather across the UK continue to have severe economic and social consequences. One key mechanism which can lead to a disaster is flooding often caused by extreme rainfall. A prime example of the costs associated with flooding can be seen in December, 2015 where record breaking levels of precipitation caused extensive flooding in Cumbria leading to at least 16,000 homes being flooded (Cumbria County Council 2018). Traditionally, design floods are calculated by fitting a statistical distribution to a sample of annual maximum events, assuming this distribution to be constant and that all observed events originate from the same underlying population. However, recent research has highlighted the importance of better understanding the underlying processes associated with individual events in order to: 1) build more robust models representing the existence of mixed populations (Kjeldsen et al. 2018), and 2) better understand how global climate change is likely to affect the type, magnitude and frequency of more localised distributions of extreme rainfall and floods (Blöschl et al. 2017).

In this context it is important to develop new methods that will allow an objective classification of event types. For example, Lavers *et al.* (2011, 2013) highlights the role of large plumes of water rising from the tropics in the form of atmospheric rivers (ARs) which cause extreme levels of precipitation across the west coast of the UK. Recent literature has shown the application of atmospheric trajectory generation and classification as a potential tool for identifying the pathways of extreme events (Santos et al. 2018; Tan, Gan, and Chen 2018; Gimeno, Drumond, et al. 2010) which would allow for the identification of atmospheric river type pathways to be identified as well as alternative pathways which cannot be classified as AR. This study extracts and classifies the atmospheric trajectories for storms resulting in extreme rainfall across 42 cities in the UK. These classifications are then compared in terms of both magnitude, frequency, spatial dependency and their relation to the North Atlantic Oscillation.

2.3.4 Storm Track Extraction

Forty-two cities spread across the UK were selected as the initiation points for the identification of extreme rainfall events. The cities, as shown in Figure 2-13, were selected to cover all 10 hydroclimatic regions of Great Britain. For each city the daily annual maximum rainfall series (AMAX) was extracted from the CEH-GEAR dataset (Tan, Gan, and Chen 2018). This data consists of gridded daily and monthly rainfall estimates between 1890-2017. Extracting the AMAX series from each of the 42 cities between 1960-2014 resulted in a total of 2598 extreme rainfall events to be analysed.

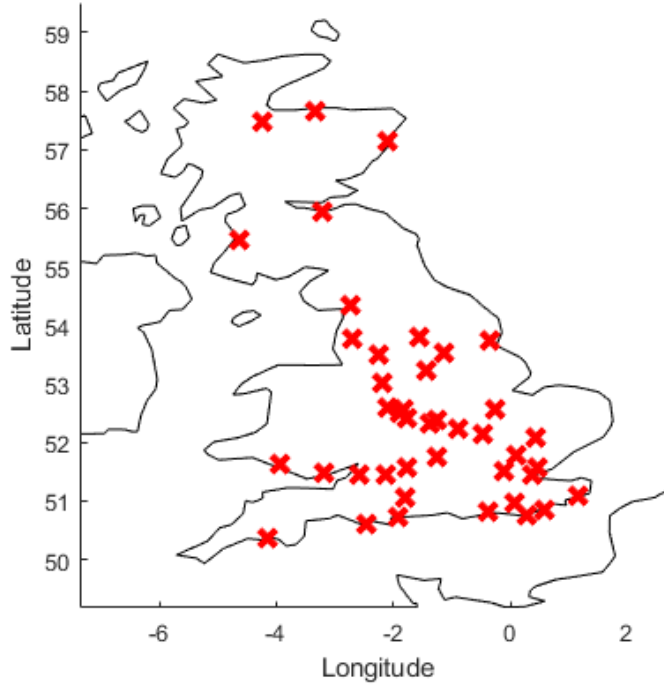


Figure 2-13: Location of 42 cities across the UK selected for this study.

Next, the AMAX series were normalised between 0 and 1 to remove the dependency of each series on the local geographical and climatological features. The normalisation equation used is as given in Eq. 2.2, where $AMAX_c$ is the series of annual maximums for city c and $NAMAX_c$ is the series of normalised annual maximums for city c

$$NAMAX_c = \frac{AMAX_c - \min(AMAX_c)}{\max(AMAX_c) - \min(AMAX_c)}, c = 1, \dots, 42 \quad (2.2)$$

and $c = 1, \dots, 42$ For each of the 2598 AMAX events, the relevant atmospheric trajectories are generated from a trajectory dispersion model called HYSPLIT (Draxler and Hess 1997) which requires an initial: longitude, latitude, altitude, extraction time, date and start time. The system also requires access to meteorological files covering the relevant dates. The extraction time indicates how many hours the model should trace the trajectory back through time from the starting location. A 48 hour extraction time and NCEP/NCAR reanalysis data (Kalnay et al. 1996) were used in this study. To generate these trajectories HYSPLIT uses a combined Lagrangian and Eulerian approach which allow the relative calculation of the advection, diffusion and particle concentrations (Draxler and Hess 1997; Draxler and Hess 1998; Stohl and James 2004).

To extract the trajectories for each of the 2598 extreme events the HYSPLIT model was initialised with two altitude starting points (500 and 1000m above sea level) and two start times per event-day (09:00 and 18:00). This resulted in 10,392 trajectories. All trajectories were standardised, thereby removing the dependency of the trajectory on the initiation point as shown in Eq. 2.3.

$$NT_n = T_n - T_0 \quad (2.3)$$

Each trajectory (T) consists of 49, 2×1 vectors representing the latitude and longitude of T at each timestep n . These points are normalised according to the trajectories initiation point T_0 to produce a new 49-point normalised trajectory (NT).

2.3.5 Pathway Classification

Three unsupervised classification methods are compared for their suitability. The three methods chosen were k-means, Self-organising maps (SOMs) and a hierarchical method using the Ward (D2) approach (Ward, 1963). For each of these methods a predetermined number of intended output classifications is required, to optimise each method a classification was carried out with a number of output classes ranging from 2 to 50. It was considered that a number of classifications beyond this point would become unwieldy for a qualitative analysis.

Next, to allow a comparison of the suitability of each method the Davies-Bouldin (Davies and Bouldin 1979) index is used to both optimise the number of clusters for each method and to compare the resulting optimum models. This index was used as it provides an accurate indicator of cluster similarity and distance (Halkidi, Batistakis, and Vazirgiannis 2001). An alternative to this is the Calinski-Harabasz (Caliński and Harabasz 1974) method. However this method performs better when clusters are well separated, an assumption which cannot be imposed on the trajectory data. The Davies-Bouldin index measures the average similarity between each cluster C_i where $i = 1, \dots, N$ and its most similar cluster C_j . The similarity measure R_{ij} as defined in Eq. 2.4, where S_i and S_j correspond to the cluster diameter (average distance of points to the cluster center), and M_{ij} is the distance between the centroid of cluster i and j .

$$R_{ij} = \frac{S_i + S_j}{M_{ij}} \quad (2.4)$$

Using this similarity measure the Davies-Bouldin index is then defined as below:

$$DB_{index} = \frac{1}{N} \sum_{i=1}^N \max(R_{ij} | i \neq j) \quad (2.5)$$

where N is the number of clusters present. As DB_{index} increases the similarity between clusters is increasing, hence a lower DB_{index} indicates better cluster separation. Figure 2-14 shows the resulting Davies-Bouldin indices and optimal number of clusters (optimal value of N) for each of the three methods selected. Each optimal N values identified are in the lower end of the possible values of N with $N = 4$ for SOMs, $N = 5$ for the linkage method and $N = 6$ for k-means. Consequently, it was decided to take a single classifier from each of the three methods using their optimal number of output classifications (clusters) namely SOM_4 , LNK_5 and KME_6 .

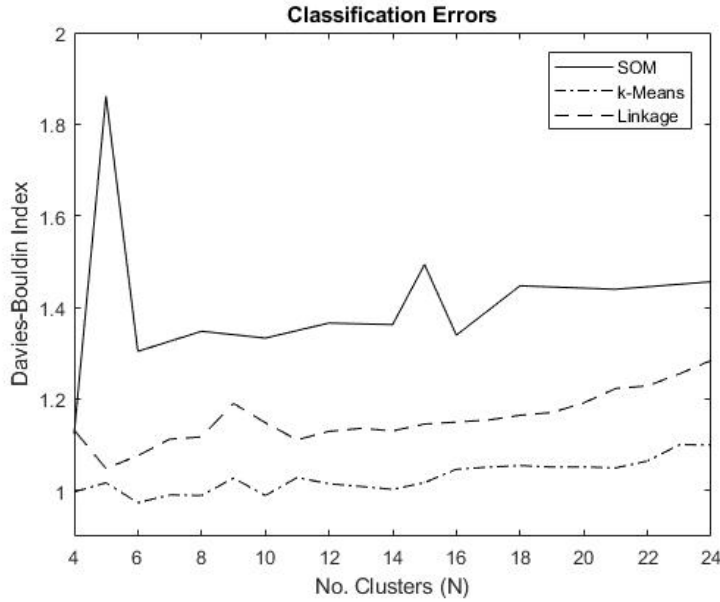


Figure 2-14: Davies-Bouldin Index for each of the three selected clustering methods with a varying number of initiation clusters. Lower values indicate better cluster separation.

2.3.6 Results

Storm types

A selection of extracted trajectories, including the centroid, is shown in Figure 2-15 for each classification as defined by the three optimal models. In addition Table 2.7 gives the proportion of the trajectories classified under each class. The proportions allocated

Classifier	Classification Proportions (%)					
	1	2	3	4	5	6
SOM_4	36.19	10.58	7.53	45.70		
LNK_5	8.36	27.36	19.65	10.76	33.87	
KME_6	13.92	25.63	9.19	12.60	24.71	13.95

Table 2.7: Proportion of trajectories classified under each classification per model.

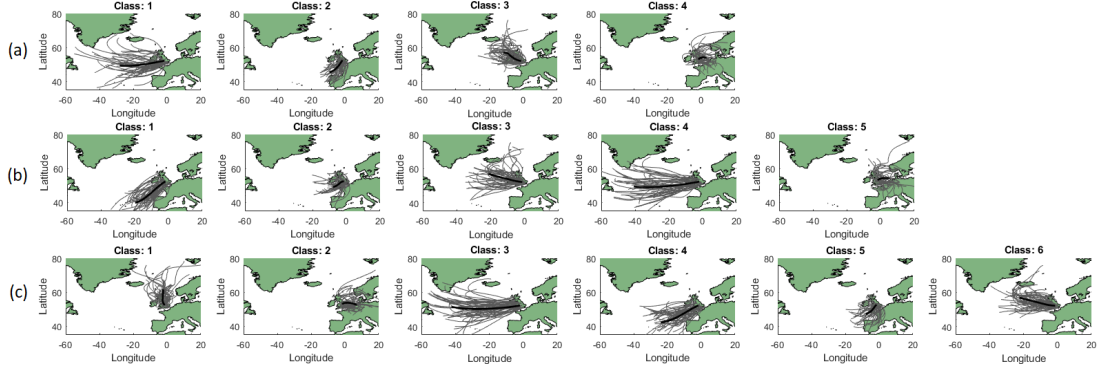


Figure 2-15: Examples of the trajectories classified under each class within the three classifiers used: SOM_4 (a), LNK_5 (b) and KME_6 (c) with the centroids shown in bold.

to each classification appear to get lower when moving from a model with only four output clusters (SOM_4) to one with six (KME_6). However, this is to be expected as more clusters allow further separation of similar trajectories.

The storms originating from the southern Atlantic, such as clusters 4 and 5 in the K-means model ($KME_6^{4,5}$), cluster 1 in the linkage model (LNK_5^1) and a small proportion of cluster 1 in the SOM model (SOM_4^1) tend to follow a similar trajectory to those of atmospheric rivers as identified by Lavers *et al.* (2011, 2012), and hence could potentially be attributed to the occurrence of such phenomena. Considering the proportions of $KME_6^{4,5}$ indicates that events caused by these atmospheric rivers could make up 37.31% of the extreme events. The second most frequent sub-set of trajectories originate from the North Sea where classes such as SOM_4^4 , LNK_5^5 and $KME_6^{1,2}$, contain 36.1%, 33.8% and 39.5% of all events. This further illustrates the reliance of extreme events on both the Atlantic and North Sea atmospheric processes. Comparing the length of the cluster centroids (as shown in bold in Figure 3) shows the Atlantic based storms namely $SOM_4^{1,2,3}$, $LNK_5^{1,2,3,4}$ and $KME_6^{3,4,5,6}$ travel a much longer distance than their North sea counterparts (SOM_4^4 , LNK_5^5 and $KME_6^{1,2}$). This suggests a stronger driving force moving the air parcels above the Atlantic Ocean at a much higher speed than those travelling from the North Sea.

Regional distribution of storm types

The spatial distribution of the classifications was considered using only KME_6 as these pathways are comparable to those in the other models, and this classifier had the lowest DB index as discussed earlier. Shown in Figure 2-16 a contrast between the eastern and western regions can be observed with regards to KME_6^2 (Fig. 3: Class 2) pathways, where the pathway leading from the North Sea westwards affect the eastern regions more than those in the west. For comparison, 42% of the trajectories ending in the North East of England belong to KME_6^2 where as only 16% of the trajectories leading to events in the North West belong to KME_6^2 . One cause of this pattern could be the existence of the Pennine Hills and the Peak District which prevent the storms from the east carrying moisture to the western side of Great Britain. Furthermore, the western regions have a larger portion of KME_6^4 type trajectories; specifically North West England, South West England and Wales have 21%, 19% and 24% of their samples classified as KME_6^4 . The East of England also shows a large proportion of KME_6^4 trajectories which total 15% in the region. This further highlights the importance of the geography of Great Britain, as these storms are unable to penetrate the elevated terrain of the Pennines and the peak district as often as they are able to make it across the mostly flat regions in the south. Finally, the most frequent pathway resulting in extreme events in Wales appears to come from the South Atlantic (KME_6^4). A similar trend is seen in South West England which corresponds to findings by Svensson and Jones (2004) who identified north-easterly moving storm tracks to have an association with high-river flows in these areas.

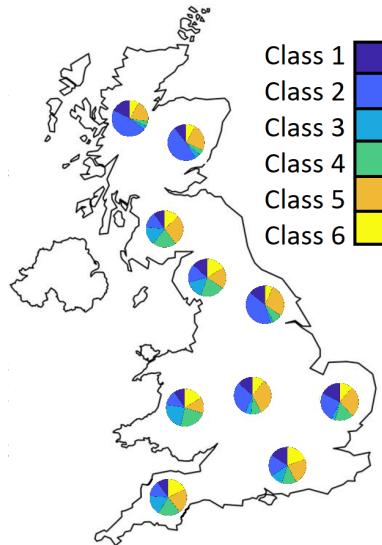


Figure 2-16: Proportion of each KME_6 storm classification per hydroclimatic region.

Classifier	Classifications					
	1	2	3	4	5	6
SOM_4	29.9	31.9	38.8	46.8		
LNK_5	30.0	42.3	33.2	30.1	46.2	
KME_6	47.1	47.6	30.1	38.3	41.1	30.9

Table 2.8: Percentage of events in each classification with a magnitude > 1 .

Magnitude of classifications

Next, the proportion of above average extremes was investigated for each of the classes in KME_6 . Table 2.8 shows for each class the proportion of events with a magnitude greater than the normalised mean of 1 (normalised according to Eq. 2.2). The classes identified as originating from the North Sea (SOM_4 , LNK_5 and $KME_6^{1,2}$) all contain the highest proportion of above-mean events where as those from the deep-west Atlantic (SOM_4 , LNK_5 and KME_6^3) have the lowest proportions. Regional difference in these magnitude variations are also matched within each region with a few key differences, 61.3% of KME_6^2 trajectories cause above average extremes in Wales where as these types only cause 38% of above average extremes in South West England.

Links to the NAO

By performing a linear regression between the magnitude of the trajectories in each classification and their relevant NAO indices we have found no significant correlation between these two variables. However, Figure 2-17 shows the empirical cumulative distribution function (CDF) of events for each classification given the NAO indices of each.

These results show KME_6^3 has the highest proportion of events falling within a positive NAO phase totalling 67% followed by KME_6^6 at 59%. This indicates events caused by pathways leading from the deep-west and North Atlantic become more frequent during a positive NAO phase. Furthermore, during the negative NAO phase it is the KME_6^2 and KME_6^5 pathways which are the most prominent with 63% and 60% of their respective trajectories falling during this negative phase. On visual inspection it appears pathways in KME_6^2 , 5 originate from close to the British Isles and form circular patterns which could indicate the existence of cyclonic activity in the south. Finally, inspecting the empirical CDF pattern of pathway KME_6^3 it appears to spike in frequency during an NAO index of 0 and 1 which could also indicate the triggering of an atmospheric event at these levels.

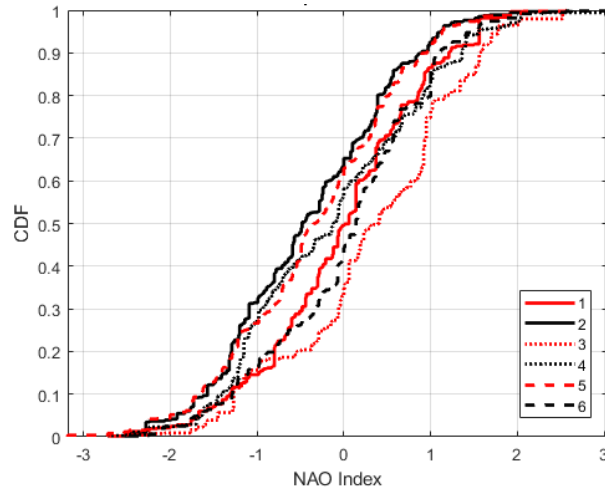


Figure 2-17: Empirical cumulative distribution function for the frequency of each trajectories within each classification for a given NAO index.

2.3.7 Conclusions

This study has developed a new framework for identifying the key-moisture pathways leading to extreme rainfall events in Great Britain through the classification of the trajectories of the storms prior to the occurrence of extreme rainfall events. This is accomplished through the optimisation of three unsupervised classification methods using the Davies-Bouldin index to select an optimal number of output nodes and analysing the resulting trajectory classes. The key findings were as follows:

1. Atlantic and North Sea storms form two subsets of the resulting classifications from all three models with 60.58% of the trajectories in the k-means classifier (KME_6) belonging to the Atlantic pathways and 39.42% originating from the North Sea.
2. Classes in each of the three models match the pathways of atmospheric rivers, a known cause of high levels of rainfall in Great Britain (Lavers *et al.*, 2011, 2012).
3. The North Sea storms cause a higher proportion of events across the eastern regions of Great Britain where as the South Atlantic storms are more commonly associated with those across the west.
4. Westerly storms from the North Sea is the most likely pathway to cause above average extreme events in Wales in comparison with the other surrounding regions.

5. A comparison of the magnitude of events in each class and the North Atlantic Oscillation showed no significant relationship between these two variables.
6. The frequency of storm originating from the North and West Atlantic increases with a positive NAO index whereas short storms originating near the British Isles become more frequent with a negative NAO phase.

These results highlight the importance atmospheric pathways have on the temporal and spatial distribution of extreme rainfall events across Great Britain. The resulting classifications presented spatial and magnitude difference across all ten hydroclimatic regions but have also opened new questions regarding the atmospheric processes which lead to these events via the pathways identified.

2.4 Postscript

This chapter presented two studies which characterise heavy rainfall events using their preceding atmospheric trajectories in response to hypothesis **Hypothesis 1**. Firstly, a methodological advance was made through the application of self-organising maps using a case-study in Northern Spain. Following this, the self-organising maps method was applied in Great Britain and compared to traditional clustering methods. In both cases the frequency and magnitude of extreme events in each of the resulting clusters were compared and contrasted.

The results presented indicate that although the self-organising maps clustering method was able to produce a selection of trajectory clusters it did not perform as well as traditional clustering methods. However, as shown in both studies all of the applied clustering methods were capable of providing a set of trajectory clusters which indicate causality for some seasonal extreme rainfall events. For example, in section 2.2 models for summer and winter extreme events present significantly different trajectory shapes with summer consisting of localised, slow moving convective systems where as the winter events consist mostly of long, fast moving trajectories generally originating from the Atlantic.

Both studies show minor differences in the magnitude or frequency distributions of the trajectory clusters which indicates an important variable relating to extreme rainfall events is either being abstracted during trajectory generation or is not included. The primary variables in the generation of the trajectories are pressure, wind speed and temperature (NOAA 2003); recent work has indicated the substantial effect mean sea-level pressure has on both the distribution of rainfall events (Ummenhofer et al. 2017; Baker, Shaffrey, and Scaife 2018; Richardson, Fowler, Kilsby, and Neal 2018 and extreme rainfall events (Richardson, Fowler, Kilsby, Neal, and Dankers 2020; Champion, Blenkinsop, et al. 2019; Allan, Blenkinsop, et al. 2020).

This has opened new avenues of questioning regarding the interplay between the studied mean sea-level pressure variations and those of temperature which has also shown to influence rainfall magnitudes (Blenkinsop et al. 2015) and is addressed in the next chapter, addressing hypothesis **Hypothesis 2**. Further to this, while the sensitivity of the results to the selection of the number of clusters is partially investigated in this chapter several sensitivity questions remain. For example, the sensitivity of the evaluation to the metrics chosen, how sensitive the results are to the length of the trajectories used and finally, how well do these moisture pathways map to measurable impact?

Chapter 3


North Atlantic air pressure and temperature conditions associated with heavy rainfall in Great Britain

3.1 Preamble

In the previous chapter extreme rainfall events were clustered using their preceding atmospheric trajectories. The findings indicated that the abstraction of preceding atmospheric conditions into atmospheric trajectories removes the sensitivity of the heavy rainfall events on low priority variables such as air temperature. The present chapter addresses the sensitivity of heavy rainfall events to the covariance of air temperature and sea level pressure. This assesses hypothesis **Hypothesis 2** using a study produced in collaboration with the UK Centre of Ecology and Hydrology, which is currently under review for the International Journal of Climatology.

The study presented in this chapter considers the covariance between mean sea-level pressure and 2m air temperature with respect to extreme rainfall events in Great Britain. To do this, previous extreme rainfall events are identified and their respective concurrent mean sea-level pressure and 2m air temperature images are extracted. The events are then clustered seasonally using the combined mean sea-level pressure and 2m air temperature images resulting in a set of weather patterns each represented by a mean sea-level pressure and 2m air temperature image (**Objective 2.1**). The resulting clusters are then compared and contrasted using their relative spatial and temporal distributions considering the effect of the large-scale atmospheric indices which were found to have influence in the previous chapter (**Objective 2.3**). The covariance of the mean-sea level pressure and 2m air temperature images is then analysed along with the relative relationships with large-scale climatic indices (**Objective 2.2**).

3.1.1 Authorship Statement

Status	Conditionally accepted in the International Journal of Climatology.
Details	Barnes, A.P., Svensson, C., Kjeldsen, T.R. (in review) International Journal of Climatology. 2021.
Authors' contribution	<p>The author of this thesis has primarily (90%) contributed to design and implementation the methodology adopted for the extraction, clustering and analysis of both the atmospheric and rainfall data. Each author's exact contributions are as follows:</p> <p>A.P. Barnes: Formulation of ideas (85%), design of methodology (95%), data collection (100%), processing and analysis of data (95%), manuscript preparation (85%).</p> <p>C. Svensson: Formulation of ideas (10%), design of methodology (5%), processing and analysis of data (5%) manuscript preparation (10%).</p> <p>T.R. Kjeldsen: Formulation of ideas (5%), manuscript preparation (5%)</p>
Date and Signature	 19-07-2021

3.1.2 Abstract

Severe flooding in the United Kingdom is often linked to the occurrence of heavy rainfall events, which can be characterized by the synoptic scale meteorological conditions over the North Atlantic region. Seasonal heavy rainfall events (summer and winter 1-day maxima) were extracted from 125 locations across Great Britain over the period 1950-2017. For each event, anomaly sea-level pressure and 2m air temperature conditions across the North Atlantic sector were extracted from the NCEP/NCAR Reanalysis dataset. In contrast to earlier studies these two datasets were combined, and clustered to identify how the pressure and temperature conditions co-vary within each half-year to produce heavy rainfall events. Distinctly different spatial patterns were found for four classes in summer and for three classes in winter. The frequency of occurrence for two summer and one winter class show opposing correlations with the North Atlantic Oscillation index (Summer class 1: $r=-0.29$; summer class 3: $r=0.44$, winter class 1: $r=0.35$) and the Atlantic Multidecadal Oscillation (Summer class 1: $r=0.37$; summer class 3: $r=-0.54$, winter class 1: $r=-0.39$), significant at the 1% level. The classes are associated with distinctly different geographical distributions of heavy rainfall events across Great Britain, and their association with large-scale circulation and temperature drivers can find application in, for example, weather generators.

3.2 Introduction

The impacts of extreme weather across the UK continue to have severe economic and environmental consequences. The cost of flood damage, often a result of heavy rainfall, is expected to increase significantly in the future, unless an average annual investment of £1 bn is made (with a benefit to cost ratio of 9:1) to protect properties and infrastructure in England up to 2065 (Environment Agency 2019). The danger to life can be shown by, for example, storms Dennis and Ciara which hit the UK during February of 2020 and resulted in at least 5 fatalities and more than £300mil in damages (Emerton 2020). Considering the risk to life and property, there is an inherent reason to try to better understand the synoptic-scale mechanisms behind heavy rainfall. However, with the climate also expected to change in future, and current climate models being better at predicting large-scale circulation patterns rather than heavy rainfall magnitudes, these patterns of large-scale forcings have received renewed attention as a research topic. Specifically, the aim of this study is to identify the key types of synoptic-scale meteorological patterns which cause heavy rainfall events in the UK.

Taylor and Yates (1967) reviewed several weather and climate classification schemes based on the atmospheric pressure pattern in the region around the UK. They found that the existing procedures were rather arbitrary and the methods almost indistinguishable from each other. Currently, the most popular weather typology, by Lamb (1972), consists of manually classified weather records from 1861 to 1971 based on their airflow patterns. Although Lamb’s types contain 27 categories in total, the bulk of the records belong to one of seven main types of air flow classification: cyclonic, anticyclonic, northerly, easterly, westerly, north westerly and southerly (Lamb 1965; Lamb 1972). Originally these weather types were determined subjectively until Jenkinson and Collison (1977) turned this into an objective classification scheme by using mean daily grid-point sea-level pressure. More recently, researchers have extended the area of influence and/or used objective methods for classification to try to capture the synoptic scale processes which create weather events in the UK. For example, Fereday et al. (2008) use k-means clustering of sea level pressures (SLP) over the North Atlantic to identify the SLP profiles for a set of 6 two-month seasons. However, they were unable to identify any common circulation types. Neal et al. (2016) identified eight distinct weather patterns which were reduced from an original set of 30 classes through clustering on the anomaly sea-level pressure patterns. Richardson et al. (2017) compared the precipitation of events classified in each of the classes generated by Neal et al. (2016) and found the reduced set of eight classes to show very high intra-class precipitation variability. It may be that including information also of moisture availability could

make for a more distinct classification scheme.

In a recent review, Gimeno et al. (2020) highlights that the key sources of European moisture come from the North Atlantic through either atmospheric rivers or cyclonic activity. Lavers et al. (2011) first identified atmospheric rivers by investigating the source regions of the atmospheric moisture feeding heavy rainfalls in the UK. Lavers et al. (2011) found that all ten of the largest floods in the UK co-occurred with an atmospheric river. These atmospheric rivers are long plumes of high-concentrations of water vapour in the atmosphere which originate from the tropics, moving northwards into the mid-latitudes. However, the concept and definition of an atmospheric river still does not provide clear evidence of the synoptic scale driving process, and further to this these events generally only occur during the winter half year (Allan, Liu, et al. 2014) hence do not explain summer extremes.

Allan et al. (2019) investigated synoptic precursors of extreme short-duration (3-hour) summer rainfall events in the UK, including dew point temperature, evaporation, geopotential height at 200hPa and sea-level pressure (SLP) anomalies, geopotential height anomalies, average moisture and evaporation patterns over northwest Europe and the North Atlantic. Their results reveal different conditions associated with intense rainfall events in different parts of the country. For example, intense rainfall events in both the South East of England and western Scotland coincide with negative SLP anomalies in the eastern Atlantic on the day prior to the event. However, for intense rainfall events in the South East of England the centre of this negative SLP anomaly is further south than for events in western Scotland. Their results highlight not only the regional homogeneity of extreme events (e.g. Champion, Blenkinsop, et al. 2019; Svensson and Hannaford 2019) in the UK but also their association with particular synoptic scale atmospheric patterns. Similarly, Ummenhofer et al. (2017) clustered SLP and precipitation patterns over Europe and identified a similar northwest and southeast regional disparity across the British Isles.

Alternative methods for investigating moisture sources have included using small-scale air parcel tracking to generalize the key moisture pathways leading to extreme events (Barnes, McCullen, and Kjeldsen 2019; Barnes, Santos, et al. 2020; Santos et al. 2018; Tan, Gan, and Chen 2018). These methods provide only the general movement of moisture in the atmosphere, but Barnes et al. (2019b) identified six distinct groups of moisture pathways leading to events in the UK. The key differences between the pathways were length and direction of travel, but the results also showed that the distributions of rainfall intensity varied between groups, and spatially across the country.

Several studies have found that temperature and circulation pattern influence rainfall magnitude. For example, for southern Italy Greco et al. (2020) highlight the importance of low-level (850hPa) temperature for the development of precipitation from convective systems while synoptic system precipitation depend on the pressure pattern. For the UK Blenkinsop et al. (2015) also found a positive relationship between precipitation and (local land surface) temperature during summer, but note that such relationships were weaker in the remaining seasons. Trambly et al. (2013) built a rainfall frequency model for southern France using temperature and pressure patterns as co-variates for the model parameters.

The present study investigates the combined effects of synoptic 2m air temperature and sea level pressure patterns in the North Atlantic region on heavy rainfall occurrence across Great Britain. Temperature is used instead of moisture, as initial investigations suggested a strong relationship between the two over the ocean. By using such a proxy, both moisture over the ocean as well as temperature over the land can be captured by a single variable, which simplifies our large-scale analysis. We use a technique to simultaneously cluster both 2m air temperature and sea level pressure patterns across the North Atlantic sector during heavy rainfall events. As far as the authors are aware, this combined clustering expands on all earlier weather typing studies for the area. The clustering results in a range of combined synoptic patterns, instead of a single composite pattern for each driver separately as in, for example, the detailed sub-daily summer rainfall studies of Allan et al. (2019) and Champion et al. (2019). Further, we investigate winter as well as summer, but look at the coarser resolution of 1-day rather than 3-h rainfall events. An advantage of using daily rather than sub-daily rainfall data is the higher confidence in the data quality. In contrast to e.g. Ummenhofer et al. (2017), the synoptic patterns are used to identify differences in geographical extreme rainfall distribution, as opposed to including the spatial rainfall pattern as part of the clustering. The average wind speeds/directions and 500hPa geopotential height pattern for each class are also investigated. Finally, the present study relates the synoptic patterns to time and climatic indices such as the North Atlantic Oscillation (NAO) and the Atlantic Multidecadal Oscillation (AMO), to investigate how long-term oscillations may influence what synoptic temperature and pressure patterns cause heavy rainfalls in different parts of Great Britain.

3.3 Data

Two types of data were used in this study: (1) individual time series of seasonal (half-year) maximum 1-day rainfalls at 125 locations in Great Britain, and (2) large-scale

gridded daily values of sea level pressure and air temperature data over the North Atlantic sector.

3.3.1 Historical Heavy Rainfall Events

Time series of heavy rainfall were extracted at 125 locations as shown in Figure 3-1, chosen at equal 0.5° latitude and longitude spacing, this equates to $\approx 35km$ dependent on latitude/longitude. This equates to 35km, depending on latitude. Although gridded rainfalls are likely to lose some variability compared with using station observations, they enable us to extract rainfalls on an even grid across Great Britain. Seasonal maximum daily rainfall (SMAX) series for both summer (May-Oct) and winter (Nov-Apr) seasons were retrieved for each location from the CEH-GEAR (Centre of Ecology and Hydrology - Gridded Estimates of Areal Rainfall) (Keller et al. 2015) dataset for the years 1950 up to and including 2017. The CEH-GEAR data uses a nearest neighbour interpolation method on observed precipitation data from the Met Office, to create a $1km \times 1km$ cell grid of daily (09:00 UTC to 09:00 UTC) total precipitation across the United Kingdom. This grid is then normalized using average annual rainfall and subsequently adjusted by monthly rainfall averages as described by Keller et al. (2015).

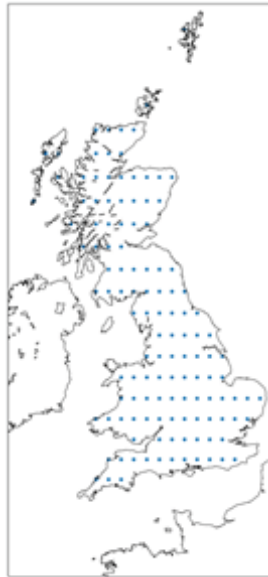


Figure 3-1: The 125 locations in Great Britain at which series of seasonal rainfall maxima are extracted.

Combining the seasonal maximum series results in a total of (68 years * 125 locations=) 8500 seasonal heavy rainfall events. The first winter of the study period is only 4-

months long (Jan-Apr), and Nov-Dec 2017 is not included in the analysis. Of the 8500 summer heavy events there are 2282 unique dates on which they occur. Similarly, for the 8500 winter heavy events there are 2010 unique dates. This is expected as locations within the same hydrometeorological region are influenced by the same atmospheric circumstances (Champion, Blenkinsop, et al. 2019; Keef, Svensson, and Tawn 2009) and therefore spatial dependence will lead to a level of co-occurrence on the same day. The rest of the analysis is carried out using the series of unique dates, to ensure that a single widespread event does not disproportionately influence the results.

3.3.2 Meteorological Data

Daily (00:00 UTC to 00:00 UTC) mean sea level pressure (SLP) and 2m air temperature (AT) data were extracted from the 2.5° gridded NCEP/NCAR Reanalysis 1 dataset (<https://psl.noaa.gov/data/gridded/data.ncep.reanalysis.html>) (Kalnay et al. 1996). This means the daily meteorological data precede the rainfall days by several hours, but we consider the data sufficiently overlapping for our purpose. The study area is limited to the region defined by 10 – 70°N and -100 – 20°E, which covers the North Atlantic sector and part of the neighbouring land areas (see e.g. Figures 2 and 3). We chose to include Greenland and part of North America to see if the temperature patterns within the polar regions influenced the resulting winter classes. Similarly, we included part of North Africa to see if the temperature there would result in a separate summer cluster for a Spanish Plume mechanism. This means our study region is slightly larger than the one considered by, for example, Allan et al. (2019).

For each heavy rainfall date a SLP and AT pattern were generated, each with a resolution of 48x24 grid cells. Following this, each cell’s daily value was then standardized by subtracting the monthly mean and subsequently dividing by the standard deviation of that cell’s SLP or AT, respectively, with the mean and standard deviation calculated over all the daily values in all years for the calendar month in which the event occurred. Identical fields were extracted from the NCEP/NCAR Reanalysis 1 dataset also for wind components and 500hPa geopotential heights, which were used to help with the interpretation of the resulting SLP and AT patterns.

To enable comparisons with larger scale climatic oscillations, the North-Atlantic Oscillation (NAO) (NOAA National Weather Service, 2005) and Atlantic Multi-decadal Oscillation (AMO) (Enfield, Mestas-Nuñez, and Trimble 2001) indices are extracted seasonally for both summer and winter, 1950-2017. The NAO provided by NOAA (<https://www.cpc.ncep.noaa.gov/products/precip/CWlink/pna/nao.shtml>) is generated using a rotated principal components analysis as described by Barnston and Livezey

(1987), which allows the location of the pressure centres to differ slightly from one season to another. The AMO, which is also provided by NOAA (<https://psl.noaa.gov/data/timeseries/AMO/>), is calculated using the weighted average over the North Atlantic sea-surface temperature of the Kaplan SST V2 dataset (https://psl.noaa.gov/data/gridded/data.kaplan_sst.html) (Kaplan et al. 1998).

3.4 Meteorological Clustering

Clustering on a combination of the anomaly SLP and AT patterns is conducted to identify a set of distinct meteorological conditions associated with seasonal heavy rainfall events.

3.4.1 Feature Set Pre-Processing

For each unique heavy rainfall day extracted from the CEH-GEAR dataset, a single data array is generated by flattening and concatenating the anomaly SLP and AT matrix for that date. Each pixel in the meteorological dataset have a size of $2.5^\circ \times 2.5^\circ$, equating to an image of size 24 by 48 = 1152 individual pixels. Because there are two meteorological images, this results in each heavy rainfall day being represented by a single vector of size $(2 \times 1152 =)$ 2304, referred to as the event's feature vector. An illustration of this procedure is shown in Figure 3-2, and an example is given for flattening in equation (3.1) and combination in equation (3.2).

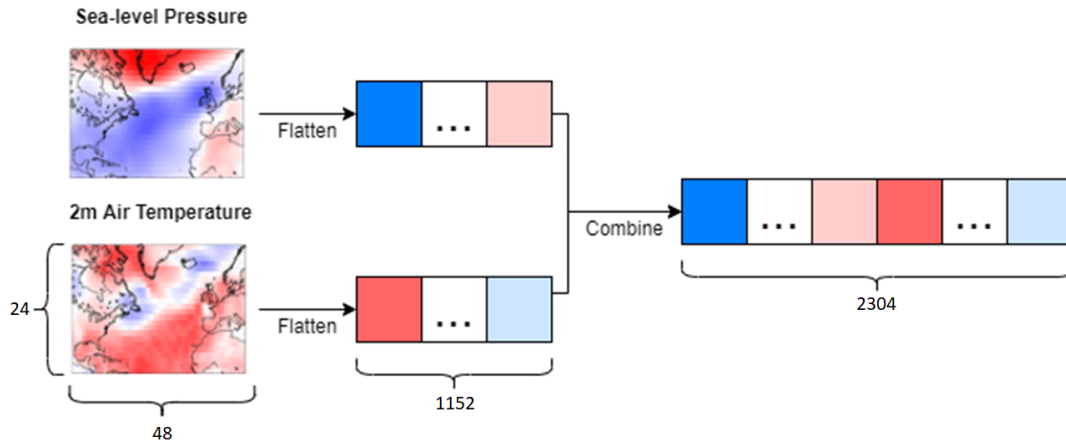


Figure 3-2: Example of feature set generation for a given heavy rainfall event. This procedure takes the SLP and AT patterns, flattens them into a single dimensional array and finally concatenates them into a final single dimensional array.

$$\text{Flatten} \left(\begin{pmatrix} x_{1,1} & \cdots & x_{i,1} \\ \vdots & x_{i,j} & \vdots \\ x_{1,j} & \cdots & x_{48,24} \end{pmatrix} \right) = [x_{1,1}, \cdots, x_{48,1}, \cdots, x_{i,j}, \cdots, x_{1,24}, \cdots, x_{48,24}] \quad (3.1)$$

$$\begin{aligned} \text{Combine}([x_1, \cdots, x_m, \cdots, x_{1152}], [y_1, \cdots, y_n, \cdots, y_{1152}]) \\ = [x_1, \cdots, x_m, \cdots, x_{1152}, y_1, \cdots, y_n, \cdots, y_{1152}] \end{aligned} \quad (3.2)$$

Combining the event feature vectors, separately for each season, results in two two-dimensional matrices where each row represents the date of a heavy rainfall event in the given season. These matrices are referred to as the training sets. The dimensions of the training set matrices are $[N \times 2304]$ where 2304 is the number of elements present in each heavy rainfall event feature set and N is the number of unique heavy rainfall days in the given season.

3.4.2 Pattern Clustering

The procedure used to class the feature sets defined in section 3.1 is k-means (Lloyd 1982) which requires a set number of output classes (k) to be pre-specified. Class models were generated for both summer and winter with k ranging from 2 to 15 which are limits based on the number of classes used by Neal et al. (2010) to allow for differences in the data. However, Richardson et al. (2017) show that only about four of Neal et al. (2016)'s 30 patterns relate to heavy rainfall events, which indicates that this may be a suitable number to consider. We found that scree plots of root-mean squared error (RMSE) versus number of clusters were not helpful for cluster selection in our case (not shown). As expected the RMSE drops with increasing number of clusters, but there is no clear break point, possibly because using the distance metrics on such high-dimensional data produce results which are often noisy (Aggarwal, Hinneburg, and Keim 2001). Instead we subjectively selected 3 classes for winter and 4 classes for summer.

3.4.3 Statistical Analysis

We used correlation analysis to explore if the frequency of occurrence of the identified classes is related to the NAO and AMO climate indices. For this, we used seasonally

averaged indices of the NAO and AMO, and seasonal counts of the number of events in each class. Before the correlation analysis was undertaken, each series was detrended. That is, the correlation analysis was undertaken on the residuals from linear regressions of each variable separately on time. Significance levels were estimated using a two-sided Student's t-test.

3.5 Results

This section presents the results of the class analysis of the daily anomaly sea-level pressure and 2m air temperatures across the North Atlantic sector, for the dates which coincide with heavy rainfall events in Great Britain. Presented below are the mean anomaly sea-level pressures and 2m air temperatures for each cluster, shown separately for summer and winter. The average wind speeds/directions and 500hPa geopotential height pattern for each class are also discussed. The relationship between the frequency of occurrence of the events in each class and indices of the NAO, AMO and time are then investigated. Finally, the classes are compared for their spatial distribution of the heavy rainfall events across Great Britain.

3.5.1 Summer Classes

Meteorological Conditions

Figure 3-3 shows both the anomaly and raw SLP patterns for the four summer classes generated using k-means. Each class is represented by the mean of all patterns which are classified under the respective cluster. Common across all four classes is an area of low pressure anomaly centred on, or to the north of, the British Isles. In addition, Classes 1, 2 and 4 share a dominant high SLP anomaly through Greenland and the Norwegian sea, with Classes 1 and 4 also showing a low SLP anomaly from the subtropical North Atlantic to northwest Europe. In contrast, Classes 2 and 3 present a dominant high SLP anomaly pattern across the sub-tropical Atlantic. Classes 1 and 3 largely reflect the expected anomaly patterns of the negative and positive phases of the summer NAO, respectively, with one anomaly centre over Iceland and another to the southeast over the North Atlantic/Europe (Figure 3a). Compared with the north-south gradient of the winter NAO (e.g. Jones, Jonsson, and Wheeler 1997), the gradients of Classes 1 and 3 are slightly rotated counter-clockwise, which is typical of the summer NAO as described by e.g. Folland et al. (2009). The two classes for which an NAO interpretation is less obvious (Classes 2 and 4), seem to be associated with a northward extension of the positive anomalies of the subtropical high pressure. This is shown as a north-south

band of high SLP anomalies in the mid-Atlantic in Figure 3-3a.

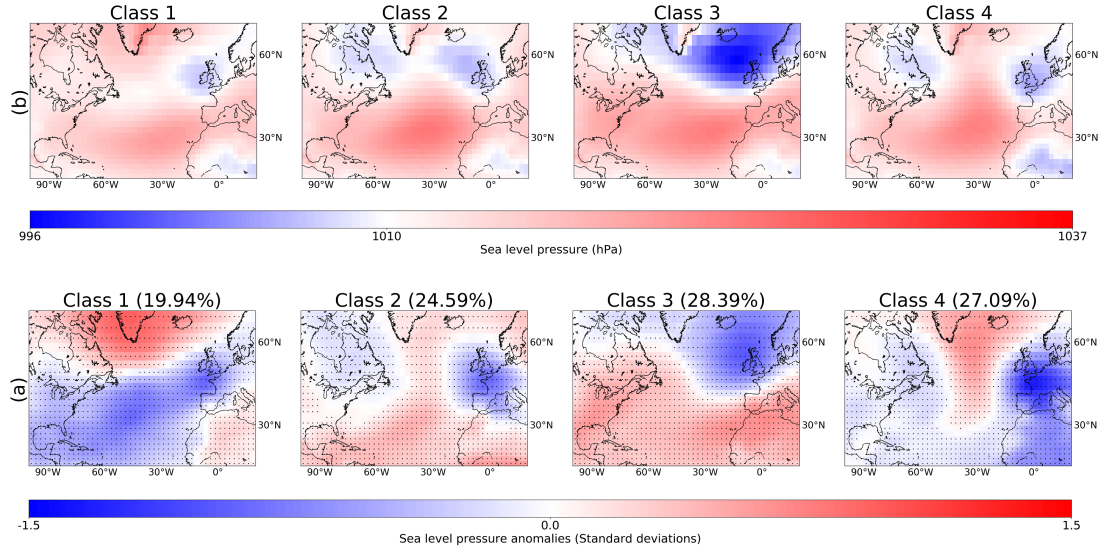


Figure 3-3: Sea level pressure patterns for the four summer classes, showing both the anomaly SLP (a) and raw SLP (b) patterns. The percentages indicate the proportion of events in each class, and the dots provided in (a) denote anomalies significant at the 2% level based on a two-sided Student's t-test.

Considering the 2m air temperature anomalies as shown in Figure 3-4, the classes can be split into anomalously warm and cool patterns with Classes 1 and 2 presenting a generally warm North Atlantic region and Classes 3 and 4 showing a predominantly cool pattern. Common to all four classes is that there is an area of cold anomalies to the west or northwest of the UK, which contrasts with a warmer anomaly to the southeast. This could signify the temperature contrast over a cold front, which would typically result in heavy rainfall as it passes eastwards across the UK.

The average wind vectors (superimposed in Figure 3-4) of the relevant classes show the presence of cyclonic activity near the British Isles, along with the indication of anti-cyclonic activity in the subtropical North Atlantic. The winds associated with the northward extended subtropical high pressure for Classes 2 and 4 presumably contributes to the development of the warm (cold) anomaly in the west (east) mid-latitude Atlantic. The direction of flow for the low temperature zones to the west and/or northwest of the British Isles has a northerly component for all four classes and is sometimes directed towards the British Isles.

The 500hPa geopotential height fields shown in Figure 3-5 indicate the directions of the paths travelled by the mid-latitude cyclones that cause the heavy rainfall events, even

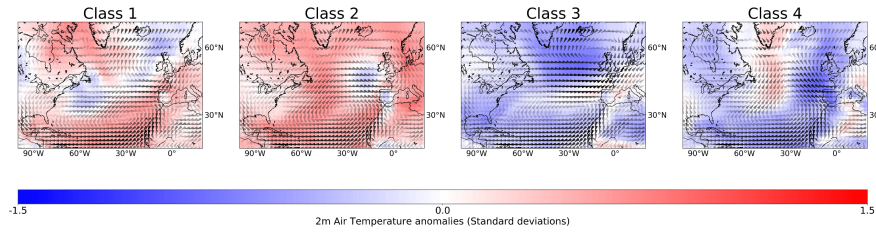


Figure 3-4: Sea-level wind speeds for summer classes. The sea-level wind speeds are overlaid on the anomaly temperature patterns for each of the four summer classes, and the opacity illustrates the strength of wind between 2 and 8 m/s. Anomaly 2m air temperature patterns are shown without wind speeds, but with points denoting significance, in supplementary information S1.

though they do not show the exact location of the jet stream. Cyclones are steered by the airflow aloft, which is parallel to the isolines of the geopotential heights. The strong north-south contrast and zonal pattern for Class 3 suggest storms are fast-moving on a straight, westerly track across the Atlantic, turning northeastward in the vicinity of the UK. Classes 2 and 4 suggest strongly meandering storm tracks (as also suggested by the northward extension of the subtropical high pressure in Figure 3-3), whereas Class 1 storm tracks seem more weakly meandering.

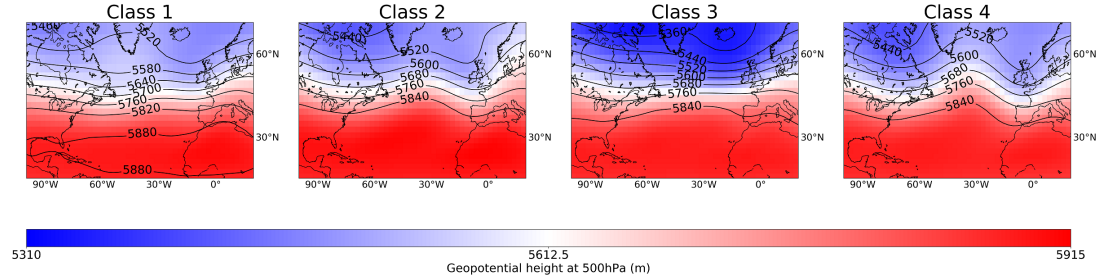


Figure 3-5: 500hPa Geopotential Heights for each summer class.

Class Variability

The top row of Figure 3-6 shows how the frequency of occurrence of the events in each summer class varies with time, while the lower two rows show how the detrended frequencies of occurrence vary with the detrended indices of the NAO and AMO. The frequencies of Classes 1 and 2 both increase with time, whereas the frequency of Class 4 decreases and Class 3 shows no temporal trend.

The events in Class 3, whose pressure pattern resembles the positive phase of the sum-

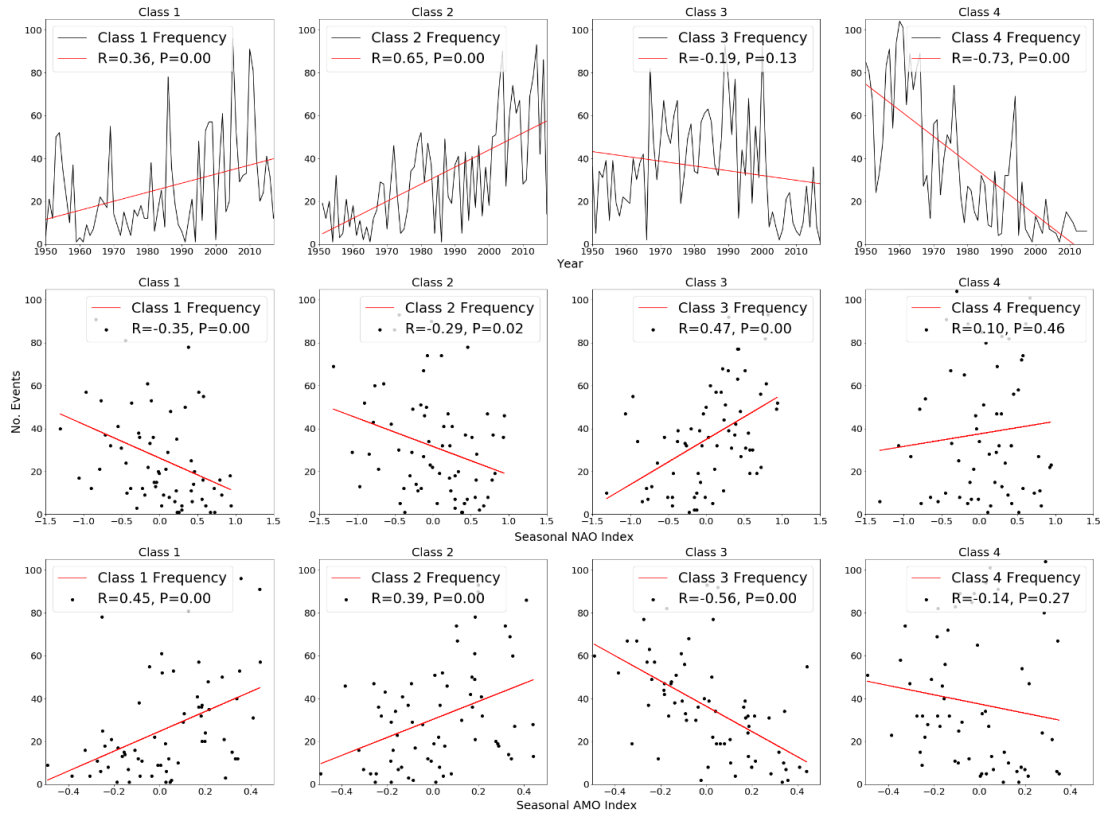


Figure 3-6: Seasonal frequency of occurrence of heavy rainfall events in the four summer classes as function of time (top row), and detrended seasonal frequencies as a function of detrended NAO index (middle row) and AMO index (bottom row). The figure also shows the correlation coefficient, R , and the significance level (P).

mer NAO, show directly opposite relationships with the NAO and the AMO to those of Class 1. This suggests that heavy rainfalls associated with the positive (negative) phase of the NAO is exacerbated by cold (warm) temperatures in the North Atlantic. A possible explanation for this would be the different tracks that storms associated with the positive and negative phases of the NAO track along, and the development of different rainfall-exacerbating sea surface temperature anomalies in the vicinity of Britain. The sea surface temperature anomaly will in turn modify the temperature of the overlying airmass.

The location of the low pressure centre for Class 3 in Figure 3-3 suggests a more northward location of storms for the positive NAO Class 3 than for the negative NAO Class 1. Cyclones tracking eastward to the north of Scotland will drive cold waters behind themselves towards Britain (and warmer waters ahead of themselves northward, where they will not affect Britain), and the aggregated action of a succession of cyclones

following a similar path may exacerbate a developing sea surface temperature anomaly. Hence, when the Atlantic is anomalously cold and the NAO is positive, the cold anomaly to the northwest of Britain will be exacerbated, and this will also be reflected in the air temperature anomaly.

In contrast, storms tracking along a path further to the south will drive warm surface waters ahead of themselves towards Britain, while a cold sea surface anomaly will be generated behind the low-pressure centres. Therefore, when the Atlantic is anomalously warm and the NAO is in its negative phase, the warm anomaly to the south of Britain will be exacerbated. There is some support for this in Figure 3-7, when contrasting the temporal evolution of the temperature anomaly patterns for Class 1 (negative NAO) with those for Class 3 (positive NAO). For Class 1, and to some extent also for Class 2, the warm anomaly off North Africa and western Europe intensifies and moves northward towards Britain in the days prior to the heavy rainfall event occurring, while a weak cold anomaly forms to the northwest, behind the cyclone. However, for Class 3 the cold anomaly that develops to the northwest of Britain is more intense than the anomaly over and around Britain. In this case the cold anomalies west of North Africa and western Europe seem to be unchanging in the days prior to the heavy rainfall. Supplementary information S3 shows the corresponding development of sea level pressure anomalies in the days prior to the heavy rainfall event.

Both Classes 2 and 4 seem to be associated with a northward extension of the subtropical high pressure in the North Atlantic (Figure 3-3), and the 500hPa geopotential height patterns in Figure 5 support the suggestion of highly meandering storm tracks. Cyclones following such paths are likely to be slow-moving, which enables the accumulation of very large rainfall amounts. Figure 8 suggests that storms in these two classes result in heavy rainfall mainly in the south and east of Britain, which is consistent with cyclones tracking across southern Britain. Mesoscale convective systems, such as associated with the Spanish Plume (e.g. Lewis and Gray 2010), mainly occur in southern Britain. However, although some classes have a warmer average temperature anomaly in western Europe and/or North Africa than others, the rarity of these events make it difficult to link them to any particular class.

The geographical distribution of heavy rainfall events associated with Class 3, whose spatial SLP pattern reflects the positive NAO, is concentrated to the north and west of the country (Figure 3-5). Here, heavy rain is likely produced along the fronts of cyclones travelling eastward, or northeastward, along a path to the north, between Scotland and Iceland, as suggested by the location of the low pressure anomaly in Figure 4 and the direction of the upper-level airflow in Figure 3-5.

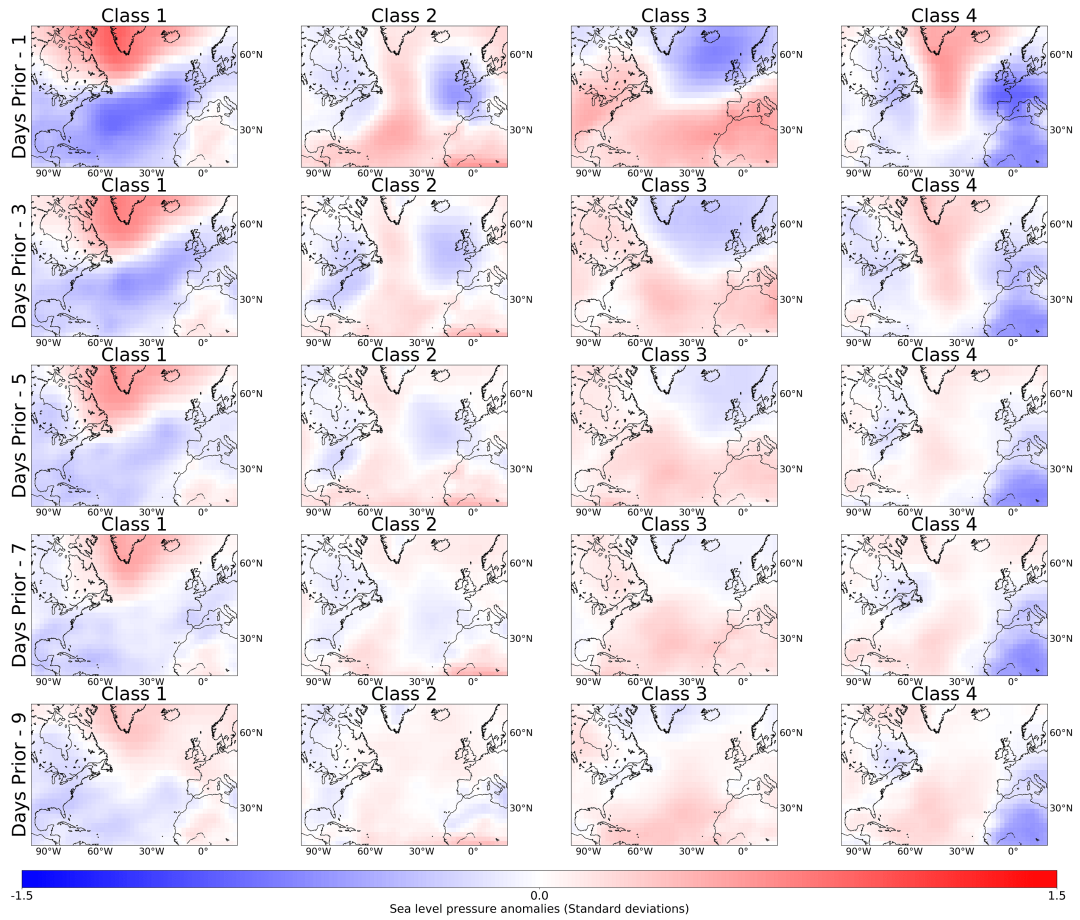


Figure 3-7: 2m air temperature anomalies in the North Atlantic region in the 1, 3, 5, 7 and 9 days prior to the heavy rainfall event occurring, for the four summer classes.

Heavy rainfall for Class 1 events, which are closely associated with the negative NAO, are more evenly spread across Britain (Figure 3-8). For this class, the location of the low pressure anomaly in Figure 3-3 suggests a track slightly further to the south of those in Class 3.

Figure S5 shows box-and-whisker plots of the standardized summer rainfall maxima for the 13 regions, separately for each of the four classes. There is not much difference in the magnitude of the standardized rainfall maxima between the regions, but rather, as shown in Figure 3-8, the difference is in the frequency of occurrence. Because we have not extracted a seasonal maximum for each class, we are unable to do a formal frequency analysis.



Figure 3-8: Geographical distribution of heavy rainfall events for each of the four summer classes, for each of 13 administrative regions of Great Britain (regions as in Hollis et al. (2019)). A high opacity indicates a higher proportion of event occurrence.

3.5.2 Winter Classes

Meteorological Conditions

The anomaly and raw SLP patterns for the three winter classes are shown in Figure 9. Both the anomaly and raw SLP patterns show a low SLP value on, or northwest of, the British Isles. In the raw patterns (Figure 3-9b) Class 1 shows a considerably stronger low SLP between Scotland and Iceland than any of the other classes, a pattern which is replicated in summer Class 3. The corresponding pressure anomalies in Figure 3-9a show a similar pattern, with strong negative anomalies between Scotland and Iceland and positive anomalies over the Azores in the subtropical North Atlantic. In contrast, the pressure anomaly pattern for Class 2 shows positive anomalies over Iceland and negative anomalies to the south. The spatial patterns formed by the pressure anomalies in Classes 1 and 2 are consistent with the positive and negative phases of the NAO, respectively (e.g. Barnston and Livezey 1987). Class 3 has similarities to the positive NAO pattern, but it is less pronounced than the Class 1 pattern, and the centre of the subtropical high pressure anomaly is shifted northeastwards, extending onto the Iberian peninsula and making it more reminiscent of the rotated summer NAO pattern.

For all three winter classes, the large-scale temperature patterns shown in Figure 3-10 are reminiscent of the Atlantic SST tripole pattern, with centres east of Newfoundland,

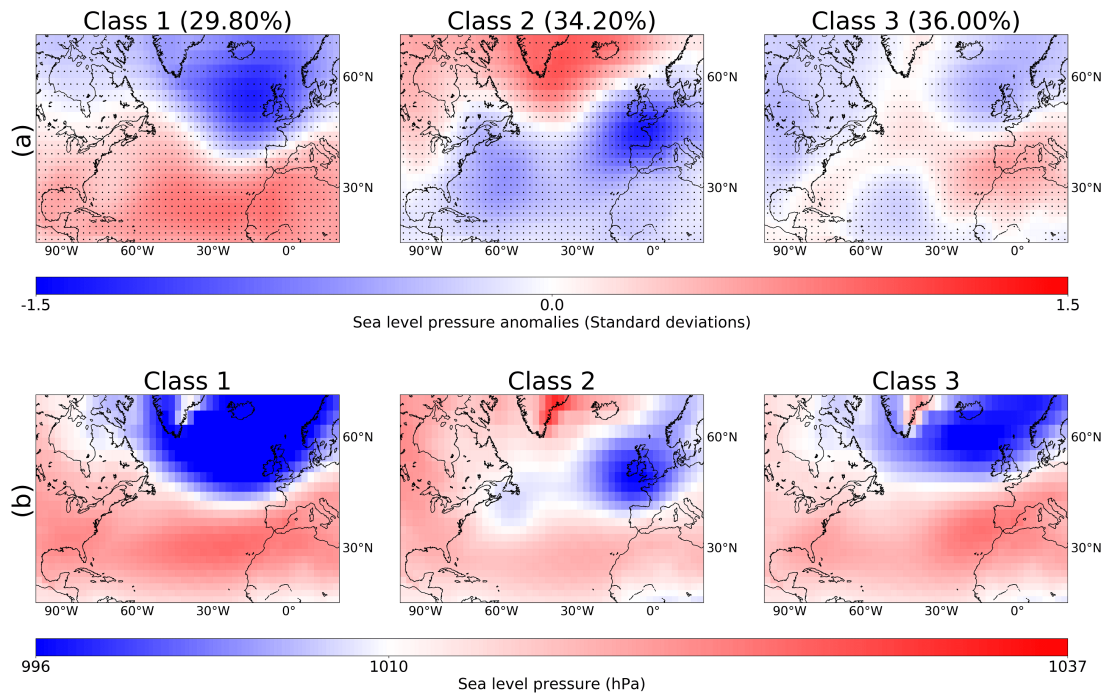


Figure 3-9: Sea-Level Pressure patterns for the three winter classes, showing both the anomaly SLP (a) and raw SLP (b) patterns. The percentages indicate the proportion of events in each class and the dots provided in (a) show the anomalies with a 2% significance value using a two-sided Student's t-test.

near the southeastern coast of the United States, and in the tropical eastern Atlantic (e.g. Fan and Schneider 2012). In addition, there is an area north of the UK (sometimes extending southwards) with a temperature anomaly of the same sign as the centre off the southeastern United States. The land areas near the Newfoundland and tropical east Atlantic tripole centres support the SST anomaly, but for the other two centres the temperature of the neighbouring land areas may differ. The wind pattern shown in Figure 10 confirms a northeastward shift of the subtropical high pressure for Class 3.

Locally near the UK, all three classes show warm temperature anomalies either across the UK and/or to the south, and southwesterly or southerly winds transporting warm air towards the UK (Figure 3-10). For all three classes there are cold temperature anomalies to the west and/or northwest of the UK. The resulting temperature contrast between these air masses provides ideal conditions for heavy rainfall at the cold front or low-pressure centre of a mid-latitude cyclone. Figure 3-9 suggests that for Class 2 the low pressure is located over Great Britain, whereas for Classes 1 and 3 it is centred further to the north and it may be the trailing cold front that is mainly responsible

for the heavy rainfall event. A difference between Classes 1 and 3 is the strength and location of the cold anomaly, which is relatively weak and centred over Iceland for Class 3 but is very strong and located to the southwest of Iceland for Class 1. The temporal evolution of the temperature anomalies (Figure 3-11) suggests that for Class 3 the anomaly develops within the last few days before the heavy rainfall event occurs, but for Class 1 the cold anomaly has existed in the same location for at least the past 10 days. Supplementary information S4 shows the corresponding development of sea level pressure anomalies in the days prior to the heavy rainfall event.

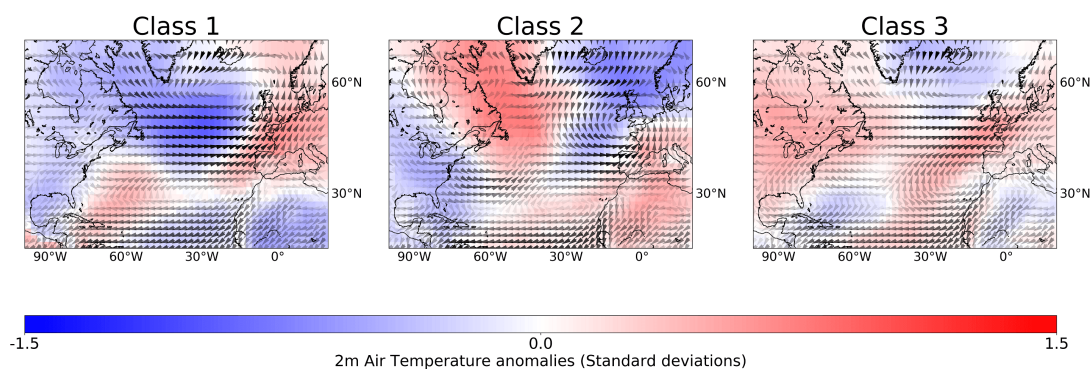


Figure 3-10: As Figure 3-6, but for the three winter classes. Anomaly 2m air temperature patterns are shown without wind speeds, but with points denoting significance, in supplementary information S2.

Figure 3-12 shows the 500 hPa geopotential heights for the three classes. For Class 2 the figure suggests a meandering storm track which is consistent with a negative NAO. In contrast, the storms for Classes 1 and 3 have travelled along a nearly straight path from a westerly to southwesterly direction.

Class Variability

The top row of Figure 3-13 shows how the frequency of occurrence of the events in each winter class varies with time, while the lower two rows show how the detrended frequencies of occurrence vary with the detrended indices of the NAO and AMO. The frequency of Class 1 increases with time, whereas the frequency of Class 2 decreases and Class 3 shows no temporal trend. The detrended event frequencies of Classes 1 and 2 show a moderately strong dependence (significant at the 1-6% level) with the detrended NAO index, with Class 1 events occurring more frequently during the positive NAO phase and Class 2 events occurring more frequently during the negative phase. This is consistent with the spatial SLP anomaly patterns in Figure 3-9a. In contrast, for Class 3 there is no significant correlation with either time or the two climate indices.

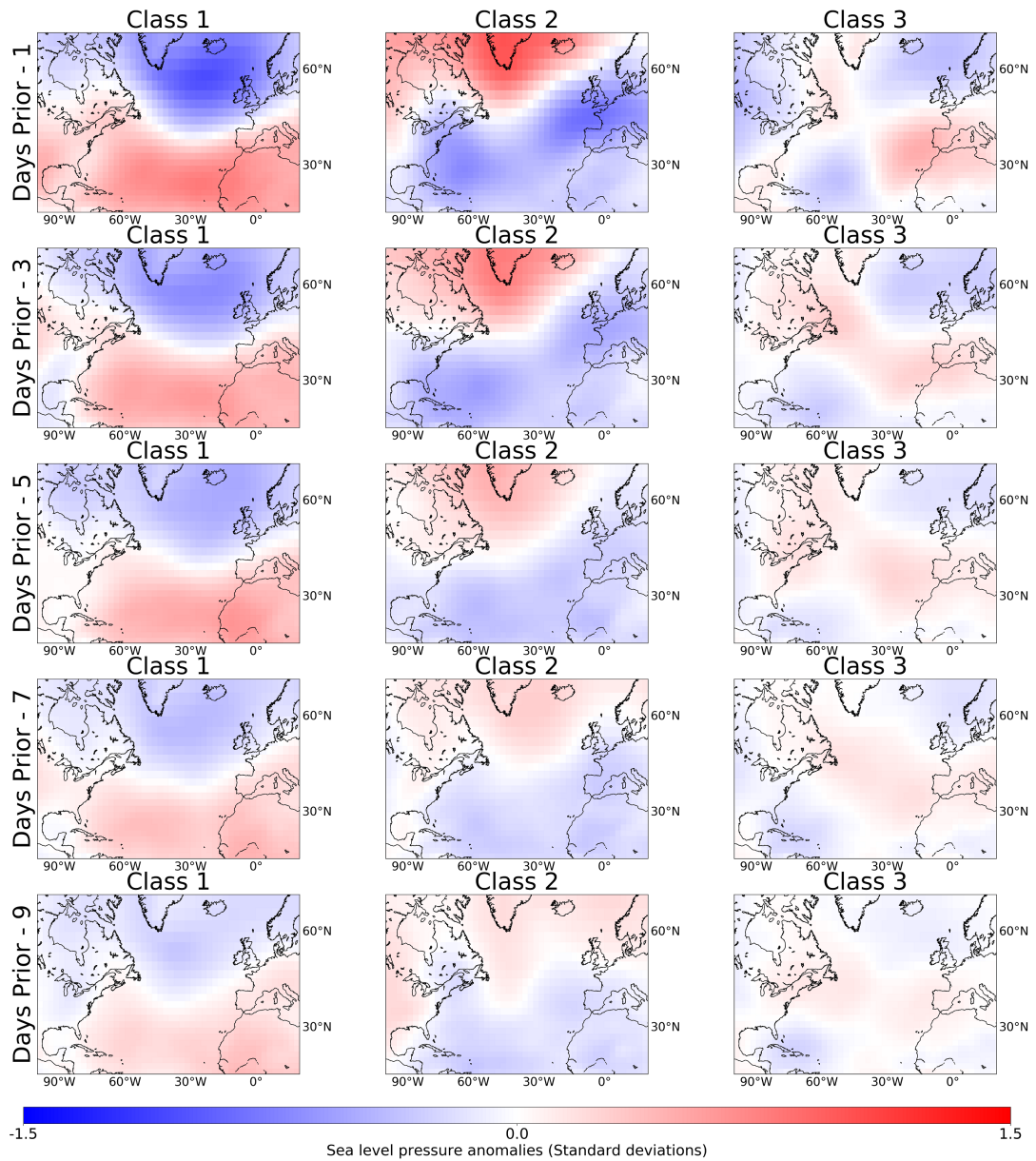


Figure 3-11: 2m air temperature anomalies in the North Atlantic region in the 1, 3, 5, 7 and 9 days prior to the heavy rainfall event occurring, for the three winter classes.

Somewhat unexpectedly for winter, we find a significant negative association with the AMO for Class 1. The cold temperature anomaly in the northwest Atlantic for winter Class 1 has persisted for at least 10 days (Figure 3-11), and it is possible that it may be so long-lasting and widespread that it influences the estimate of the AMO index for the season. The negative correlation with the AMO, and the positive correlation with the NAO, for Class 1 in winter is similar to the correlations for Class 3 in summer.

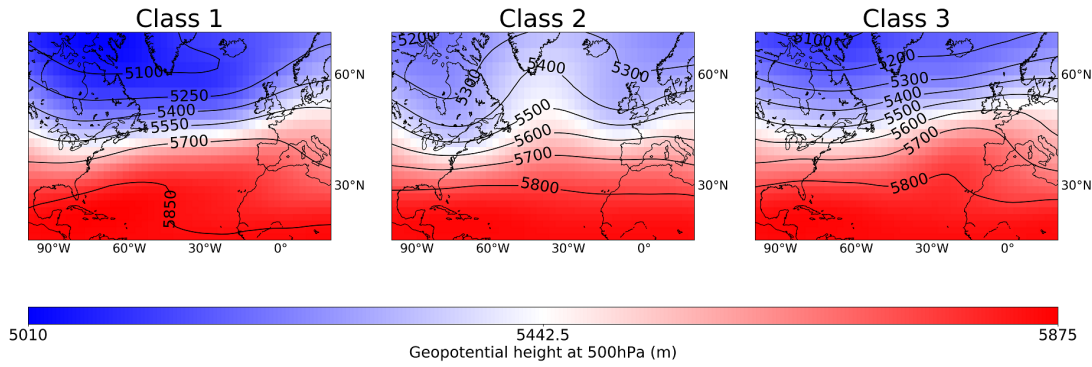


Figure 3-12: 500hPa Geopotential Heights for each summer class.

The pressure patterns for these classes are also similar (Figures 3-3 and 3-9).

Comparing the frequency of occurrence regionally across Great Britain (Figure 3-14) reveals different distributions for each of the three classes. Heavy rainfall events in Class 2 show a preference for occurring in the south and east, as can be expected for a SLP pattern reflecting the negative phase of the NAO. The location of the SLP anomaly in Figure 9 suggests cyclones are tracking across Britain, and prolonged rainfall in eastern Britain often occurs in onshore winds on the northern side of depressions (e.g. Wheeler 2013).

Class 1 events cause heavy rainfalls mainly in western Britain, with their low-pressure centres located further north compared with events in Class 2 (Figure 3-9). Class 3 events are concentrated in the far northwest, and the spatial rainfall distribution is rather similar to that for the summer Class 3 events. The SLP patterns for both summer Class 3 (Figure 3-9) and winter Class 3 (Figure 3-14) display a slight counter-clockwise rotation of the high pressure centre (shifted northeastwards from the North Atlantic onto the Iberian peninsula) compared with the more standard winter NAO pattern of Class 1. This seems to shift the low pressure, and the main rainfall area, slightly further north for Class 3 compared with Class 1.

Again, similarly to summer, there is not much difference in the magnitude of the standardized winter rainfall maxima for the 13 regions, for the three winter classes (Figure S6). The difference is in the regional frequency of occurrence (Figure 3-14).

3.6 Discussion

Including 2m air temperature across the North Atlantic sector as an extra feature set to the meteorological clustering, which is traditionally done only on atmospheric pressure

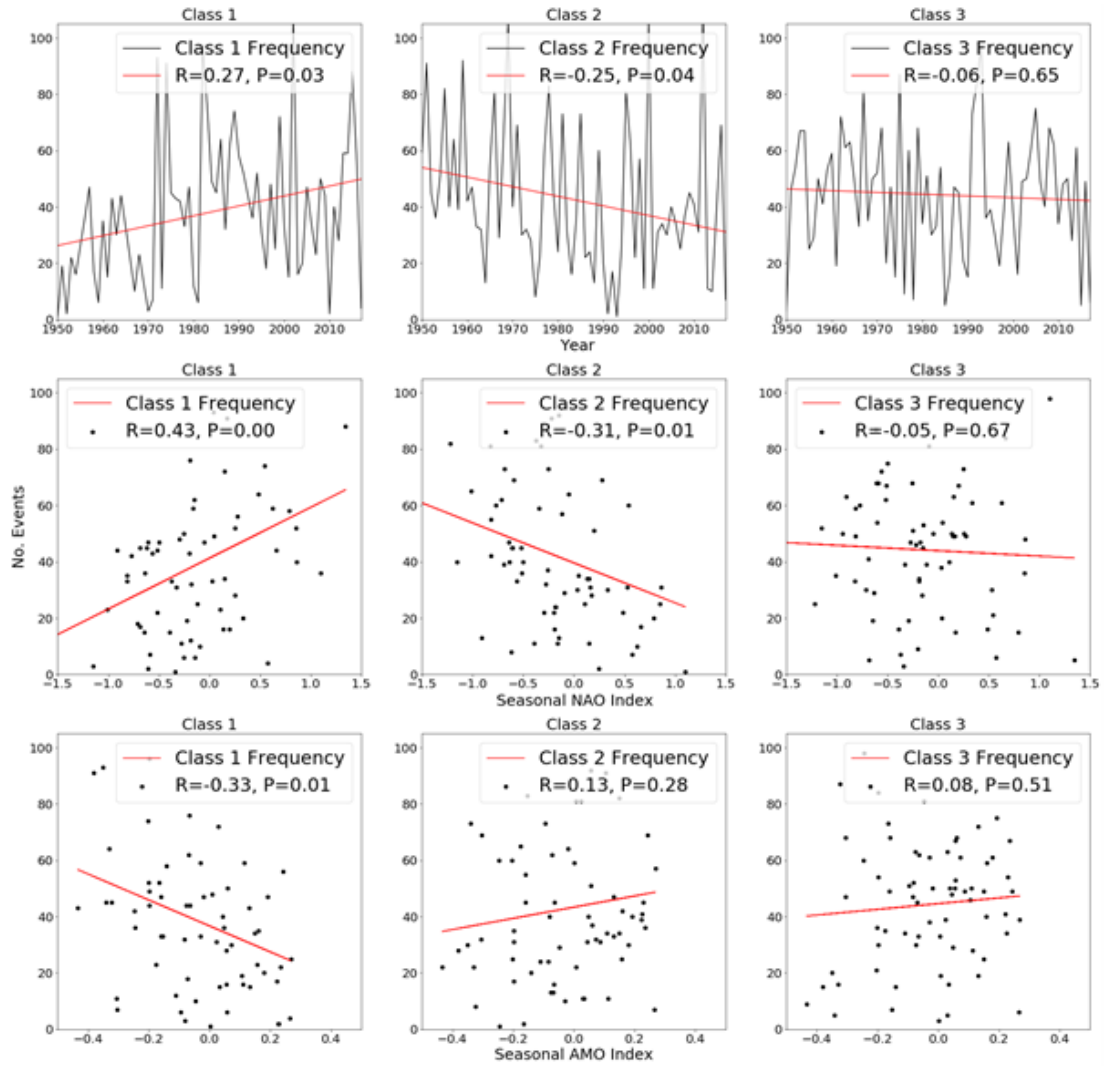


Figure 3-13: As figure 3-6, but for the three winter classes.

patterns, has provided a new view of the conditions leading to heavy rainfall events in Great Britain. The four identified classes in summer, and the three classes in winter, are each associated with different geographical distributions of heavy rainfall events. The temperature and circulation patterns identified in this study indicate local areas whose temperature and/or pressure has the potential to be used as additional predictors for weather generators such as for example described by Serinaldi & Kilsby (2012). Future work could also involve investigating the large-scale temperature and pressure patterns predicted by global climate models, and the expected effect these would have on heavy rainfall characteristics in different parts of Britain.

In this context we compare the circulation patterns derived in the present study using



Figure 3-14: Geographical distribution of heavy rainfall events for each of the three winter classes for each of 13 administrative regions of Great Britain. A high opacity indicates a higher proportion of event occurrence.

both the SLP and 2m air temperature anomalies, with the classes from previous studies which are based on atmospheric circulation only, but for which the associated UK rainfall has also been assessed (sections 5.1 and 5.2). We then discuss the sensitivity of the results to the choices of data and methods (section 5.3).

3.6.1 Summer

Neal et al. (2016) present 30 circulation patterns over the North Atlantic – European region, for which Richardson et al. (2017) calculate regional UK median rainfall and rainfall variability (inter-quartile range). Our summer Classes 1, 2, 3 and 4 show some similarities in SLP anomalies (Figure 4) and wind directions (Figure 5), with circulation patterns number N28, N29, N21 and N11, respectively, identified by Neal et al. (2016) (an “N” has been inserted before the pattern number to distinguish them from our Classes). Richardson et al. (2017) show that patterns N29 and N21 are both associated with high rainfalls in most of the country, but for N29 particularly in the south and east, and for N21 particularly in the north and west. This is in general

agreement with the rainfall distributions for our Classes 2 and 3, respectively (Figure 8). For patterns N28 and N11 Richardson et al. (2017) find that rain mainly falls in the south and east (similar to our Classes 1 and 4), but the median rainfall is only moderate. However, the rainfall variability is rather high, which suggests that the patterns include both wet and dry events. Since the Classes in our study are by design associated with high rainfall events, a contributing factor to distinguishing between the wet and dry events in Neal et al.’s patterns may be the temperature patterns associated with our Classes (Figure 3-5).

3.6.2 Winter

Despite the significant correlation with the NAO, the winter Class 1 seems to have more similarities with Neal et al. (2016)’s pattern N21 than with the six patterns they label typical of the positive NAO phase; Class 1 has a southwesterly, rather than westerly, wind direction over the UK. The winter Class 2 has similarities to Neal et al. (2016)’s pattern N11, and Class 3 to pattern N2 (which is similar to N21, but has a weaker low pressure). The principal rainfall areas largely overlap for Class 1 and N21 (north and west) and Class 2 and N11 (south and east). The rainy regions for Class 3 and N2 are both mainly in the north and west of the country, and for pattern N2 Richardson et al. (2017) again suggest a combination of a moderate rainfall median and a higher rainfall variability.

For winter, further comparisons can be made between our classes and those found by Ummenhofer et al. (2017), who show circulation patterns and associated rainfall patterns over Europe. However, these comparisons are less clear due to the fewer and more generalised classes used by Ummenhofer et al., and the disparity in spatial rainfall domain. The circulation patterns (Figures 3-10 and 3-11) of our Classes 1 and 3 both show similarities to UB and UE, and Class 2 to UC, where U_i indicates pattern i in Ummenhofer et al. (2017). The strongest similarities are between Class 2 and UC, which is also reflected in the regional distribution of rainfall which favours eastern and southern Britain (Figure 3-14). Classes 1 and 3, and UB and UE, all occur mainly in the north and west of Britain.

3.6.3 Methodology

The results of the study are sensitive to the selection of data and methods. Non-stationarity of the data means that the period of record used will influence the classification results, including the derived quantities such as rainfall magnitude and geographical distribution associated with each class. Figures 3-6 and 3-13 show how the

number of events in each class vary with time. We have explored two potential co-variates that are known to influence the region, the NAO and AMO climate indices, but other oscillations and phenomena have not been investigated.

Some subjective choices have been made regarding the clustering algorithm, initialization conditions and the preselection of atmospheric variables. The algorithm used (k-means) will tend to generate clusters of roughly equal size, and the results depend heavily on the initial number of clusters chosen, k . In this study we chose a k -value based on subjective analysis of the clustering results, and the results of earlier studies as discussed in Section 3.2.

Other factors which influence the sensitivity of the analysis include the spatial domain and the product from which the meteorological data was extracted. As we wanted to investigate also the influence of temperature on land areas neighbouring the North Atlantic, we selected a larger domain than used in some earlier studies (e.g. Richardson, Fowler, Kilsby, and Neal 2018; Ummenhofer et al. 2017), and this will have affected the results compared with those studies. We used the NCEP/NCAR Reanalysis 1 product for the meteorological data, but different results may have been found if, for example, a similar reanalysis product from the European Centre for Medium range Weather Forecasts (ECMWF) had been used, or if moisture rather than temperature data had been used.

3.7 Summary and Conclusions

Meteorological conditions over the North Atlantic were extracted from NCEP/NCAR Reanalysis Data (Kalnay et al. 1996) for seasonal heavy rainfall events (summer and winter 1-day maxima) at 125 locations across Great Britain. The anomaly sea level pressure and 2m air temperature patterns associated with each event were clustered jointly to find how the meteorological conditions over the North Atlantic sector co-vary to produce heavy rainfall events.

Four classes were identified for summer. Two of them suggest that heavy rainfalls are affected by opposing combinations of the seasonal NAO and AMO: negative (positive) NAO and positive (negative) AMO for Class 1 (Class 3). The remaining Classes 2 and 4 are both associated with a northward extension of the subtropical high pressure in the North Atlantic, highly meandering storm tracks, and heavy rainfall predominantly in southeast Britain. Although these classes are associated with opposing North Atlantic temperatures (Figure 3-4), only the event frequency for Class 2 is borderline significantly (6%) correlated with the seasonal AMO.

Whereas in summer the temperature patterns show either predominantly cold or warm anomalies over most of the North Atlantic, in winter two phases of a smaller-scale four-pole temperature pattern emerges. This resembles the SST tripole pattern (e.g. Fan and Schneider 2012), plus a centre north of the UK with a temperature anomaly of the same sign as the centre off the southeastern United States.

The number of events in winter Class 1 shows significant positive correlation with the NAO and negative correlation with the AMO. There is a strong, widespread and persistent cold anomaly in the SST centre off Newfoundland, which may influence the seasonal AMO index. Heavy rainfall events mainly occur in western Britain. In contrast, the number of Class 2 events is borderline significantly (6%) negatively correlated with the NAO, and the meandering storm tracks result in heavy rainfall mainly in the south and east.

The pressure pattern for winter Class 3 shows some similarity with that typical of the positive phase of the NAO, but with the subtropical high-pressure anomaly shifted eastwards onto western Europe. There is no correlation with either the NAO or AMO. The pressure pattern is similar to the summer Class 3 pattern, and both these classes result in a strong focus of heavy rainfall events in the far northwest of Great Britain. The cold temperature anomaly to the northwest of the UK develops over a matter of days prior to the heavy rainfall occurring, similar to the events in summer, and in contrast to the longer-lasting cold anomaly of winter Class 1.

3.8 Acknowledgements

The authors gratefully acknowledge the NCEP Reanalysis, NAO and AMO data provided by the NOAA/OAR/ESRL PSD, Boulder, Colorado, USA, from their website at <https://www.esrl.noaa.gov/psd/> as well as the CEH-GEAR rainfall dataset provided by UKCEH, available through their website at <https://catalogue.ceh.ac.uk/documents/ee9ab43d-a4fe-4e73-afd5-cd4fc4c82556>. Andrew Barnes acknowledges funding as part of the Water Informatics Science and Engineering Centre for Doctoral Training (WISE CDT) under a grant from the Engineering and Physical Sciences Research Council (EPSRC), grant number EP/L016214/1. The contributions by Cecilia Svensson were supported by the UK Natural Environment Research Council (NERC) National Capability award NE/R016429/1, UK-SCAPE (UK Status, Change and Projections of the Environment), <https://www.ceh.ac.uk/ukscape>.

3.9 Postscript

The study presented in this chapter used cluster analysis on the concurrent mean sea-level pressure and 2m air temperature fields of the North Atlantic during extreme rainfall events in the UK in response to **Hypothesis 2**. The study clusters extreme rainfall events in Great Britain using their relative mean sea-level and air temperature fields across the North Atlantic.

The results showed strong contrasts between the mean sea-level pressure and air temperature patterns for each of the clusters. Specifically, the results highlight the spatial and temporal variability between the clusters; this indicates the role of mean sea-level pressure and air temperature fields in the generation of the extreme rainfall events are interdependent and that the variability of these fields can result in very different spatial and temporal impact distributions.

Previously studies have focused on the interpretation of extreme or heavy rainfall events using the mean sea-level pressure patterns (Allan, Blenkinsop, et al. 2020; Champion, Blenkinsop, et al. 2019; Richardson, Fowler, Kilsby, and Neal 2018; Ummenhofer et al. 2017). However, the ability to distinguish between regular and extreme rainfall events using these patterns is left unattended. The study presented in this chapter highlights the importance of this question which is addressed through **Hypothesis 3** in the next chapter.

While this work shows potential application to weather generators however there are also opportunities to further study the relationships between other meteorological variables by clustering these different variables in various combinations. For example, clustering GpH and integrated water vapour, or specific humidity and wind vector fields and then performing regression analysis between the resulting clusters and rainfall metrics. Moreover, the sensitivity of these atmospheric variables to the clustering methods and similarly to Chapter 4 the sensitivity of the results to the number of cluster are also open avenues for investigation. Further work in this area could enable the advancement of current weather generators and improve the current understanding of how and when extreme events occur.

Chapter 4

Identifying and interpreting extreme rainfall events using image classification

4.1 Preamble

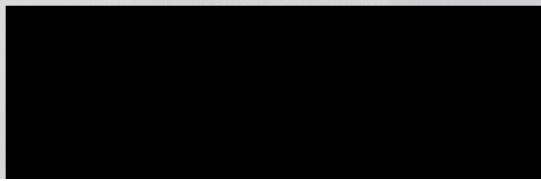
In the previous chapter the covariance of both mean sea-level pressure and air temperature fields relevant to heavy rainfall events is evaluated using a cluster analysis of combined atmospheric fields. This chapter seeks to answer whether extreme and regular rainfall events can be distinguished based on their mean sea-level pressure fields through addressing hypothesis **Hypothesis 3**.

To do this, a study was carried out which extracted extreme and regular rainfall events for two hydrologically diverse regions of the UK (**Objective 3.1**) and developed a set of neural network based classification models (**Objective 3.2**) to differentiate between the following subsets of the rainfall events:

1. Extreme and regular rainfall events in the North West of England.
2. Extreme and regular rainfall events in the South East of England.
3. Extreme rainfall events in the North West of England and extreme rainfall events in the South East of England.

The neural networks used the mean sea-level pressure fields of the North Atlantic to distinguish between the events in each experiment. Following this, the resulting classifiers were evaluated for their accuracy in correctly identifying the relative events (**Objective 3.3**). Finally, a sensitivity analysis of the models was carried out to identify the regions of the North Atlantic that were most responsible for resulting classifications.

4.1.1 Authorship Statement

Status	Accepted in the Journal of Hydroinformatics.
Details	Barnes, A.P., McCullen, N., Kjeldsen, T.R. (in review) Journal of Hydroinformatics. 2021.
Authors' contribution	<p>The author of this thesis has primarily (90%) contributed to design and implementation the methodology adopted for the extraction, clustering and analysis of both the atmospheric and rainfall data. Each author's exact contributions are as follows:</p> <p>A.P. Barnes: Formulation of ideas (100%), design of methodology (95%), data collection (100%), processing and analysis of data (95%), manuscript preparation (90%).</p> <p>N. McCullen & T.R. Kjeldsen: design of methodology (5%), processing and analysis of data (5%), manuscript preparation (10%).</p>
Date and Signature	 19-07-2021

4.1.2 Abstract

This study presents the first attempt to identify extreme rainfall events based on surrounding sea-level pressure anomalies, using neural network-based classification. Sensitivity analysis was also performed to identify the spatial importance of sea-level pressure anomalies. Three classification models were generated: the first classifies the patterns between extreme and regular rainfall events in the north west of England, the second classifies the patterns between extreme and regular rainfall events in the south east of England, and the third classifies between the patterns of extreme events in the north west and south east of England. All classifiers obtain accuracies between 60-65%, with precision and recall metrics showing that extreme events are easier to identify than regular event. Finally, a sensitivity analysis is performed to identify the spatial importance of the patterns across the North Atlantic, highlighting for all three classifiers the local anomaly sea-level pressure patterns around the British Isles is key in determining the difference between extreme and regular rainfall events. In contrast the pattern across the mid and western North Atlantic shows no contribution to the overall classifications.

4.2 Introduction

Flooding caused by extreme rainfall events can have severe social, environmental and economic consequences. Although variations in yearly flood trends have been studied extensively (e.g. Robson 2002; Prosdocimi et al. 2019) such trends do not help in identifying the processes which lead to the extreme cases. For example, in February 2020 storms Ciara and Dennis passed over the United Kingdom (UK), resulting in up to 177mm of rainfall in a single 24-hour period (Met Office, 2020) and is estimated to have resulted in insured losses of up to £200 million (Finch 2020). To provide improved risk analysis and support flood management, the processes which cause these extreme rainfall events need to be better understood and differentiated from those of regular rainfall events.

The occurrence of extreme rainfall events in the UK has a strong dependence on the concurrent and prior meteorological conditions across north western Europe and the North Atlantic. For example, Brown (2017) shows the dependence of extreme daily rainfall in the UK on large-scale meteorological indices: North Atlantic Oscillation (NAO), Pacific Decadal Oscillation (PDO), El Niño – Southern Oscillation (ENSO) and Atlantic Multidecadal Oscillation (AMO). These indices represent the difference in either sea-level pressure (NAO, PDO) or sea-surface temperature (ENSO, AMO) across their specified regions. Brown found the biggest impact was made by the NAO (the difference in sea-level pressure between Iceland and the Azores), a positive NAO increases the likelihood of extra-tropical cyclones developing over the North Atlantic. This relationship is further demonstrated by Richardson et al. (2017) and Schillereff et al. (2019) which both show a negative NAO correlates strongly with increased high-river flows.

Extra-tropical cyclones are known to be the main contributors to extreme precipitation across the globe (Pfahl and Wernli 2012) and have also been linked to the development of atmospheric rivers (ARs) (Gimeno, Vázquez, et al. 2020). ARs are long plumes of highly concentrated water vapour in the atmosphere which originate from the mid to lower latitudes, with those affecting the UK moving upwards towards North Western Europe from the Caribbean. Lavers et al. (2011) found ARs occurred during the ten largest floods in the UK. Following this, Lavers and Villarini (2013) analysed the frequency and intensity of ARs with several climate change scenarios, concluding that both the intensity and frequency of the strongest ARs is expected to increase in the future. In contrast, Champion et al. (2015) found that less than 35% of winter and of 15% of summer ARs are associated with an extreme rainfall event. This highlights the

need to be able to determine the difference between atmospheric phenomenon which cause extreme rainfall events and those which produce more moderate rainfall events of little or no interest in flood management.

Attempts to address this need have focussed on the identification of key meteorological patterns across the North Atlantic relating to extreme rainfall events derived from large-scale climate data. Neal et al. (2016) presents 30 sea-level pressure anomaly (SLPA) patterns (MO-30) identified through the application of the k-means clustering algorithm (Lloyd, 1957). These patterns represent the types of SLPA patterns which can be present over the North Atlantic on any day. The patterns were then combined subjectively into 8 SLPA patterns (MO-8), some of which are shown to strongly correlate with the NAO. Richardson et al. (2018) investigated the applicability of these cluster sets for identifying regional precipitation and drought climatology throughout the UK, finding that the smaller set of 8 clusters do not aid in explaining precipitation variability. However, magnitude variation between patterns was observed, with some patterns producing consistently higher levels of median daily rainfall across all regions of the UK. However, this does not allow easy distinction between extreme and regular rainfall SLPA patterns in the various regions.

Ummenhofer et al. (2017) attempted to cluster SLPA patterns using the anomaly precipitation spatial variation across Europe and found a dipole in SLPA across the UK can determine whether precipitation anomalies in the UK will be positive in the north west or south east. This relates to the findings by Champion et al. (2019), who found that summer extreme rainfall events in the north west are typically associated with a positive SLPA region over the UK. However, no such relationship was found when analysing extremes in the south east.

The large-scale meteorological patterns being considered by the studies above are represented by images, 2D matrices with pixel colour representing the numerical value of the meteorological variable in question (for example, SLPA). Neural networks have proven to be effective at image classification across various domains, from the classification of YouTube videos (Karpathy et al. 2014) to tumour feature extraction (Yang, Yang, et al. 2019) but, up until now, they have not been used effectively to classify meteorological patterns such as distinguishing between SLPA of extreme events. This study SLPA applies neural networks to identify the differences in SLPA patterns across the North Atlantic for extreme and regular rainfall events, applied to both the north west and south east of England. In particular, the study demonstrates the differences in SLPA between:

1. Daily extreme and regular rainfall events in the north west of England.
2. Daily extreme and regular rainfall events in the south east of England.
3. Daily extreme rainfall events in the north west and south east of England.

Following this, a sensitivity analysis was conducted to compare which regions of the North Atlantic are most important to determining between the above classifications.

4.3 Data

4.3.1 Rainfall Events

Extreme and regular daily rainfall series were extracted from the administrative regions of north west and south east of England. The rainfall series used was the UK Centre of Ecology and Hydrology’s CEH-GEAR dataset (Tanguy et al. 2015). This dataset combines data from the Met Office database of observed precipitation data using a natural neighbour interpolation method to generate a regular grid of rainfall based covering the British National Grid with daily rainfall values from 1890-2017. The application of the natural neighbour interpolation allows grid cells to be generated based on the closest viable rainfall monitors. To extract representative rainfall for each region (north west and south east England), a regular grid of coordinates is generated for each region at 30km intervals, bounded by the North West and South East administrative regions. Figure 4-1 shows the position of these points in both the North West (a) and the South East (b). For each day, the rainfall magnitude for a region is given by the total rainfall at each of the points identified. The days on which the rainfall total is greater than that of a trace level ($>0.5\text{mm}$ at each location) is considered a rainfall day and is added to the non-trace rainfall series for the region. Following this, each non-trace event is standardized based on the mean and standard deviation of the month in which it occurs, using the following equation:

$$r_{l,m} = \frac{r_{l,m} - \overline{r_{l,m}}}{std(r_{l,m})}, l = 1, \dots, 12 \quad (4.1)$$

Here, $r_{l,m}$ represents the non-trace rainfall series for region l for all non-trace rainfall events in month m , $\overline{r_{l,m}}$ is the mean and $std(r_{l,m})$ is the standard deviation of the series. Following standardization, the magnitude of each event represents the deviation of that event’s magnitude from the mean of its respective location and month. Selecting extreme rainfall days from a rainfall series can be achieved by taking the maximum

rainfall day in each time-period (e.g annual maximum rainfall); alternatively, a threshold can be applied such that all days with a daily rainfall quantity greater than the threshold are selected. In this study the later approach is used as maxima approaches require a rainfall day to be selected in each time-period which can lead to the selection of rainfall days which in the context of the rainfall series are not extreme events such as in a particularly dry year. Selecting the events with the highest 10% of standard deviations from the mean provides a set of extreme rainfall events, the 10% of events closest to 0 can then be chosen as the regular rainfall dataset as these represent the expected or mean amounts of rainfall in a given month for a given location.



Figure 4-1: Locations of the regions and points from which rainfall is extracted for both the north west region (b) and south east region (c).

This extraction resulted in 3008 individual events (1504 extreme and regular rainfall, respectively) in the North West and 2290 events (1145 extreme and regular events) in the South East. The disparity here is due to there being fewer non-trace rainfall days in the South East, with the North West having 15,046 non-trace rainfall days and the South East having only 11,450.

4.3.2 Meteorological Patterns

To classify each event the anomaly sea level pressure (SLPA) pattern is required across the North Atlantic. For each of the regular and extreme rainfall days for both the north west and south east regions SLPA patterns are extracted across the North Atlantic. The patterns are extracted from the 2.5° gridded NCEP/NCAR Reanalysis 1 dataset (Kalnay et al. 1996), with each pattern bounded between 15-70 latitude and -80-15 longitude.

$$\mathbf{P}_{i,m} = \frac{\mathbf{P}_{i,m} - \overline{\mathbf{P}_m}}{std(\mathbf{P}_m)}, m = 1, \dots, 12 \quad (4.2)$$

Here $\mathbf{P}_{i,m}$ represents the 2D pattern for event i in month m which is standardized using element-wise operations using $\overline{\mathbf{P}_m}$ and $std(\mathbf{P}_m)$. The monthly mean $\overline{\mathbf{P}_m}$ and standard deviation $std(\mathbf{P}_m)$ are defined using all daily patterns in month m , each resulting in a 2D matrix with each cell representing a single pixel across the North Atlantic.

4.4 Classification

To classify the rainfall events a neural network-based classification method is used, the classifiers are trained using the anomaly sea-level pressure patterns for each event over the North Atlantic. Three classifiers are required; the first classifies the north western extreme and regular event patterns, the second classifies the south eastern extreme and regular patterns, finally the third classifier classifies the extreme event patterns from both the north west and south east. The exclusion of a fourth model distinguishing between north west and south east regular events is intentional as the focus of this paper is on the identification and comparison of extreme events. Table 1 describes each of these classifiers (M_{NW} , M_{SE} , M_{comp}) and indicates which data sets are used in each model and which class they represent. This section introduces the neural-network classification method and the optimisation procedure including how the data is split for training.

Model	Description	North West		South East	
		Extreme	Regular	Extreme	Regular
M_{NW}	Distinguishes between North Western extreme and regular events.	1	0		
M_{SE}	Distinguishes between South Eastern extreme and regular events.			1	0
M_{comp}	Distinguishes between North Western and South Eastern Extremes.	1		0	

Table 4.1: This table indicates the purpose of each model and the datasets which are used. The numbers indicate the class of the given dataset in the given model.

4.4.1 Neural Network Architecture

A neural network consists of at least two layers of nodes connected through edges. Figure 4-2 shows an example architecture with three layers: an input layer, a hidden layer and an output layer. Assigned to each edge in the graph is a weight which is optimised through training and is indicated by W_x where $x = 1, \dots, 8$ is the edge label.

When propagating an input vector the input nodes in the neural network take on the values of their relevant features, in the case of figure 4-2 there are only two input nodes

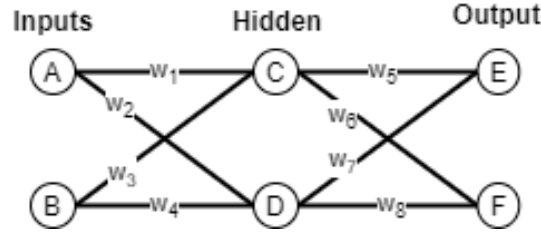


Figure 4-2: An example neural network structure consisting of three layers where each node is connected via weights (as given by w_x) to the nodes in the layers both before and after.

and hence two features in the input vector. Following this, the value propagated out of each edge can then be calculated by multiplying the value of the input node by the weight assigned to the edge, in the case of the edge 1 the value can be calculated as:

$$C = \max(0, \text{edge}_1 + \text{edge}_3) = \max(0, Aw_1 + Bw_3) \quad (4.3)$$

A similar calculation can be done for node D and then the values at nodes C and D can be propagated forwards in the same manner to nodes E and F along their respective edges. In figure 4-2 two output nodes are given, indicating a binary classification, a choice of two class nodes: either E or F . For classifiers M_{NW} and M_{SE} the output nodes will represent whether the input pattern is an extreme event or a regular event and in case of M_{comp} these will indicate whether the pattern is a south eastern or north western extreme. To make the process of selection easier a soft-max function is applied to the output nodes such that the output from node E is,

$$\text{softmax}(E) = \frac{\exp(E)}{\exp(E) + \exp(F)} \quad (4.4)$$

where E is the output from node E , F is the output from node F and $\exp(\dots)$ is the exponential function. Softmax forces the output to be between 0 and 1 giving a probability of the given pattern being in classes E and F .

4.4.2 Classifier Training

Each of the three models introduced at the beginning of this section (M_{NW} , M_{SE} and M_{comp}) require different datasets and hence three datasets are produced consisting of a labelled set of input vectors. Each dataset is represented by a matrix of n rows and m columns where n is determined by the number of events and m is the number of cells

(or pixels) in a given pattern. The row which represents a given pattern is generated through the flattening of its matrix, which is done through the concatenation of each row in the matrix to each other resulting in a vector. Through this operation each 22x38 cell pattern is converted to a single vector of size 836. Each set of events is then split into two subsets: a training and a test set. The training set consists of 80% of the input vectors and is used to train the neural network, the remaining 20% is the testing dataset and is used to validate the accuracy of the network on unseen data. The actual selection of events as belonging to either the training or testing datasets is randomised.

Training the network involves the optimisation of the weights between the nodes in the network, this optimisation is done using stochastic gradient descent (Bottou 1998) and the backpropagation algorithm (Rumelhart, Hinton, and Williams 1986). Back propagation is a way to propagate the error calculated at the output nodes back through the weights of a neural network (Leung and Haykin 1991). To do this, an objective function is required, in this study the cross-entropy loss function (Courville, Bengio, and Aaron 2016) is used to determine the error between the output nodes and the intended classification label (extreme or regular). The cross-entropy error will take the log difference between the true label and its calculated probability, resulting in the two output nodes containing the probability of each class being correct.

To further provide refinements to the final model we trial models with a varying number of hidden nodes. In the example given in figure 2 only two hidden nodes are used; however, in the SLPA classifiers the number of hidden nodes is trialled from 10 to 100 in increments of 10. This will enable the selection of a suitable number of hidden nodes for the final representative model.

4.5 Results

The accuracy and interpretation of the three-anomaly sea-level pressure (SLPA) classifiers are given in this section. The first part of this section discusses the accuracy of each classifier and then the sensitivity of the classifiers to regions of the north Atlantic's SLPA.

4.5.1 Model Accuracy

North West Classifier (model M_{NW})

The results presented in Figure 4-3 (c) show that the testing accuracies during training plateau at approximately 60%, in contrast the training accuracies continue to increase

close to 100% for classifiers with 90 and 100 hidden nodes. The classifier with 30 hidden nodes ends the 100 epochs of training with the highest testing accuracy of 62% and hence is selected for further investigation.

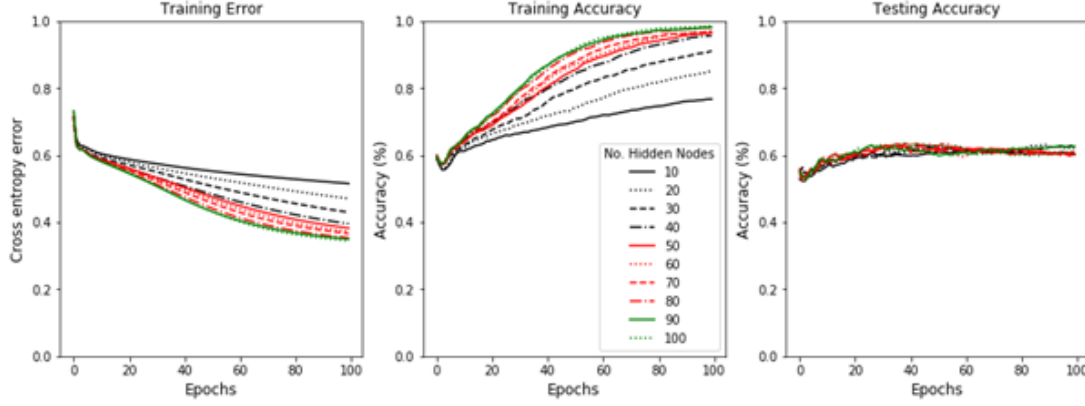


Figure 4-3: Loss and accuracies for models classifying between SLPA patterns relating to north west extreme and regular rainfall events.

Investigating the $M_{NW,30}$ classifier, precision between the extreme and regular event classifications differ at 68% and 55% respectively. This indicates the classifier is better at identifying only extreme events, with fewer false positives. However, when comparing the recall scores of each classification, which are 60% for extremes and 63% for regular events, this shows the classifier is equally good at labelling positive extreme and regular events alike.

South East Classifier (model M_{SE})

Similarly to the north west classifier a plateau occurs when attempting to train a neural network to classify between south eastern extreme and regular rainfall event SLPA patterns across the North Atlantic. As presented in figure 4-4, the training accuracy increases as the training error of these classifiers decreases; however, as found in the training for M_{NW} , the testing accuracy remains consistent at around 60%.

For M_{SE} the optimal classifier contains 10 hidden nodes ($M_{SE,10}$), this classifier finishes the 100 epochs with a 60% testing accuracy and 84% training accuracy. Breaking this into the precision and recall values a similar trend again is seen to $M_{NW,30}$ with precision values for both regular and extreme events being similar at 55% and 59% respectively. Further to this, the recall values also show a similar trend with the extreme event patterns having a recall higher than that of the regular event patterns (61% and 53% respectively).

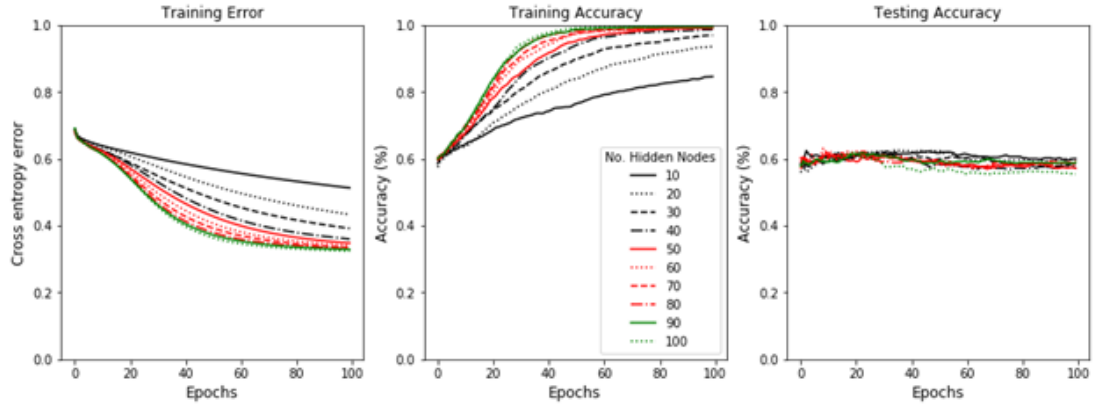


Figure 4-4: Loss and accuracies for classifiers classifying between the SLPA patterns relating to south east extreme and regular rainfall events.

Extreme event classifier (model M_{comp})

The final classifier (M_{comp}) looked to distinguish between extreme event patterns for north west and south east, similarly again to M_{NW} and M_{SE} a plateau of testing accuracy occurs, as shown in figure 4-5, but with a slight variability depending on the number of hidden nodes used. The spread of training accuracies and training errors is also marginally lower than those presented in the previous classifiers.

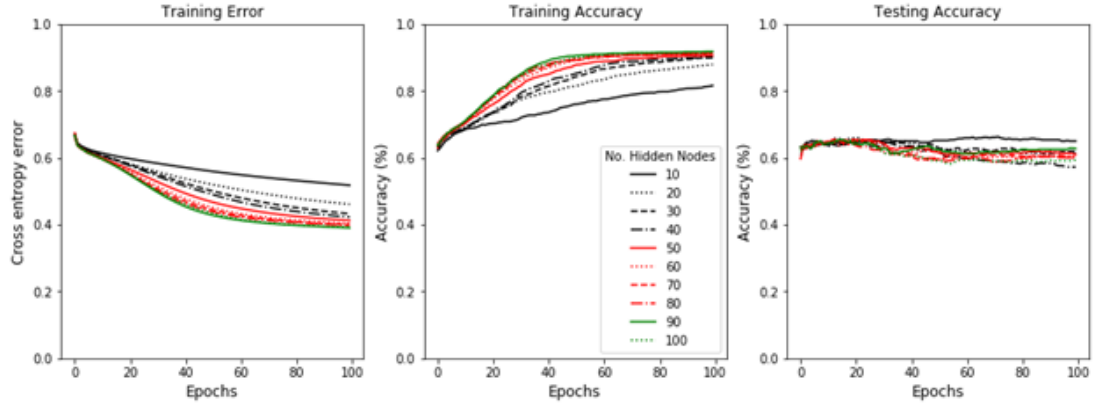


Figure 4-5: Loss and accuracies for models classifying between SLPA patterns relating to extreme events in the north west and south east.

Despite this, the most accurate classifier has 10 hidden nodes ($M_{comp,10}$) and gives a testing accuracy of 65% and a training accuracy of 81%. In contrast to the $M_{NW,30}$ and $M_{SE,10}$ models, the precision and recall values of identifying south eastern extremes (66%, 67%) are both higher than those of identifying north western extremes (55%, 54%). This is counter intuitive as the model was trained using 31% more examples of

north western extremes indicating the model would have more experience classifying these types of extremes.

4.5.2 Spatial Sensitivity

To identify the regions of interest to each classifier a saliency map is created, representing the relative contribution of each cell (input feature) to the overall classification. To calculate the contribution of each cell to the overall classification the back-propagation algorithm is used on a baseline image which is a pattern consisting of only 0s and a given classification, for example an extreme event in M_{NW} . The error generated by the network is then propagated back through the network, the weights of edges will show a stronger difference if they are important to the given classification where as those with little relevance will not change by a comparatively large amount (Simonyan, Vedaldi, and Zisserman 2014). When the errors reach the input nodes, they can be rank ordered to identify which pixels were contributing the most to the given classification, in this study this is achieved by normalizing between 0 and 1 the contribution values calculated.

Figure 6 shows the spatial contribution patterns for both $M_{NW,30}$ (left) and $M_{SE,10}$ (right). Both maps show little contribution from cells in the mid and western regions of the North Atlantic, however a strong contribution is present closer to the British Isles. $M_{NW,30}$ presents higher levels of contribution from both the Irish and North Seas whereas $M_{SE,10}$ relatively weak contributions from these regions but a higher level of contribution from coast of Brittany in north western France. Ummenhofer et al. (2017) shows the difference in SLPA across the North Atlantic for various precipitation anomaly patterns; the key difference in the patterns presented is the SLPA just west and south west of the British Isles (a positive SLPA leads to negative precipitation anomalies in the north west and negative SLPA indicates positive precipitation anomalies). Similarly, $M_{SE,10}$ shows interest over the south west of the UK which continues to match the findings of Ummenhofer et al. (2017).

Next, the saliency map for $M_{comp,10}$, which distinguishes between extreme events in the north west and extreme events in the south east, is shown in figure 4-7 and presents high level of contributions across the North of England, the Irish Sea and the coast of Brittany. This reinforces the case of local meteorological conditions creating the difference not only between extremes and regular rainfall events but also the difference between north west and south east extreme events. Further to this, both Figures 4-6 and 4-7 indicate on the day of occurrence the conditions across the rest of the North Atlantic are not contributing to the resulting classifications. This raises the question

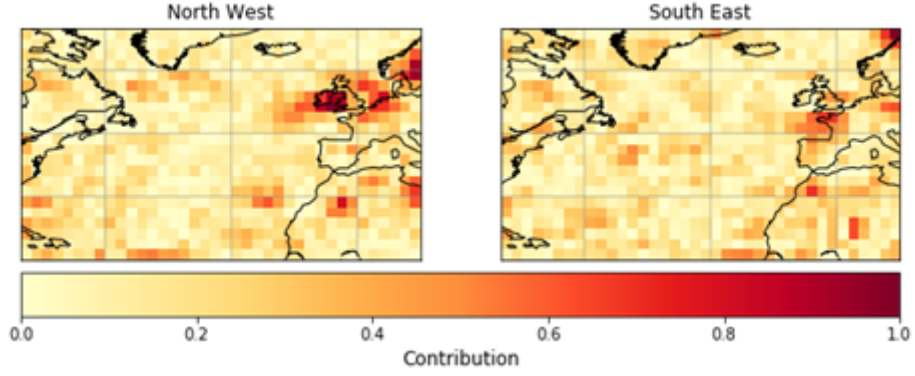


Figure 4-6: Saliency map showing the spatial contributions of SLPA patterns to classifying extreme and regular rainfall events for both $M_{NW,30}$ (left) and $M_{SE,10}$ (right).

of how these contributions could change if the classifiers were trained using patterns of the days prior to an event, as it is known that certain prior meteorological conditions are common to some extreme rainfall events (Allan, Blenkinsop, et al. 2020)).

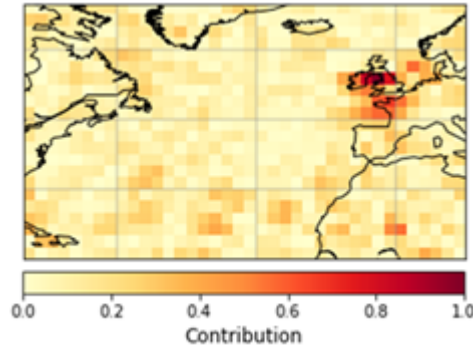


Figure 4-7: Spatial contributions of SLPA patterns in determining the difference between north west and south east extreme events.

4.5.3 4.3 Limitations

The neural network based approach used in this study relies heavily on the data used to train and test the models. As neural networks were trained to differentiate between extreme/regular rainfall events hence the training process is sensitive to how extreme events were selected. In this study a threshold method is used, which selects the top 10% of standardised rainfall days in each region to represent extreme events. The reasons for this selection are outlined in section 2.1; however, the use of an alternative threshold (e.g. 5%) or maxima based method would result in a set of models which vary greatly from the models presented here.

Furthermore, the method used for calculating the representative daily rainfall total for each region and day is the result of a trade-off, between computational time and accuracy. As presented in section 2.1 the representative sample for each day is collated from a regular grid of points at 30km intervals, the CEH-GEAR dataset is provided at 1km intervals; however, increasing the resolution of the regular grid would substantially increase the computational time required to calculate the average daily regional rainfall total. This trade-off was considered reasonable as the present study only uses the magnitudes to determine the extreme and regular events within each region. If, however we were to compare the magnitudes between regions then a different approach using higher resolution representations would be necessary.

Finally, the sensitivity analyses shown in section 4.2 highlights some interesting disparities between regular and extreme events in both regions. However, the interpretability and reliability of the sensitivity analysis are tied to the how effective the optimisation of the neural network’s parameters was during training. Hence with further fine tuning of the network’s parameters the resulting sensitivity analyses should reveal clearer disparities and offer further insight into the differences.

4.6 Conclusions

Neural network-based image classification was used to identify the concurrent, anomaly sea-level pressure (SLPA) differences across the North Atlantic between the following types of daily rainfall events for two homogenous rainfall regions in the UK:

1. Extreme and regular rainfall events in the north west of England.
2. Extreme and regular rainfall events in the south east of England.
3. Extreme rainfall events in the north west and south east of England.

Through the generation and optimisation of several neural network classifiers to represent each of the above scenarios the following conclusions can be drawn:

1. The differences in SLPA for extreme and regular rainfall events in both the north west and south east of England are close enough to make numerical classification difficult.
 - (a) Classifying between north western extremes and regular rainfall events has an accuracy 2% higher than classifying between south eastern extremes and regular events (62% and 60% respectively).

- (b) In both regional classifiers the precision and recall of extreme events are higher than those of the regular rainfall patterns, indicating extreme event SLPA patterns are more defined than regular events.
 - (c) In determining the differences between extreme events in the north west and those in the south east both recall and precision are higher for south eastern extremes, indicating the patterns relating to these events are more defined than those in the north west.
2. Saliency maps have been used to identify the spatial regions of SLPA which contribute to the classifications.
- (a) The local SLPA patterns across the British Isles is key to determining the difference between extreme and regular rainfall events in both the north west and south east.
 - (b) The mid and western North Atlantic however has been shown not to provide any substantial contribute to any of the classifications developed in this study.

Finally, the patterns presented in the sensitivity analysis indicate the potential for this method to be used to identify the spatial importance of meteorological variables in the days prior to extreme or regular events. This will aid meteorologists target the regions of importance without the need to incorporate global data, reducing computational requirements. Furthermore, opening this method to the application to other meteorological variables such as precipitable water, sea-surface temperature and geopotential height may enable further inference to be gained on why extreme events are different.

4.7 Acknowledgements

The authors gratefully acknowledge the NCEP Reanalysis data provided by the NOAA/OAR/ESRL PSD, Boulder, Colorado, USA, from their website at <https://www.esrl.noaa.gov/psd/> as well as the CEH-GEAR rainfall dataset provided by UKCEH, available through their website at <https://catalogue.ceh.ac.uk/documents/ee9ab43d-a4fe-4e73-afd5-cd4fc4c82556>.

4.8 Postscript

This chapter presented a study which addresses **Hypothesis 3**. To do this a new neural network based classification scheme was developed to distinguish between heavy and regular rainfall events for two hydrologically diverse regions of the UK. Three classification models were developed to distinguish between the following subsets of rainfall data from the two regions:

1. Heavy and regular rainfall events in the North West of England.
2. Heavy and regular rainfall events in the South East of England.
3. Heavy rainfall events in the North West of England and heavy rainfall events in the South East of England.

The models were trained to make this distinction using the mean sea-level pressure fields of the North Atlantic. The resulting models for each of these experiments were then compared using their accuracy in distinguishing between the event types. Finally, a sensitivity analysis was carried out to identify which regions of the mean sea-level pressure fields used were important in the models' classification.

The results of these experiments highlight that although the neural network models were capable of distinguishing between the heavy and regular rainfall events they are only able to achieve mild improvement on random guessing achieving 60-62% accuracy. The sensitivity analysis however did reveal that for all three experiments the localised mean sea-level pressure fields to the west of the UK contribute the most to the resulting classifications with little to no influence being given by the mid to western Atlantic.

Although these results indicate the neural network architecture used in this chapter is not practically capable of providing useful distinctions between the MSLP patterns responsible for extreme rainfall events in different regions of Great Britain. However, they do indicate that neural network do have potential in interpreting the atmospheric fields. Considering the approach in this chapter methodologically the process used to define heavy and regular rainfall events would have a substantial impact on the model's ability to differentiate them. Further to this, Richardson *et al.* (2020a, 2020b) indicates the pressure fields surrounding the UK can be used for sub-seasonal forecasting of both drought and flood conditions.

Future work, could investigate the sensitivity to the classification procedure to the architecture and other hyper-parameters of the neural network. Moreover, the inclusion of other meteorological variable combinations could be used to identify a high-performing

classification model while providing further inference as to what makes extreme events different. This leads to the question of whether alternative neural networks would be able to improve forecasting potential through the analysis of these fields instead of distinguishing between heavy and regular events. This question is answered in the next chapter which addresses **Hypothesis 4**.

Chapter 5

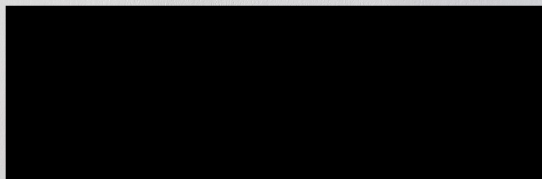
Forecasting sub-seasonal rainfall in Great Britain using convolutional-neural networks

5.1 Preamble

Chapters 3 and 4 have shown how atmospheric patterns across the North Atlantic can be used to identify and distinguish rainfall events; chapter 3 specifically highlighted the dependence of mean sea-level pressure and air temperature. In the present chapter new neural network based methodology is developed for forecasting sub-seasonal rainfall events hence addressing **Hypothesis 4**.

This chapter reports on a study currently in review for Meteorological Applications. The study begins by extracting regional, monthly rainfall values for all administrative regions of Great Britain. For each of the rainfall events both the mean sea-level pressure and air temperature patterns from across the North Atlantic were extracted using ECMWF SEA5 hindcasts at 1, 3 and 6-month leadtimes (**Objective 4.1**). A new neural network model is produced for each leadtime which accept a mean sea-level pressure and air temperature pattern as input to produce a regional series of rainfall values for the representative month (**Objective 4.2**). Finally, these models are evaluated both in terms of accuracy and bias, with a comparison made to the original ECMWF SEAS5 precipitation hindcasts (**Objective 4.3**).

5.1.1 Authorship Statement

Status	In Review in Theoretical and applied climatology.
Details	Barnes, A.P., McCullen, N, Kjeldsen, T.R. (in review) Theoretical and applied climatology. 2021.
Authors' contribution	<p>The author of this thesis has primarily (90%) contributed to design and implementation the methodology adopted for the extraction, clustering and analysis of both the atmospheric and rainfall data. Each author's exact contributions are as follows:</p> <p>A.P. Barnes: Formulation of ideas (100%), design of methodology (95%), data collection (100%), processing and analysis of data (100%), manuscript preparation (85%).</p> <p>N. McCullen & T.R. Kjeldsen: design of methodology (5%), manuscript preparation (15%)</p>
Date and Signature	 19-07-2021

5.1.2 Abstract

Traditional weather forecasting approaches use various numerical simulations and empirical models to produce a gridded estimate of rainfall, often spanning multiple regions but struggling to capture extreme events. The approach presented here combines modern meteorological forecasts from the ECMWF SEAS5 seasonal forecasts with convolutional neural networks (CNNs) to improve the forecasting of total monthly regional rainfall across Great Britain. The CNN is trained using mean sea-level pressure and 2m air temperature forecasts from the ECMWF C3S service using three lead-times: one month, three months and six months. The training is supervised using the equivalent benchmark rainfall data provided by the CEH-GEAR (Centre for Ecology and Hydrology, gridded estimates of areal rainfall). Comparing the CNN to the ECMWF predictions shows the CNN out-performs the ECMWF across all three leadtimes. This is done using an unseen validation dataset and based on the root-mean square error (RMSE) between the predicted rainfall values for each region and benchmark values from the CEH-GEAR dataset. The largest improvement is at a one-month leadtime where the CNN model scores a RMSE 6.89mm lower than the ECMWF. However, these differences are exacerbated at the extremes with the CNN producing, at a one-month leadtime, RMSEs which are 28.19mm lower than the corresponding predictions from the ECMWF. Following this, a sensitivity analysis shows the CNN model predicts increased rainfall values in the presence of a low sea-level pressure anomaly around Iceland, followed by a high sea-level pressure anomaly south of Greenland.

5.2 Introduction

Rainfall variation plays a significant role in the UK’s long-term investment strategy and this variation takes two forms. The first is the effect of droughts, or prolonged periods of lower-than expected rainfall, such as the dry summer of 2012, which resulted in farmers struggling to grow and harvest crops and a heightened risk of wildfires (Huntingford et al. 2014). The second effect is flooding from high levels of precipitation, with two prominent examples of this being storms Ciara and Dennis from February 2020, which resulted in over £300 million worth of damage and costing the lives of five people (Emerton 2020). However, these are not isolated events but form an increasingly apparent change in rainfall intensity, with increasingly wetter winters and drier summers (e.g., Murphy et al. 2020). Therefore, it is important to increase our understanding of how and why these extremes occur.

Previous research has demonstrated that the magnitude and spatial distribution of rainfall are tied to the patterns of atmospheric circulation (Utsumi, Kim, et al. 2017; Baker, Shaffrey, and Scaife 2018; Gimeno, Vázquez, et al. 2020). This is especially true during winter, when the precipitation variability over the British Isles is heavily influenced by the North Atlantic Oscillation (NAO), an index which is characterized by the pressure difference between the Azores and Iceland (Brown, 2018). The NAO has been found to exert a strong influence on the storm track and strength of extra-tropical cyclones crossing the North Atlantic Ocean (Huntingford et al. 2014). These storms which originate over the North Atlantic are the main contributors to European rainfall (Gimeno, Vázquez, et al. 2020). Other studies have identified links between NAO and flood levels (e.g. Hannaford and Marsh 2008; Macdonald, Phillips, and Mayle 2010).

Neal et al. (2016) created two classification models to investigate the synoptic atmospheric conditions leading to dry and wet periods, respectively, across the entire United Kingdom. The classification models grouped daily atmospheric conditions into either one of thirty or one of eight types depending on which model was being used. These models were developed by using daily sea-level pressure patterns across northern Europe and the North Atlantic and clustering them using a simulated annealing variant of the k-means clustering algorithm. Neal’s models use the mean sea-level pressure anomalies across the North Atlantic to classify every day into one of thirty different circulation types. Subsequently, the set of 30 circulation types was reduced to a smaller set consisting of eight circulation types; the most prominent of which represent the positive and negative phases of the NAO. Using these eight patterns, Richardson et al. (2017) were able to show how certain patterns such as a negative NAO with a blocking

pattern or anticyclonic conditions over the UK result in drier conditions than average. Furthermore, Richardson et al. (2017) also showed how a positive NAO pattern or a strong cyclonic pattern to the south west of the UK can result in wetter than average conditions. Similarly, Ummenhofer et al. (2017) used clustering techniques to group the precipitation rates across Europe into five types. The average sea-level pressure anomalies for each of these types were grouped together and showed strong relationships between the dominant pressure systems over the Arctic and Europe to the precipitation variability over the UK. None of the studies listed above appear to include temperature as a covariate despite the key relationship between temperature and rainfall via the Clausius-Clepyeron (CC) relation which states a warmer atmosphere can hold more water than a cooler one (Blenkinsop et al. 2015). The relationship between temperature and rainfall via the CC relation is evident but vary across a spatial domain even as small as the UK (Blenkinsop et al. 2015). Further studies also show a stark contrast in synoptic temperature conditions related to heavy or intense rainfall events (Allan, Blenkinsop, et al. 2020).

Baker et al. (2018) used several linear regression models to explain up to 76% of regional rainfall variability in the UK using a series of selected sea-level pressure metrics. Richardson et al. (2020) further expanded the work on the original circulation pattern analysis of Richardson et al. (2017), to show that weather patterns can be used to inform both medium-range precipitation forecasting, highlighting that the use of the weather patterns in forecasting increased the accuracy of the drought forecast. Recently there has been a move towards the use of neural networks to predict future rainfall. A review by Pham et al. (2020) found that neural networks can generally predict daily and sub-daily rainfall to within 10mm or less. Kumar et al. (2019) used a neural network to predict the monthly- rainfall totals across several hydrologically homogeneous regions in India. However, the greatest success was reported by Haidar & Verma (2018), who developed a one-dimensional convolutional neural network (CNN) using climate variables (including, but not limited to, max temperature, min temperature, southern oscillation index, dipole mode index and interdecadal pacific oscillation) to predict monthly rainfall total in eastern Australia. They found that the resulting model showed higher predictive performance than the recently released Australian Community Climate and Earth System (Hudson et. al. 2017). Recently, CNNs have been shown as capable at predicting gridded precipitation; first Larrando et al. (2019) uses Geopotential Height fields across the North Atlantic to predict total 3-hourly precipitation across Western Europe presenting more accurate results than alternative traditional machine learning approaches such as regression. In contrast, Rasp and Thuerey (2021) used a large number of input variables including geopotential height, temperature, wind speeds, specific

humidity and 6h accumulated precipitation to predict gridded rainfall estimates with cells 5.625° . Although both studies present promising results neither provided a true sub-seasonal forecast. An image-based CNN would allow the interpretation of images, such as those used by Neal et al. (2016) but using the powerful inference offered by the CNN architecture shown by Haidar & Verma (2018), Larrando et al. (2019) and Rasp and Thuerey (2021).

The present work fills this gap by producing a novel sub-seasonal rainfall forecasting methodology which uses image-based convolutional neural networks along with the meteorological forecasts from the ECMWF. The convolutional neural networks used are a novel deep learning approach, which combine both high-resolution sea-level pressure and 2m air temperature forecast patterns across the North Atlantic to produce regional, monthly rainfall predictions. These models are then compared to the ECMWF SEAS5 precipitation forecasts (Johnson et al., 2019) using three different lead times (one month, three months and six months). To begin with, this study describes the datasets and pre-processing carried out (section 2), before introducing CNNs in section 3, detailing the architecture and training progress of the selected model in section 3. The forecasts from the CNN are then compared with those from the SEAS5 system (section 4), before making concluding remarks regarding the potential for CNNs to be used to predict regional rainfall.

5.3 Data

Training the CNNs requires three key datasets: (1) the benchmark (observed) regional precipitation, (2) the forecasted mean-sea level pressure, and (3) 2m air temperature (2AT) patterns across the North Atlantic. Forecast precipitation is then also required to allow a comparison between the accuracy of the CNN model and that of the ECMWF SEAS5 model. This section begins by describing the extraction of the observed and forecasted regional rainfall before describing the process of extracting forecasted North Atlantic mean sea-level pressure (MSLP) and North Atlantic 2AT data. Finally, this section concludes by describing the separation of the dataset into training, testing and validation.

5.3.1 Regional Precipitation

Regional, series of observed monthly precipitation totals (mm) covering the land surface of Great Britain are extracted from the CEH-GEAR (Tanguy et al. 2015) and the forecasted precipitation totals (mm) extracted from the ECMWF SEA5 (Johnson et

al. 2019). The CEH-GEAR dataset represents the benchmark precipitation and is used to train the CNN model. The predictions made by the CNN are then compared to the precipitation hindcasts made by the ECMWF SEA5 service. Both datasets are used to produce average cumulative monthly rainfall between 1993 and 2017 for the 13 regions administrative regions of Great Britain (Figure 5-1).



Figure 5-1: The 13 regions of Great Britain (a) and the corresponding 20km by 20km points (b) used to aggregate monthly rainfall totals (mm).

Benchmark regional rainfall

The CEH-GEAR dataset is a daily-mean rainfall dataset provided on a $1\text{km} \times 1\text{km}$ grid covering the British Isles. The dataset spans the years 1950 to 2017, however only data from 1993 to 2017 were used in this study due to the more limited range of the ECMWF hindcasts dataset as described in the section 2.1.2. First, the daily CEH-GEAR data were aggregated to monthly values (mm). Next, the monthly rainfall data were further aggregated spatially to represent rainfall in each of the 13 regions. This was achieved by defining 598 points at 20km intervals across the UK as shown in Figure 5-1 (a). For each region, a representative monthly rainfall value is represented by the average monthly cumulative total of all points within the region's boundaries.

ECMWF SEAS5 forecast regional rainfall

Forecast of bias-corrected rainfall data provided by the ECMWF SEA5 model was retrieved through the for three different lead times, one month, three months and six months. As the ECMWF SEA5 results are provided as an ensemble of 52 model realisations, the ensemble mean is used. Rainfall data for each lead time variant is provided in cumulative monthly values (mm) at a global resolution of $1^\circ \times 1^\circ$ cells, the

data used in this study is bound between $[100^{\circ}\text{W}, 70^{\circ}\text{N}]$ and $[20^{\circ}\text{E}, 10^{\circ}\text{N}]$. This data is then aggregated for each region to produce a total monthly rainfall value for each region for the months available. To do this for a given region and month, the month's rainfall data is first retrieved and is represented by a matrix of $1^{\circ} \times 1^{\circ}$ cells. Next, each point within the selected region takes the value of the CEH-GEAR cell which contains it. Finally, the values for each point can be averaged to produce a total monthly rainfall value for the given region during the given month. Completing this operation for each month and each region produces a rainfall data matrix of size $[13, 288]$ ([N-Regions, N-Months]).

5.3.2 Meteorological Data

Similarly to the rainfall data discussed in section 2.1.2, the large-scale atmospheric dataset used in this study is provided at a $1^{\circ} \times 1^{\circ}$ resolution and is obtained from the ECMWF SEA5 system and provided bias-corrected (Johnson et al. 2019). The variables of interest are the bias-corrected MSLP and bias-corrected 2AT. Both variables are provided globally and are forecasted using multiple lead times, with the MSLP provided in units of Pascal and the 2AT provided in Kelvin, as discussed above the ensemble mean is taken for both the MSLP and 2AT patterns. As this study is focussing on the synoptic conditions in the North Atlantic Ocean, a subset of the data between -100° -20° longitude and 10° -70° latitude was extracted for each of the three chosen lead times (one month, three months and six months). For each lead time, each month is then represented by two matrices of size 121×61 , one for the 2AT and the second for the MSLP with each entry representing a $1^{\circ} \times 1^{\circ}$ spatial cell. The resulting dataset consists of 288 matrices for AT and 288 matrices for MSLP, one for each month covering the 24-year study period (1993 – 2017).

5.3.3 Data Separation

The final step in data preparation is to distinguish the data used for training, testing and validation. The training data will be used to train and optimise the network, the testing data will be used in a hold-out testing scheme to ensure the models are not overfitting and finally the validation data will be used to evaluate model performance after development. To begin, the validation dataset is set to contain the data from the years 2013 to 2017, then the remaining months are split randomly between training (70%) and testing (30%).

5.4 Forecasting Method

Three convolutional neural networks (defined below) were developed to forecast the monthly regional rainfall values across Great Britain using three different lead times, the inputs and outputs of each CNN are shown in Figure 5-2. This section introduces convolutional neural networks, their components and the architecture of the network followed by an outline of the training method including details on the data standardization procedure used prior to training. CNNs are selected due to their capabilities of interpreting image data where traditional neural networks would fail, covering a wide variety of applications from tumour identification (Yang, Yang, et al. 2019) to video classification (Karpathy et al. 2014).

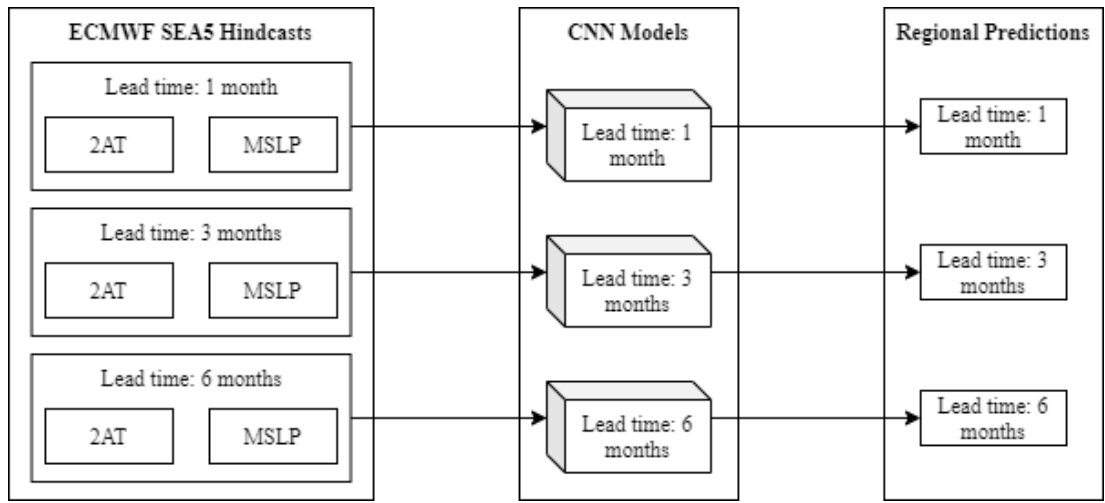


Figure 5-2: The three forecast models showing their inputs and outputs.

5.4.1 Network Structure

Convolutional neural networks (CNNs) are a type of neural network that specialise in interpreting data that are in image form, which in the present case are images consisting of two matrices: the 2AT and the MSLP patterns. The resulting input matrix for each month is a 3D matrix of size $[2 \times 121 \times 61]$, the first $[121 \times 61]$ slice containing the MSLP and the second containing the 2AT. During training this matrix is fed through the layers in the CNN with each layer performing a unique matrix transformation, the layers used in the models for this study are detailed below.

The name (CNN) is derived from the networks' use of convolutional (i.e., a layer which performs many different operations on the input) layers. An example convolutional layer is provided in Figure 5-3. Here the layer accepts a $[3 \times 3]$ matrix as its input

matrix, it then passes a predefined kernel (mask) over the image in increments (also known as the step-size) of one pixel. At each step the kernel is multiplied by the pixels underneath it, then summing the resulting values to produce the output of this step. The outputs of each step are put back together to form a new lower-resolution image. In this case the kernel (defined here as a 2x2 block with a row of two 1s above a row of two 0s, indicating the kernel is looking for a horizontal line) has identified a horizontal line at the top of the image and no horizontal lines below this. This can be seen in Figure 5-3 where a 2 is produced for both the top left and top right hand corners indicating both of these contain some or all of a horizontal line. In practice it is common to use multiple kernels at each layer such that each layer can capture many different features. These result in an output matrix larger than that of the input matrix; for example, if three kernels of size $[2 \times 2]$ were used on a $[3 \times 3]$ matrix input the resulting output would be $3 \times [2 \times 2]$ (three kernels of size $[2 \times 2]$).

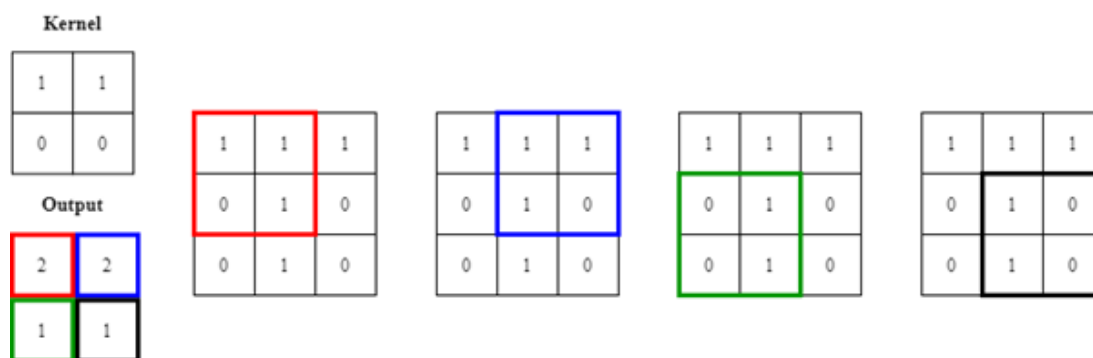


Figure 5-3: A convolution applied to a 3-by-3 image using a 2-by-2 kernel. The kernel is moved over the image by one pixel at a time, calculating the value of the subsection by multiplying the kernel by the pixels highlighted.

Using multiple kernels in a single layer then presents a problem of complexity, increasing the size of the data as it moves through the convolutional layer further increases the computational resources needed for processing. To counteract this the implementation of max-pooling layers are used, which also reduce the dimensionality of the data. Max-pooling layers look through a kernel but instead of multiplying the pixels under it, the patch simply takes the maximum pixel value and uses this to represent its output. This process is illustrated in Figure 5-4 using a variation of the $[3 \times 3]$ matrix present in Figure 5-3. As the max pooling layers generally follow a convolutional layer the input they receive is a multi-dimensional matrix, in the example described in the above paragraph the output provides $3 \times [2 \times 2]$ matrices (one $[2 \times 2]$ for each kernel). Each kernel's output is processed independently, such that the number of matrices outputted by max pooling layers stays the same as the number which are given to them. However, these matrices

will have reduced dimensions. Take for example an output from a convolutional layer of $5 \times [3 \times 3]$ matrices, feeding this into a max pooling layer as shown in Figure 5-4 will produce $5 \times [2 \times 2]$ matrices.

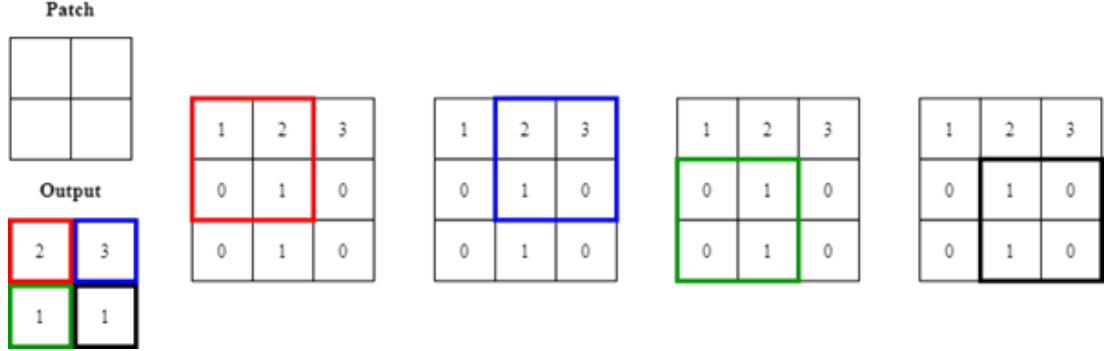


Figure 5-4: A max-pooling operation applied to a 3-by-3 image using a patch of size 2-by-2. As the patch moves across the image it extracts the maximum pixel value at each timestep.

Max-Pooling layers enables the CNN to reduce the dimensionality of the data. Relating this back to the datasets described in section 5.3, the input is a 3D matrix ([variables, latitude, longitude]=[2, 61, 121]) but the output is a vector of length 13 (a monthly rainfall value for each of the 13 regions), so a final set of layers is needed to convert the multi-dimensional outputs of the convolutional/max-pooling layers to a 1D matrix. To do this, a linear layer is used; an example of which is shown in Figure 5-5. The linear layer consists of several nodes each of which is connected by a weighted edge to every pixel in the output of the layer before it (also referred to as fully connected layers). The output (y) for all nodes in the linear layer can then be calculated as:

$$\mathbf{y} = \mathbf{x}\mathbf{W}^T + \mathbf{b}, \quad (5.1)$$

where \mathbf{x} is an array containing the output of the previous layer and the weights matrix \mathbf{W}^T is of size $[|\mathbf{x}| \times |y|]$ and \mathbf{b} is a randomly initialised bias term (of size $[1 \times |y|]$). The resulting vector \mathbf{y} is then passed through an activation function, which in this case is a rectified linear unit function on each element, this activation function applies an absolute function to the values, ensuring all output values in \mathbf{y} are positive.

The architecture of the CNNs produced for this experiment is shown in Figure 5-6. Figure 5-6 also shows how the size of the data moving through the network is changing, in the first convolutional layer for example the original input image is split into a $16 \times [30 \times 60]$ matrices. This indicates that in the first convolutional layer there

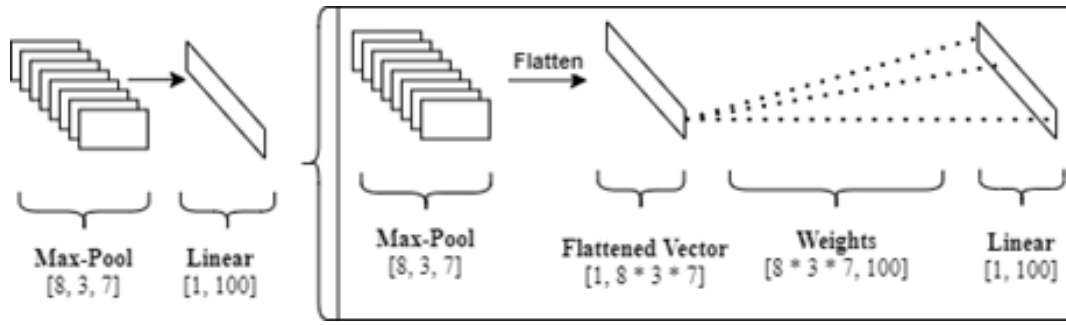


Figure 5-5: A linear layer example following a max pooling layer. This example shows a max pooling layer with output dimensions $[8, 3, 7]$ feeding into a linear layer of size $[1, 100]$. The max-pooling output is first flattened into a 1D vector. Each value in this vector is then connected to every node in the linear layer via a weighted edge which results in a weights matrix of size $[8 \times 3 \times 7, 100]$. The linear layer then uses these weights and the flattened max-pooling vector to calculate the layer's output as described by Equation 5.1.

are 16 randomly generated kernels (all kernels used are of size $(2, 2)$), the kernels are randomly generated to enable to identification of features which may not have been previously known. An activation layer then follows each convolutional layer using the ReLU function $\max(x, 0)$. These are then reduced in size through the first max-pooling layer before being fed into the second convolutional and max-pooling layers. Following these the output is passed through two linear layers, the first containing 100 neurons and the second containing 13. This final linear layer of 13 neurons outputs the monthly rainfall predictions for each of the 13 regions.

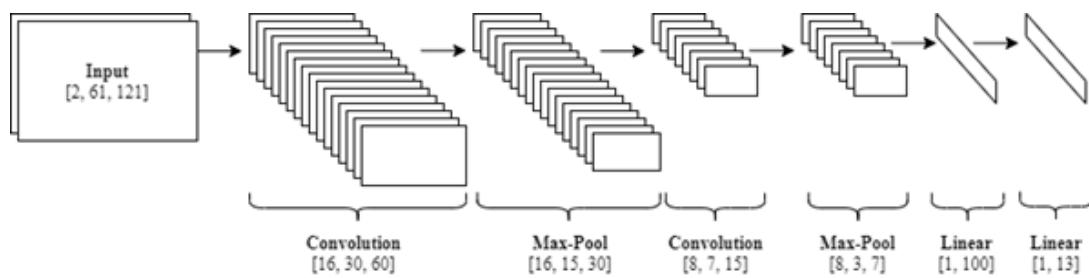


Figure 5-6: Architecture of the convolutional neural network model. Each layer is provided with the number of dimensions of its output matrix. For example, the first convolutional layer has an output size of $[16, 30, 60]$, this also indicates the number of filters used in the layer (16). These are followed by max-pooling layers and finally two dense linear layers.

5.4.2 Training

As two separate variables with different scales and units are used for the input, they are standardized separately, such that both the 2AT matrix and mean sea level pressure were standardized by the mean and standard deviation of each of their individual matrix elements. Once standardized these images were recombined into the $[2 \times 61 \times 121]$ matrices required for training. Next, to reduce the potential for overfitting the data are split randomly into two groups; a training and a validation dataset. The training dataset was used for training the weights of the CNN, whereas the validation data was used to compare the model predictions to those of the ECMWF system. Hence, of the data available, the months between 2013 and 2017 were retained for validation purposes and the remaining months between 1993 –2012 were used for training. To train the weights of the CNN the Adam optimisation (Kingma and Ba 2015) method is used along with the root mean-squared error (MSE) defined as,

$$RMSE(x, y) = \sqrt{\frac{\sum_{i=1}^n (y_i - x_i)^2}{n}}. \quad (5.2)$$

Finally, to ensure the models are optimal a stopping condition is used through a hold-out testing scheme, on each epoch the testing data is used to calculate a testing loss. If after 5 epochs the testing loss does not reduce the training scheme will revert the parameters to the epoch with the lowest testing error.

5.5 Validation Results

This section details first a comparison between the forecasting capability of the trained CNN model developed in this study and the existing ECMWF model using only the validation dataset which was not used during training, then breaks down the CNN model to identify what features have been identified in the large-scale data as being most influential for informing the predictions (section 5.5.2).

5.5.1 Model Comparisons

To ensure a fair comparison only validation data is used to compare the ECMWF and the CNN models. Figure 5-7 shows both the CNN and ECMWF predictions against the benchmark rainfall for the validation dataset. For all three lead times the CNN shows wider spread in its predictions, especially when predicting the lower rainfall values. Decreasing the lead time from six months to three months appears to make little difference to the distribution of the predictions. However, at a one month lead

time the ECMWF predictions present a smaller range of predicted rainfall which comes at the cost of constant over prediction of the lower rainfall values and under-prediction of the higher rainfall values. Contrary to this, the CNN model yields a larger variation in the predictions of very low and very high rainfall amounts but appear to be less biased.

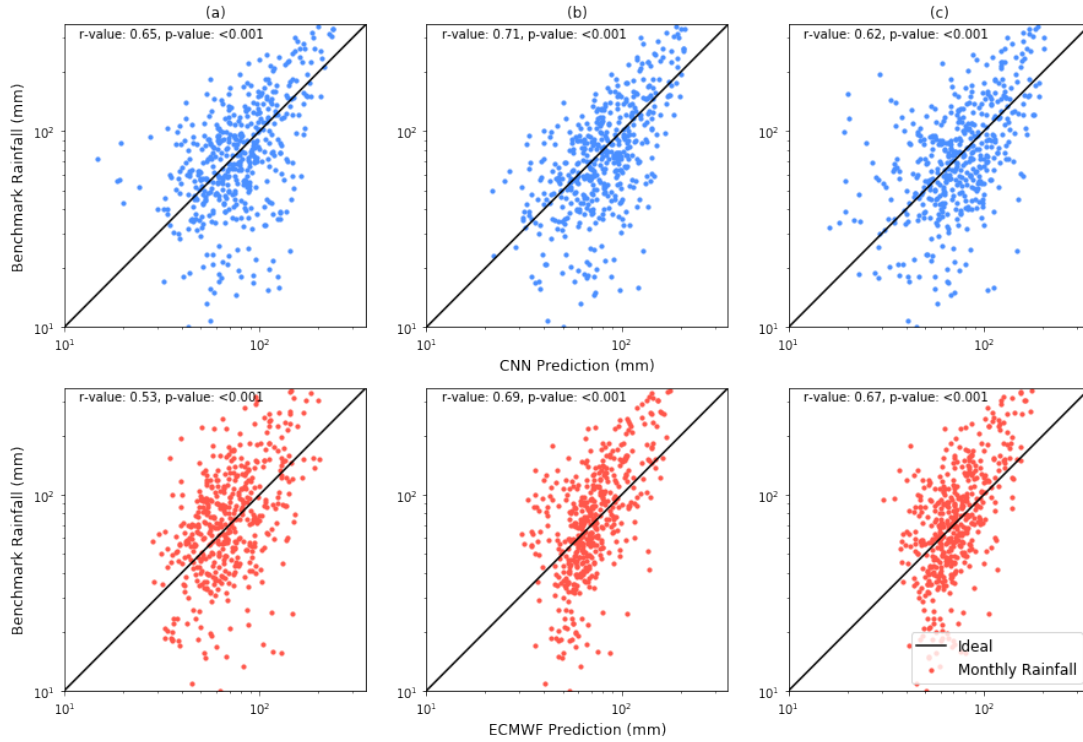


Figure 5-7: Validation rainfall predictions against benchmark rainfall for both the CNN and ECMWF methods in all three lead times: (a) one month, (b) three months and (c) six months.

As shown in Table 5.1 the three-month variants of both models perform the best, with the lowest RMSE scores. This trend is found in both the validation RMSE scores and the overall dataset RMSE scores. In all leadtimes and in both dataset variants the CNN outperforms the ECMWF model, this is to be expected in the overall dataset (training, testing and validation) as the CNN was specifically trained using the data being evaluated. However, this does not explain the increased accuracy the CNN has in the validation dataset which was not available during training.

Further investigating the bias in the models towards the central range of rainfall values Figure 5-8 shows a summation of the residuals (differences between the benchmark and predicted rainfall) against the benchmark rainfall values for a three-month lead time.

Model	Leadtime	RMSE	
		Validation	Overall
CNN	1	46.47	38.09
	3	43.27	37.99
	6	48.53	39.02
ECMWF	1	53.36	47.50
	3	48.65	45.86
	6	49.60	52.26

Table 5.1: The RMSE scores for both the CNN and ECMWF models covering all three leadtimes given the validation dataset, the top 5% of all events in each region and the complete, overall dataset are given.

This illustrates the strong under prediction of the higher rainfall values in both the CNN and ECMWF predictions; moreover, this highlights a weaker bias in the CNN model with approximately half the final cumulative residual compared to the ECMWF predictions. Following this, a weaker bias can be seen in the rainfall values leading up to 100mm with a general trend of over prediction in both models, of which the CNNs bias appears stronger. A similar trend is seen for both one-month and six-month lead time predictions.

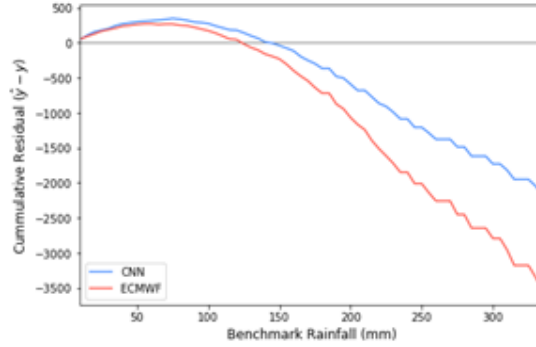


Figure 5-8: Cumulative residual of both methods using a three-month lead time against the actual regional rainfall.

Following this, it is important to identify any regional or seasonal bias in the predictions, to do this proportional errors are generated for each of the 13 regions across Great Britain and for each of the 12 months of the year. Figure 5-9 (top row) shows the proportional error for each region and each month of the year. To do this, the mean-absolute error (MAE) is used to calculate the differences between the two series, the general equation for the MAE is defined as,

$$MAE(x, y) = \frac{\sum_{i=1}^n |y_i - x_i|}{n}. \quad (5.3)$$

Subsequently, the MAE can then be used to calculate the proportional regional error (PRE) for a given region i ,

$$PRE_i = \frac{MAE(p_i, \hat{p}_i)}{\bar{p}_i}. \quad (5.4)$$

Here the mean-absolute error between the benchmark rainfall series (p_i) and predicted rainfall series (\hat{p}_i) is divided by the mean benchmark rainfall (\bar{p}_i) for the given region i . This indicates how far away the predictions are based on the region's average rainfall value. Similarly, the proportional monthly error (PME) can be calculated as:

$$PME_m = \frac{MAE(p_m, \hat{p}_m)}{\bar{p}_m}. \quad (5.5)$$

As with equation 3, the difference between the benchmark series (p_m) and predicted rainfall series (\hat{p}_m) is divided by the mean benchmark rainfall (\bar{p}_m) for month m where $m = 1, \dots, 12$.

The values of PREs are below 52% for all lead times and all regions; despite this, at a one-month lead time there is a disparity between the CNN and the ECMWF predictions. The CNN errors at a one-month lead time are highest for regions in the south east of Great Britain (London, South East England and East of England) whereas the ECMWF errors are higher for the west of Great Britain (Wales, South West England and North West England). This can be attributed to the known rainfall gradient across the UK, where western regions are likely to receive higher levels of rainfall and geographic effects produce a rain-shadow over the east (Mayes and Wheeler 2013). As described above and shown in Figure 5-8, the ECMWF model produces larger errors for the higher rainfall values which are those occurring more in the west and north west regions where as, the CNN provides more accurate predictions for the higher rainfall values which according to Figure 5-9 comes at the cost of predicting east and south eastern rainfall. However, due to the different drivers of rainfall across the UK (Baker, Shaffrey, and Scaife 2018) this error could be representing the CNN identifying one rainfall driver and discounting the others.

The bottom row of Figure 5-9 shows values of PME and highlights significant bias in the forecasted precipitation between month of the year. First, the CNN across all three lead times produces high errors for April, June and September, whereas the ECMWF forecasts have the largest proportional errors for April, September and October. However, the magnitude of these errors is different, with the CNN mis-predicting June

rainfall by 100% of June's average rainfall whereas the ECMWF forecasts only mispredicts June by 47.5%. September is shown to be difficult to predict with both models producing an error of 91.1% of the average September rainfall.

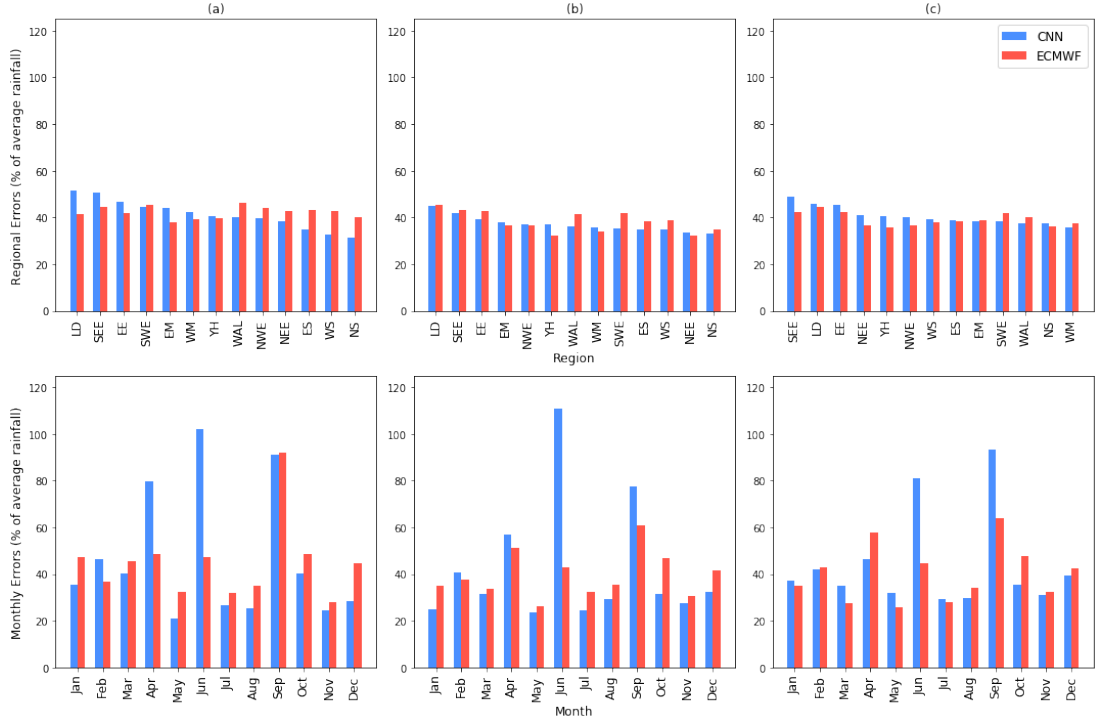


Figure 5-9: Regional and monthly rainfall areas as a proportion of the average rainfall for the given month or region. This is given for both methods and all three lead times: (a) one month, (b) three months and (c) six months.

5.5.2 Sensitivity Analysis

The benefit of using a convolutional neural network is that the weights between each layer can be used to identify the pixels of the input matrix which attribute the most to a given region's rainfall prediction. To do this the integrated gradients method is employed (Sundararajan, Taly, and Yan 2017). Integrated gradients determines the importance of each pixel in the original image for, in this case, increasing the predicted rainfall value. For example, a negative attribution value indicates a pixel lowered the resulting rainfall prediction whereas a positive attribution increases the resulting rainfall value. Figure 5-10 shows the normalized attribution of each MSLP (a) and 2AT (b) pixel for both North West England (top) and South East England (bottom).

Figure 5-10(a) shows three dominant areas of interest for both NW and SE England; firstly, a strong negative attribution can be seen south west of Iceland, stretching

towards the south west of the UK. This negative attribution will increase the magnitude of the rainfall prediction for both NW and SE England if the meteorological patterns contains a negative MSLP anomaly. Should the region instead contain a positive MSLP anomaly the rainfall values will decrease. In contrast the second and third areas of interest as shown by the positive attribution values to the east of Newfoundland and surrounding Cape Verde, west of Africa. These regions of positive attribution will amplify the rainfall predictions if they contain positive MSLP anomalies and decrease the prediction if they contain negative MSLP anomalies.

The amplification of rainfall values due to a low-pressure anomaly to the west of the British Isles as shown in Figure 5-10(a) agrees with the findings of previous studies (Richardson, Fowler, Kilsby, and Neal 2018; Ummenhofer et al. 2017; Baker, Shaffrey, and Scaife 2018; Richardson, Fowler, Kilsby, Neal, and Dankers 2020). However, Figure 10(a) also shows an extra region of higher pressure, south of Greenland, which further amplifies rainfall magnitude. This extra high-pressure anomaly could aid in the creation of a deep pressure gradient, increasing wind speeds between the centres and further enhancing mixing of the cold polar air from the North and the warm moist air from the south. This mixing of cold and warm air is further shown by Figure 10(b) which presents a combination of both positive and negative 2AT attributions around the UK. All leadtimes present a band of negative 2AT attributions stretching from the North Atlantic Ocean in a north easterly direction across the south of Great Britain towards Sweden and Norway. This band of negative 2AT is surrounded by mostly positive 2AT attributions and indicates a strong 2AT gradient in the area. However, for increasing the prediction for SE England the attributions show a less distinct characterisation between the air masses indicating strong mixing of the cold and warm air masses.

Furthermore, the MSLP positive attributions around Cape Verde could indicate the models are also enhancing rainfall when the MSLP anomaly differences between the north and mid-Atlantic Ocean are highest. This agrees with the findings of Baker et al. (2017), who also show that a pressure difference between a point between Scotland and Iceland and a point near Africa correlates strongly to rainfall in the UK. These MSLP differences appear to simulate the North Atlantic Oscillation index (NAO) which determines the MSLP difference between Iceland and the Azores. A heightened NAO is known to correspond to increased rainfall in the UK as highlighted by Brown (2018).

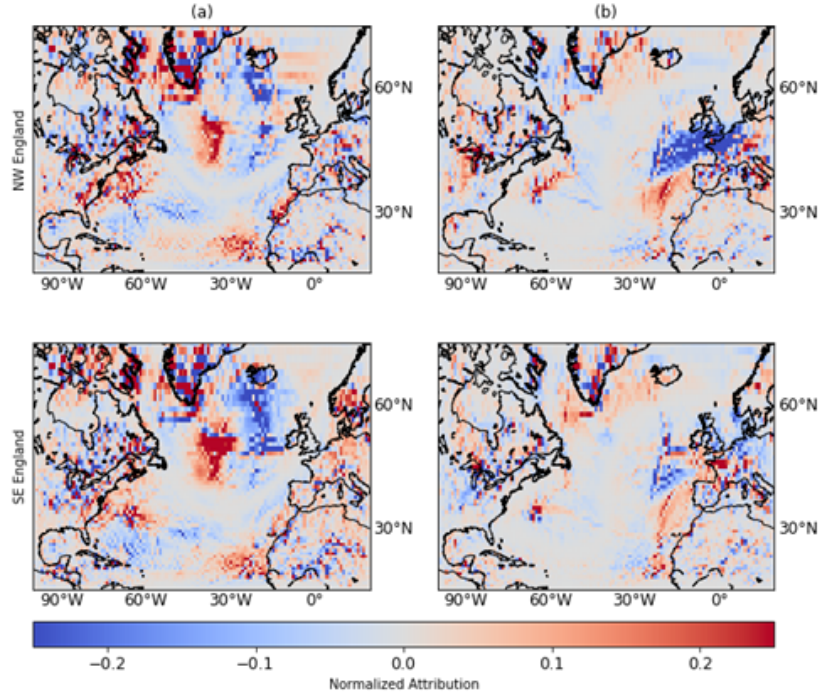


Figure 5-10: Normalized attribution values for increasing rainfall predictions in both NW England (top) and SE England (bottom) for both MSLP (a) and 2m air temperature (b).

5.6 Conclusions

This paper has shown for the first time that convolutional neural networks (CNN) can be used as a tool for enhancing monthly, regional rainfall forecasting in the UK through the interpretation of forecasted mean sea-level pressure and 2m air temperature patterns. Three CNN models were trained using monthly, regional rainfall from the CEH-GEAR dataset and MSLP & 2AT anomaly patterns from the ECMWF monthly hindcasts. Each model was trained using a different lead time – either one month, three months or six months. A validation dataset was then used to compare the predicted regional rainfall values with those of the ECMWF precipitation hindcasts given at the same lead times. The CNN models were then analysed using an integrated gradients technique to explore how it made its predictions. The key results are as follows:

1. The CNNs provided more accurate regional monthly rainfall totals than the ECMWF SEAS5 model across all three leadtimes.
 - (a) The CNN predicts the validation regional monthly rainfall totals with a lower RMSE than the ECMWF SEAS5 model for all three leadtimes. The RMSE

improvements are as follows: 6.89mm (one-month), 5.38mm (three-months) and 1.07mm (six months).

- (b) Predicting the entire dataset including the training, testing and validation data series the CNN models continue to outperform the ECMWF SEAS5 predictions by the following RMSE differences for each leadtime: 8.96 (one-month), 7.87 (three-months) and 13.24 (six-months).
 - (c) The CNN model's residuals indicate the CNN has higher accuracies when predicting the heaviest rainfall events compared with the ECMWF SEA5 model.
2. The CNN models show spatial and seasonal bias in its predictions.
- (a) The CNNs provide the most accurate results for northern and western regions of Great Britain but do not perform as well for the eastern and south-eastern regions.
 - (b) The CNNs perform well for some months of the year (December, July, August, November and May) but produce very large errors for the months of June, September and April (over double the average rainfall for the month of June).
3. Sensitivity analysis was performed to identify how the CNNs were making their predictions, resulting in the following findings:
- (a) A strong negative MSLP anomaly to the west of Great Britain is a key feature relating to increased rainfall predictions. However, a positive MSLP anomaly to the west of Great Britain will decrease the amount of rainfall predicted.
 - (b) A positive MSLP anomaly to the east of Newfoundland but to the west of the negative MSLP anomaly identified in point 1, and another positive MSLP anomaly over Cape Verde, will also enhance rainfall magnitudes over Great Britain. If these regions were to contain negative MSLP anomalies instead, the rainfall predictions would be reduced.
 - (c) A combination of positive and negative 2AT anomalies over the British Isles will also increase the monthly rainfall total predictions made by the CNN models.

While the study presented here was limited on the available data, future work could

focus on the application of this forecasting method to provide higher-resolution forecast in both time and space dimensions. There is also now the opportunity to explore other meteorological variables using CNNs to identify where these variables may matter using an integrated gradients analysis. Another potential option is to modify the method presented in this paper to output a probabilistic forecast instead of a point-forecast which could form a future body of methods capable of improving both rainfall forecasting and our understanding of the processes which lead to rainfall.

5.7 Acknowledgements

All data used in this paper is freely available either through the ECMWF’s Copernicus data explorer (<https://cds.climate.copernicus.eu/cdsapp#!/dataset/seasonal-monthly-single-levels?tab=overview>) or the UK Centre of Ecology and Hydrology’s CEH-GEAR data platform (<https://catalogue.ceh.ac.uk/documents/5dc179dc-f692-49ba-9326-a6893a503f6e>).

5.8 Postscript

This chapter addressed hypothesis **Hypothesis 4** by showing the application of convolutional neural networks to forecast sub-seasonal rainfall across the 13 regions of Great Britain. This study is the first attempt to use convolutional neural networks on atmospheric patterns to predict rainfall.

The results of this study show the new neural network based methods provide higher level of accuracy than the conventional ensemble based model. More specifically the new method showed larger improvements for extreme/heavy rainfall events than it did for lower levels of rainfall. This did however come with some seasonal and regional bias; for example, at a one month leadtime the neural network method is more accurate for northern and western regions of Great Britain and the months December, July and August. However, the new model did provide substantial errors for the months June, September and August. This indicates although the method does produce some biases it is possible to use the mean sea-level pressure and air temperature patterns of the North Atlantic to forecast rainfall in the UK.

Following the comparison of the resulting rainfall values each model underwent a sensitivity analysis to identify which regions of the north Atlantic mean sea-level pressure and air temperature were responsible for increasing/decreasing the resulting forecasted rainfall values. This sensitivity analysis confirmed that a strong negative mean sea-level pressure to the north west of the UK is a key feature to increasing the amount of

rainfall. Similarly, if this negative body is followed by a positive body of mean sea-level pressure this rainfall amount will likely increase further. In all cases a strong contrasted front of positive and negative air temperature contributions can be found around the UK.

This highlights the capabilities of the new neural network architecture are not limited to that of forecasting but also allow an understanding of how the forecast was made and what meteorological patterns may be available to improve our understanding of the processes involved. With results indicating that the neural networks are capable of using single images to improve rainfall forecasts there is now the question of reducing the time dimension of the inputs to further improve the rainfall predictions. This is discussed in the next chapter.

However, alternative work could address the sensitivity of this method to not only other meteorological variables but could also investigate the scale of improvements made by such complex models. For example, a study could investigate how the current state-of-the-art model, along with the models generated in this chapter compare to a linear regression model. This would enable a quantification of the improvements made with the increase in data and computational power required and ideally provide a useful reference for operational forecasters to choose the right tool for their forecasts.

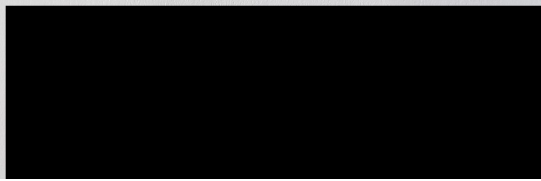
Chapter 6

Video based forecasting of regional, sub-seasonal rainfall

6.1 Preamble

In partial answer to **Hypothesis 4**, chapter 5 investigated the use of static, synoptic meteorological images for sub-seasonal rainfall forecasting. To expand on the answer to **Hypothesis 4** the present chapter expands on the work of chapter 5 to generate new forecasting models which use a sequence of synoptic images rather than just a single image. Specifically, this chapter describes a study which creates a series of CNN models capable of regional monthly rainfall forecasting using a sequence of forecasted mean sea-level patterns and 2m air temperature patterns (**Objective 4.1 & 4.2**). The resulting models are first compared with the current state of the art MetOffice GloSEA5 model and then combined with it to generate improved monthly rainfall forecasts (**Objective 4.3**).

6.1.1 Authorship Statement

Status	In Review in IEEE Geoscience and Remote Sensing Letters.
Details	Barnes, A.P., McCullen, N, Kjeldsen, T.R. (in review) IEEE Geoscience and Remote Sensing Letters. 2021.
Authors' contribution	<p>The author of this thesis has primarily (90%) contributed to design and implementation the methodology adopted for the extraction, clustering and analysis of both the atmospheric and rainfall data. Each author's exact contributions are as follows:</p> <p>A.P. Barnes: Formulation of ideas (95%), design of methodology (95%), data collection (100%), processing and analysis of data (100%), manuscript preparation (85%).</p> <p>N. McCullen & T.R. Kjeldsen: Formulation of ideas (5%), design of methodology (5%), manuscript preparation (15%)</p>
Date and Signature	 19-07-2021

6.1.2 Abstract

This study presents a new methodology for improving forecasts of current monthly, regional precipitation using video-based convolutional neural networks (CNNs). Using 13 administrative regions of Great Britain as a case study, three CNN architectures are trained for each region to forecast monthly rainfall totals given forecasted mean sea-level pressure and 2m air temperature videos from the MetOffice GloSEA5 model and a benchmark rainfall data. The forecasts generated by the CNN and the GloSEA5 precipitation forecasts are both compared directly against a benchmark rainfall dataset for each of the regions. Following this, the CNN models are combined with the GloSEA5 forecasts to generate a new ensemble for each region which is then compared to the benchmark rainfall. The results show that the trained CNNs produce errors similarly to the GloSEA5 model with RMSEs of 63mm (Single Frame), 44mm (Slow Fusion) and 37mm (Early Fusion) compared to the GloSEA5 error of 33mm. However, the CNN models all outperform GloSEA5 in the prediction of extreme events. Furthermore, treating the forecasts as an ensemble result in errors of 32mm (CNN ensemble) and 31mm (post-processing ensemble) both of which improve on the independent GloSEA5 forecasts.

6.2 Introduction

Flooding is becoming more frequent and the number of global deaths and economic losses due to flooding is on the rise; The World Meteorological Organization show that in the first half of 2020 alone more than 9.8 million people were displaced due to hydrometeorological events (World Meteorological Organisation 2021). Accurate prediction of extreme rainfall is therefore a key challenge to science and engineering.

Modern datasets allow efficient interpretation of the large-scale (synoptic) conditions and their relevance to the description and prediction of local rainfall; for example, Richardson et al. (2017) uses a set of 30 weather patterns to explain regional rainfall variation in the United Kingdom based on mean sea-level pressure (MSLP) patterns across the North Atlantic. The weather patterns used by Richardson et al. (2017) were originally defined by Neal et al. (2016) using MSLP data covering the North Atlantic to evaluate the performance of forecast models under the different weather conditions. Despite the regional variation between MSLP patterns observed in the North Atlantic and the resulting impact on observed rainfall patterns across the UK shown by Richardson et al. (2017) these approaches fail to consider temperature as a key variable. The relationship between temperature and rainfall is captured by the thermodynamic Clausius-Clapyeron relation can vary across a spatial domain as small as the UK (Blenkinsop et al. 2015). Further studies also show a stark contrast in synoptic temperature conditions related to heavy or intense rainfall events (Allan, Blenkinsop, et al. 2020).

Weather patterns and synoptic conditions have also been used to directly predict future climatological variables. In a review by Pham et al. (2020) neural networks were shown to be capable at predicting both daily and sub-daily rainfall values to within 10mm across spatial domains varying from local station scales to state-scale such as Florida. More advanced neural network structures have also been adopted to forecast rainfall. For example, Haidar & Verma (2018) used a range of climatic indices such as minimum and maximum temperature, the Southern Oscillation index (SO), the North Atlantic Oscillation index (NAO) and many others with a convolutional neural network (CNN) architecture to predict rainfall in a specific Australian suburb (Innisfail). Haidar & Verma (2018) were able to achieve lower root-mean squared errors than both the ACCESS-S1 hindcasts and a standard neural network architecture. More recently, approaches have used CNNs to interpret synoptic-scale images comprising of multiple meteorological variables. For example, Rasp and Thuerey (2021) used geopotential height, temperature, wind speeds and specific humidity among others at multiple pre-

ceding time steps to predict precipitation at lead-times of 6-hours and 1, 3 & 5 days within 2-3mm on a 5.625° spatial resolution grid. Despite this, they highlight the importance of higher resolution models and conclude that larger networks generally offered higher accuracy scores. However, they used a single architecture neural network (2015).

Karpathy et al. (2014) presented four options for including a time dimension in the structure of a CNN for classification of videos. The first method takes a single frame representation of the video (Single Frame), the second takes two images at either end of the video, passing them through the network individually before combining them at the end (Late Fusion). The third approach passes the entire video through the network from start to finish (Early Fusion) and finally, the fourth approach passes time-defined subsets of the video through the network separately, slowly merging them through the network until they are eventually recombined at the end (Slow Fusion). Their results highlight advantages of the different architectures however an ensemble approach combining all architectures is found to be best in this domain.

This paper takes a different approach to current literature, rather than analyzing static images of the preceding conditions (e.g. Neal et al. 2016) these conditions are characterised by a sequence of images (i.e. ‘a video’) representing the temporal evolution of the synoptic conditions. The meteorological videos are then interpreted by the video-based CNN variants proposed by Karpathy et al. (2014). A case-study using the regional, monthly rainfall of the 13 regions of Great Britain are used in this study. Regional forecasting models are generated using each of the variants and are then combined into two ensembles, the first is a combination of the CNN variants as shown by Karpathy et al. (2014) and the second includes forecasts from the MetOffice’s GloSea5 model (Maclachlan et al. 2015). These approaches are then compared and contrasted both against each other and against a benchmark rainfall dataset.

6.3 Data

Two data sources are used to train and evaluate the CNN models. First, the Centre of Ecology and Hydrology Gridded Estimate of Areal Rainfall (CEH-GEAR) (Tanguy et al. 2015) is used to represent the benchmark rainfall totals, providing gridded monthly rainfall across Great Britain between 1890 and 2017. Next, from the MetOffice GloSea5 hindcasts (MOS5) (Maclachlan et al. 2015) daily forecasted MSLP and 2AT patterns are used to train the CNNs to predict the benchmark rainfall data from CEH-GEAR using a 1-month lead-time. Also, from the MOS5 dataset monthly rainfall totals are

extracted for each region. However, due to the temporal limits of the MOS5 data (1994-2020) and the CEH-GEAR data (1890-2017) the temporal range of this study is limited within 1994 to 2017.

6.3.1 Rainfall

Great Britain has been split into 13 administrative regions as indicated by Figure 6-1, each of these regions is then further split into a set of points spaced equally at 30km×30km. The monthly rainfall total (mm) for a given region is calculated by averaging the total monthly rainfall from each point within the region. Both the CEH-GEAR and MOS5 datasets are provided in a gridded format and as such each point assumes the value of the grid cell which contains the point. Following this each region's rainfall dataset is standardized as follows,

$$\widehat{p}_{i,t} = \frac{p_{i,t} - \bar{p}_i}{std(p_i)} \quad (6.1)$$

where $p_{i,t}$ is a regional series of monthly rainfall totals (mm) where $i = 0, 1, \dots, 12$ indicating the region being standardized and $t = 1, \dots, 275$ indicating which timestep (month in the series) is currently being calculated. Standardizing the regional rainfall in this way removes biases of regions with particularly high rainfall, for example the North West of England compared to regions of low rainfall such as the South East of England. The result of this extraction and standardization are two matrices of rainfall events of size $[275, 13]$ where 275 is the number of months available to forecast (275 instead of 276 because a one-month lead-time is required which removes 01-1994 as available data) and 13 is the number of regions.

6.3.2 Meteorological Data

Synoptic patterns of MSLP and 2AT were extracted from the MetOffice GloSea5 Hindcasts (Maclachlan et al. 2015), these patterns were extracted for the middle 28 days of every month used in the study (02-1994 to 12-2017) and covered a synoptic extent between $[100^\circ W, 10^\circ N]$ to $[20^\circ E, 70^\circ N]$. The middle 28 days was chosen to represent most of the month while ensuring all months had the same amount of data available. The MOS5 data were available on a $2.5^\circ \times 2.5^\circ$ grid-format, meaning each pattern is represented by a matrix $[121, 61]$ in size. Each pattern was extracted from the final day of the preceding month; for example, patterns for days 01-02-1995 up to and including 28-02-1995 were extracted using forecasts ran on the 31-01-1995. Next, the resulting sets of MSLP and 2AT patterns were standardized separately as follows:

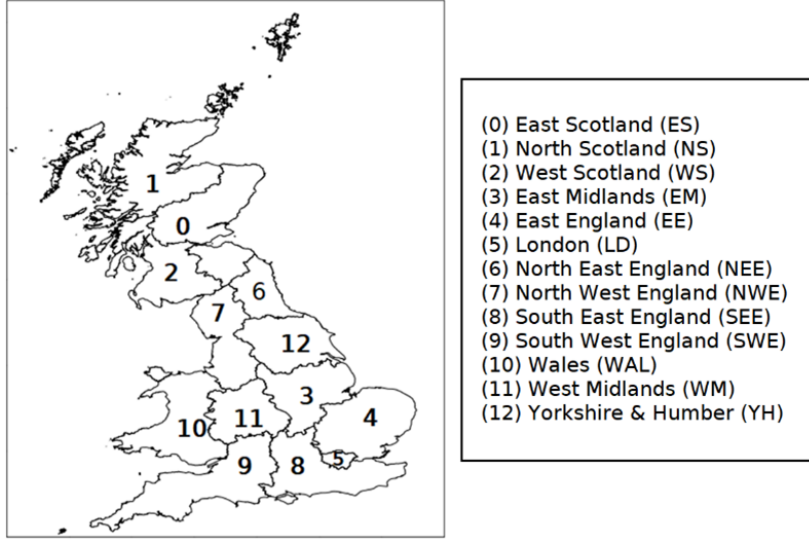


Figure 6-1: The 13 administrative regions of Great Britain.

$$\widehat{z_{x,y}^{var}} = \frac{z_{x,y}^{var} - \overline{z_{x,y}^{var}}}{std(z_{x,y}^{var})} \quad (6.2)$$

here $z_{x,y}^{var}$ represents the set of cells at a given position where, $x = \{1, \dots, 121\}$ and $y = \{1, \dots, 61\}$ for the variable given by $var = \{MSLP, 2AT\}$. The resulting two sets of matrices are of size $[276, 121, 61, 28]$ ([Number of months, longitude cells, latitude cells, number of days]) and are finally combined to give a single matrix of size $[276, 121, 61, 28, 2]$ such that each dimension represents [Number of months, longitude cells, latitude cells, number of days, variables].

6.3.3 Training, testing and validation

To reduce overfitting and provide a fair comparison between the developed CNN models and the MOS5 predictions the dataset was split into training, testing and validation. The training data was used to optimize the CNN, the testing data was used to ensure overfitting does not occur and finally the validation dataset was be used to compare the resulting CNN models to the MOS5 predictions. To ensure seasonal consistency between both training and validation datasets the validation dataset consisted of all data for years taken at a 4-year interval (1997, 2001, 2005, 2009, 2013, 2017) which equates to 26% of the total data and the remaining years are allocated to training (74% of total data). During the training process the training dataset was further split into training (70%) and testing (30%).

6.4 Forecasting Method

In this section the CNN variants used are followed by a description of the two ensemble approaches which are used for evaluation.

6.4.1 CNN Variants

To forecast regional monthly rainfall totals using the videos representing the forecasted meteorological images, as described in section 6.3.2, three CNN architecture variants are trained for each region resulting in a total of 39 CNN models. Each of the three models will incorporate the time dimension (number of days) into the CNN differently and are based on the architectures proposed by Karpathy et al. (2014).

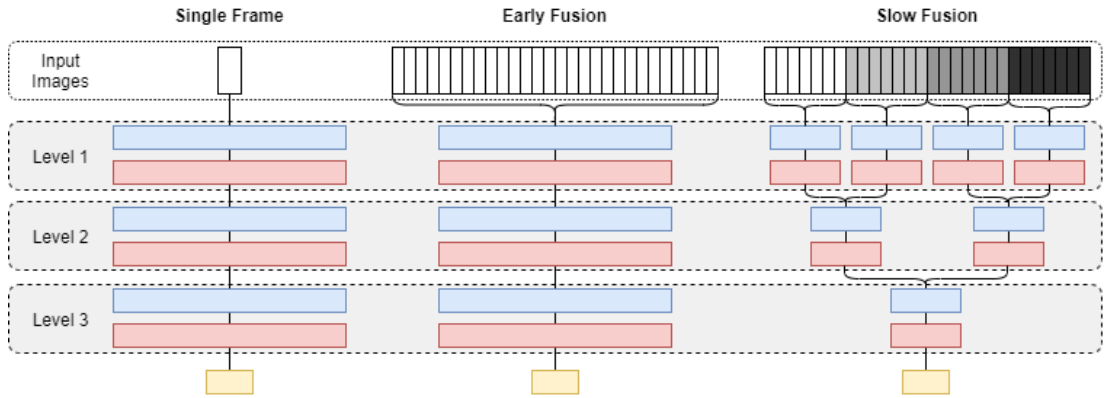


Figure 6-2: Three CNN architectures for including a temporal dimension, adapted from Karpathy et al. (2014). Blue boxes indicate convolutional layers, red boxes indicate max-pooling layers, and the yellow boxes indicate fully-connected linear layers.

Firstly, a single-frame (SF) approach is adopted which takes a mean across the time dimension, creating a new matrix containing the average MSLP and 2AT patterns across the 28 days. This in turn, reduces the number of dimensions from 4 ([longitude cells, latitude cells, number of days, variables]) to 3 ([longitude cells, latitude cells, variables]). This 3D matrix is then interpreted as a static image and used to train the CNN. Next, an early-fusion (EF) approach processes the entire 4D matrix at once without any pre-processing. This involves the convolutional and max-pooling layers having 3D filters with kernels covering latitude, longitude and temporal dimensions. Finally, a slow-fusion (SlowF) approach splits the initial 4D matrix along the temporal dimension into four equally sized (weekly) matrices of [longitude, latitude, $(28 / 4 = 7)$ 7, variables]. Each of these weekly matrices is then passed through the first level of the network individually before being recombined into two bi-weekly matrices by concatenating the results of the first across the temporal dimension. The ‘bi-weekly’

matrices are then passed through a second level of the network, concatenated into a single matrix and then passed through a final third level of the network. A summary diagram of the architectures is shown in Figure 6-2.

At each layer kernels of size 2 were used such that the single frame model uses kernels of size $[2, 2]$ and the Early Fusion/Slow Fusion models use kernels of size $[2, 2, 2]$ to incorporate the temporal dimension convolutions. Both the single frame and early fusion models were generated using 128 filters in each layer whereas the Slow Fusion model uses 32, 64 and 128 filters in each respective layer. These sizes were chosen following several trials which varied the number of filters in each architecture.

Each of the CNN models was trained using a learning rate of 0.0001 and the Adam optimization method (Kingma and Ba 2015) As mentioned in section 2.3 the training data is split into training and testing data with a split of 70% training to 30%. For each region and architecture variant combination three training cycles were completed and the model with the lowest final test error was selected to represent the region and architecture combination, this is to provide an accurate representation of the architecture/region selection which is not influenced by a poor training cycle.

6.4.2 Ensemble Forecasting

Regional forecasts of rainfall across the 13 regions were also made by combining the outputs from the CNN and MOS5 into two ensemble means Firstly, the CNN Ensemble (CNNE) is defined as the mean of the predictions made by all three CNN architecture variants (Single Frame, Slow Fusion and Early Fusion). Karpathy et al. (2014) found that an average of the outputs improved accuracy compared to the individual CNN architectures alone; thus this ensemble approach was adopted in this study. The second approach is a Post-Processing Ensemble (PPE) which is defined as the mean of the CNNE and the MOS5 prediction. An overview of these ensembles for a given month is given in Figure 6-3.

6.5 Results

This section first provides a comparison of the developed CNN models for each region against the MOS5 predictions, followed by a discussion of the combined CNNE and PPE ensemble predictions. All results presented in this section refer to a comparison of the output from the models using a validation dataset as described in section 6.3.3, this data was kept separate from training and testing to ensure the networks had not been exposed to the validation data.

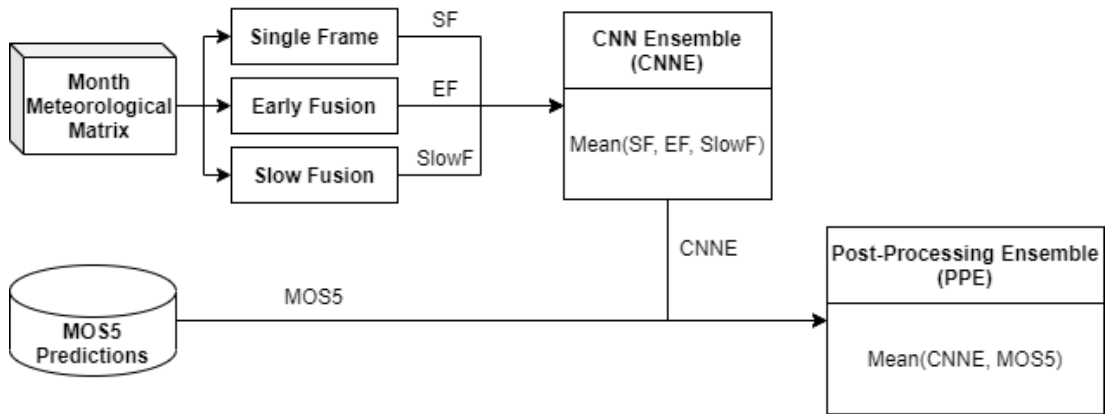


Figure 6-3: Two ensemble approaches are presented. First the CNN Ensemble (CNNE) is calculated through taking the mean of all three CNN Results for a given month. Then, the mean of the CNNE and the MOS5 prediction is taken as the post-processing ensemble (PPE).

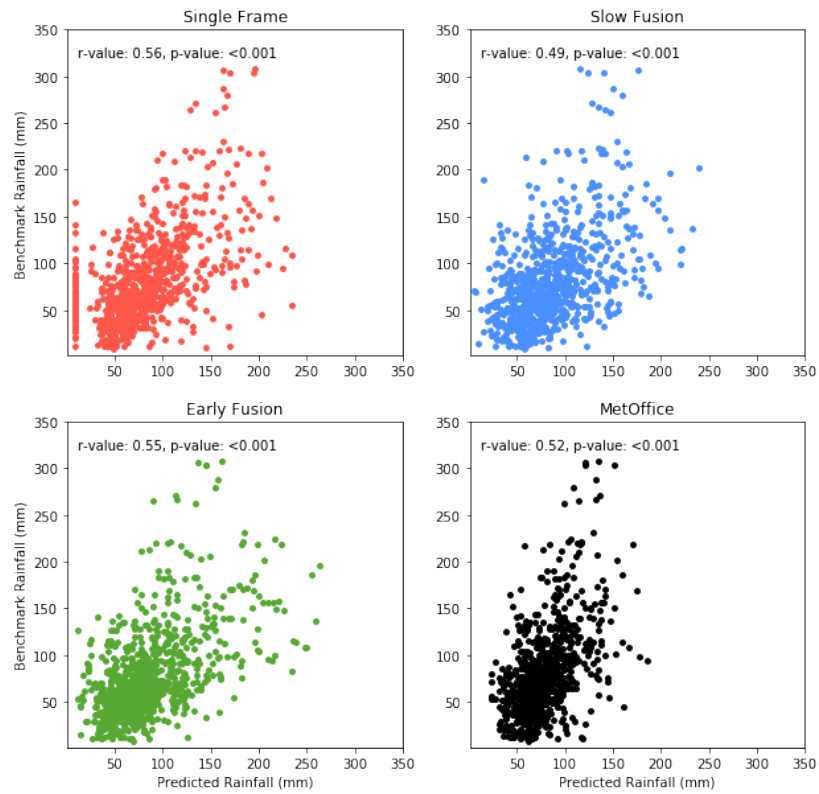


Figure 6-4: Predicted rainfall against the benchmark rainfall value for all months in the validation dataset.

The average validation root-mean squared errors (RMSEs) for the CNN variants and MOS5 predictions across all regions are as follows: 63mm (SF), 44mm (SlowF), 37mm (EF), 33mm (MOS5). The MetOffice GloSea5 outperforms all three CNN variants on the validation dataset across all regions. Despite this, the prediction patterns highlighted in Figure 6-4 show the MOS5 predictions never exceeded 200mm of rainfall whereas all three CNN variants appear capable of doing so. This is especially true regarding the EF and SlowF variants which show strong positive correlations between predicted and benchmark rainfall, even though this comes with an increase in variance.

Figure 6-5 shows the contribution to the root mean-squared error (RMSE) values from across the regions. The results show that the regional bias of the models remains consistent with each model presenting a graph with broadly similar shapes with higher RMSE errors produced for regions known for higher levels of rainfall such as the three Scottish regions, Wales and North East England. Notably the SF variant producing a larger error for Yorkshire and Humber which relate to a subset of predictions of 1mm in (Figure 6-4 Single Frame) indicating a lack of convergence of the CNN.

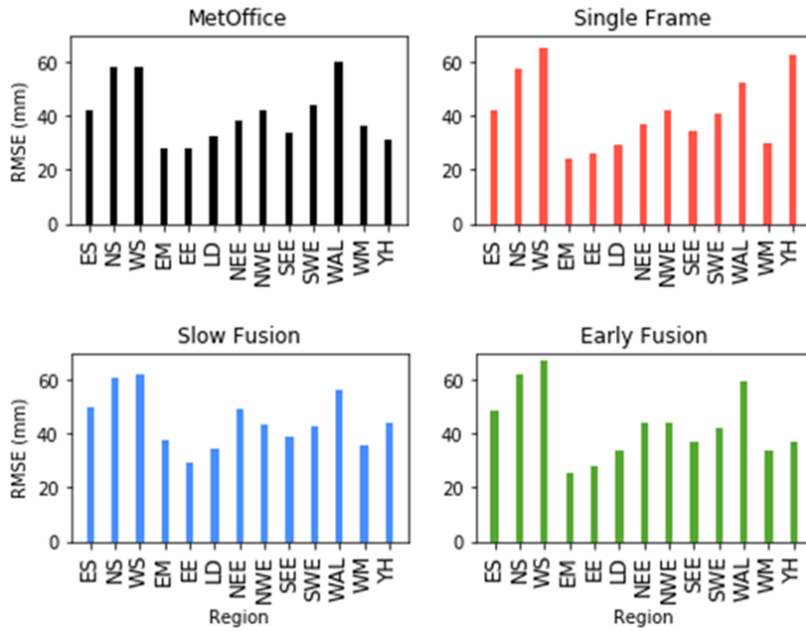


Figure 6-5: Regional RMSEs for each model for the validation dataset.

Next, the ensemble means are generated as described in section 6.3.2. Figure 6-6 shows the validation dataset predictions for the CNNE (left) and PPE (right); the variation of both plots highlight the similarity between the two prediction models. The RMSEs for the CNNE and PPE are 32mm and 31mm respectively across all regions, comparing

this with the 33mm RMSE found for MOS5 these results indicate an ensemble approach with the CNN variants has the potential to provide more accurate rainfall forecasts. These results also further confirm those of Karpathy et al. (2014) who also concluded that an ensemble approach improved their results.

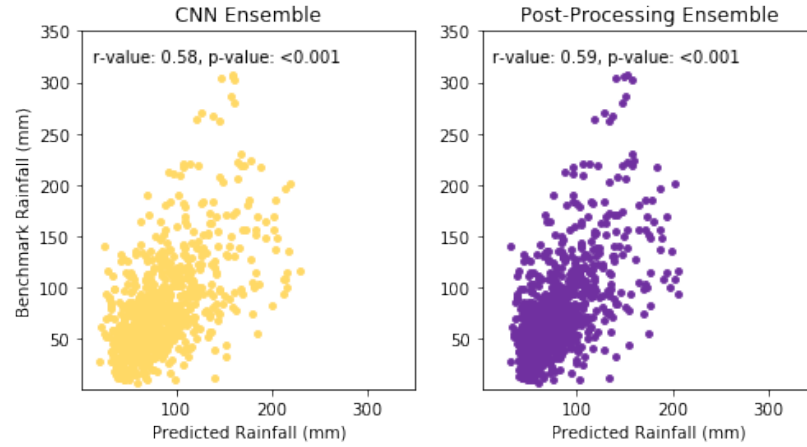


Figure 6-6: Ensemble predictions for the validation dataset compared to the benchmark monthly rainfall totals (mm). Left: CNNE, and right: PPE.

Finally, Figure 6-7. Shows the cumulative residual of each CNN and ensemble variant alongside GloSea5 for rainfall values increasing from 0mm to 350mm. This figure illustrates that although the individual models appear less accurate at a high-level, they do make significant improvement in the under prediction of heavy rainfall events shown by the GloSea5 model. This is an important result as period of high rainfall are often responsible for flooding.

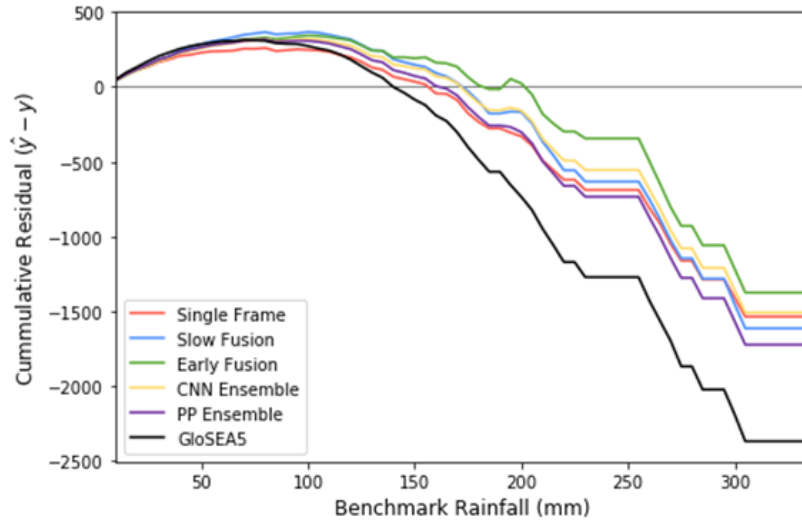


Figure 6-7: The cumulative residual for all forecasting methods including the MetOffice’s GloSea5 model.

6.6 Conclusions

This paper introduces a new technique for sub-seasonal rainfall forecasting using video based convolutional neural networks. Regional CNNs were constructed using three different architecture variants and trained using forecasted daily mean sea-level pressure and 2m air temperature patterns with a leadtime of one month. The forecasted images occur throughout a given month and are used to predict the regional rainfall. Following this, two ensemble models were produced, one of which used took the mean of the CNN variants and the second took the mean of the CNN variants and the MetOffice GloSea5 (MOS5) model. All models were then compared with the MOS5 predictions with the following findings:

1. Individually the CNN variants were able to provide regional rainfall predictions based on forecasted MSLP and 2AT patterns.
2. No regional bias was found between the CNN variants. Higher errors were found in regions with higher levels of rainfall however this was to be expected due to the magnitude of the events.
3. The ensemble models both produced RMSEs lower than the MOS5 predictions.
4. All CNN and ensemble approaches showed increased accuracy for heavy rainfall events in comparison to the MOS5 model.

These findings highlight the applicability of video-based convolutional neural networks to rainfall forecasting. This study was limited by the quantity of data used; however, the results show the use of an ensemble of different CNN architectures could provide invaluable post-processing to traditional numerical weather prediction models, especially focusing on improving the prediction of the most extreme events. To improve the models further a cross-validation approach could be taken to increase the amount of data used during training and to further increase the amount of data available data augmentation techniques could be applied to create a synthetic data set, providing more training examples.

6.7 Acknowledgements

All data used in this study is freely available. The Centre of Ecology and Hydrology’s CEH-GEAR dataset is available from their portal (<https://catalogue.ceh.ac.uk/documents/ee9ab43d-a4fe-4e73-afd5-cd4fc4c82556>). The meteorological and gridded rainfall data extracted from the MetOffice GloSEA5 model is available through the ECMWF’s Copernicus service (<https://cds.climate.copernicus.eu/cdsapp#!/dataset/seasonal-monthly-single-levels>).

6.8 Postscript

The present chapter builds on chapter 5 to develop an enhanced answer to **Hypothesis 4**. This is achieved by expanding the architecture of the neural networks used in chapter 5 to include a temporal dimension. To do this three neural network architectures capable of accepting videos as inputs are developed to forecast the regional monthly rainfall across Great Britain. Following this, the models are compared with MetOffice GloSEA5 predictions and later combined with the GloSEA5 predictions to produce ensemble means.

The results of this chapter highlight the forecasting power of video enabled CNNs and the increased accuracy available when making use of these techniques through ensemble forecasts. Despite this, the final accuracies remained low and with the exception of the ensemble methods none were able to achieve accuracies lower than the MetOffice’s GloSEA5 forecast. However, All model architectures showed significant improvement for the extreme rainfall values within each region which indicates the CNN Architectures are less biased towards expected rainfall quantities.

Opportunities presented by this study include the retraining of higher resolution models

using a larger architecture than the one trialled in the present study. Enhancing the size of the network through increasing the number of layers and the number of filters within each layer will result in higher accuracies and potentially could help further identify synoptic patterns related to extreme rainfall events. Moreover, how the variation of the video's temporal window could affect resulting forecasts, reducing the window size may enhance forecasts but come at the cost of higher computational complexity during training. However, by investigating this further future work will be able to identify the corresponding complexity/accuracy alignment.

Chapter 7

Conclusions

7.1 Thesis Summary

The overarching aim of this thesis is to develop new machine learning methods to aid both our current understanding of extreme rainfall events and provide rainfall forecasting improvements. This thesis achieves this aim by addressing four hypothesis as given in Section 1.3. Starting with an introduction to extreme rainfall and current analysis methods which builds a case for the hypotheses presented in section 1.3. These hypotheses are then tested through Chapters 2 to 6. In this section an overview is given of Chapters 2 to 6 and is followed.

Chapter 2 addresses **Hypothesis 1** (Heavy rainfall events can be characterised by their preceding atmospheric trajectories) by following two studies which cluster extreme rainfall events using atmospheric trajectories extracted using the HYSPLIT model (Draxler and Hess 1997). The first study (section 2.2) presents a methodological advance in the use of self-organising map (SOM) based neural networks for clustering atmospheric trajectories related to extreme rainfall events in a case-study region of the Duoro catchment in Northern Spain. The second study (section 2.3) evaluated: k-means, hierarchical, and SOM based clustering methods on a case-study of the UK. The results of these experiments show his form of clustering can provide inference into the distributions of extreme rainfall and be used to seperate extreme rainfall events into subsets with different magnitude distributions.

Chapter 3 then expands this analysis to evaluate the effect covariance between 2m air temperature (2AT) and mean sea-level pressure (MSLP) has on heavy rainfall events to address **Hypothesis 2**. Heavy rainfall events were identified across Great Britain and their concurrent mean sea-level pressure and 2m air temperature synoptic patterns were clustered using k-means. The resulting groups of heavy rainfall events were then compared to asses the existence of spatial and temporal trends. Next, these groups were linked with large-scale climatic indices such as the NAO and AMO using detrended correlation anaylsis. The results show that the spatial and temporal variability of heavy rainfall events shows significant correlation to a co-variance between MSLP and 2AT which also present significant correlations with large-scale meteorological variables such as the NAO and AMO.

Chapter 4 addresses **Hypothesis 3** by reporting an experiment which uses the synoptic MSLP patterns of both extreme and non-extreme rainfall events to distinguish between the two using two hydrodynamically distinct regions (NW England and SE England). Several deep neural networks were trained to distinguish between the patterns and then undergo a sensitivity analysis to identify what differences in the synoptic patterns

cause a pattern to be classified as 'extreme' or 'non-extreme'. The results show that despite the neural networks achieving an accuracy of 60% the initial selective decision on what constitutes an extreme and non-extreme rainfall event is fundamentally subjective. Despite this, the sensitivity analysis did reveal the most important regions of the North Atlantic are the ocean around Ireland and the Irish Sea.

Chapter 5 combines the findings of Chapters 3 and 4 into a new method for developing interpretable seasonal to sub-seasonal rainfall forecasts in answer to **Hypothesis 4**. Using convolutional neural networks (CNNs) to simultaneously forecast monthly rainfall for all 13 regions in Great Britain. Differing from current approaches which focus on using individual meteorological variables this study instead combines the synoptic patterns of both MSLP and 2AT across the North Atlantic. The resulting models were then compared to the ECMWF's SEA5 forecasting model. Next, a sensitivity analysis was performed to identify which areas of the synoptic patterns were attributing to the resulting forecast rainfall quantities.

Finally, Chapter 6 builds on Chapter 5 by trialling multiple neural network based forecasting architectures to expand on the answer to **Hypothesis 4**. Video based CNNs were developed to use a series of forecasted MSLP and 2AT synoptic images to predict regional monthly rainfall across Great Britain. The resulting models are then compared to the current state of the art MetOffice GloSEA5 forecast model. Following this, the models are combined with the MetOffice GloSEA5 model to produce a series of ensembles which improve on the current state of the art model.

7.2 Results

This section provides an overview of the results from each hypothesis and chapter.

Beginning with **Hypothesis 1**, which states "Heavy rainfall events can be characterised by their preceding atmospheric trajectories", Chapter 2 addresses this hypothesis with two experiments. First, the preceding atmospheric trajectories for heavy rainfall events in the Duoro catchment in northern Spain are clustered using SOMs. This clustering procedure allowed the development of models which provided classification schemes with varying number of classes (2 to 10). The study presented highlights four models in particular:

1. 4-Class SOM using all latitude and longitude points
2. 9-Class SOM using all latitude and longitude points

3. 9-Class SOM using all altitude, latitude and longitude points
4. 9-Class SOM using only summer latitude and longitude points
5. 9-Class SOM using only winter latitude and longitude points.

These four models highlight the variability in atmospheric trajectory available to the small case-study region, the 4-class and 9-class models which used just the latitude and longitude points produce a separation between short and long trajectories. In both cases the shorter, slower trajectories account for the majority of extreme events as also found by Jorba *et al.* (2004). However, in separating winter and summer by using separate models the study shows that the majority of summer related events are caused by the shorter, slower trajectories whereas in the winter model the majority of the trajectories originate in the mid-Atlantic and are faster moving. Through analysis of the magnitude of the rainfall events the study also showed that during summer the trajectories which originate from the North Atlantic produce 4.5% higher magnitude events than the recirculatory, continental patterns.

Next, in comparing the models which did not use altitude and the one which did the study highlights altitude increases the error of the clustering and produced results which did not provide clear separation in magnitude of events. However, in consideration of this the study highlights the curse of dimensionality a known problem when dealing with datasets with a large number of features (Kohonen and Honkela 2007; Marimont and Shapiro 1979). Despite this, the study did successfully highlight the ability of clustering techniques to identify meaningful differences in extreme rainfall distributions using preceding atmospheric conditions.

Finally, Chapter 2 presents a second study which compares k-means, SOMs and linkage based clustering methods in the clustering of atmospheric trajectories using Great Britain as the case study. Here AMAX events were extracted from 42 cities across Great Britain, their preceding atmospheric trajectories extracted and then clustered using each of the methods mentioned previously. Each clustering method was trialled using a variable number of clusters from 4 to 24, with a intra-cluster similarity (Davies-Bouldin index (DB)) metric taken for each model run, the runs with the lowest DB index are selected for analysis.

From the three models it was found that the lowest DB indices were found with a four cluster SOM, 5 cluster linkage and a 6 cluster k-means model. The 6-cluster k-means model was shown to have the lowest DB index and was then used in further analysis to show that 60.58% of the extreme rainfall events used were attributable to the North

Atlantic and 39.42% were attributable to the North Sea.

With a distinct dependence between the heavy rainfall events and the composite meteorological variables it then became necessary to identify to what extent the interdependence of the meteorological variables influences the heavy rainfall events. To do this Chapter 3 addresses **Hypothesis 2** through clustering the concurrent synoptic scale mean sea-level pressure and 2m air temperature patterns of the North Atlantic during heavy rainfall days in the UK.

The results from Chapter 3 indicate a strong interdependence of synoptic scale 2AT and MSLP patterns. During summer three out-of four classes showed a strong anomalous low pressure center west of the UK, the remaining class presented a strong negative MSLP anomaly between Scotland and Iceland with a strong positive MSLP anomaly over the Iberian peninsular. Despite this, all four MSLP patterns show similarities with some identified by Neal *et al.* (2016), with common low pressure anomalies dominating the western/north western UK. The frequency of each event class distribution across the UK also revealed similarities with work by Richardson *et al.* (2017) who showed the magnitude of Neal *et al.*'s (2016) event classes across various regions of the UK. However, because the rainfall events used in this study are heavy rainfall events Richardson *et al.*'s (2017) work shows more rainfall variability. Further regression analysis was conducted using the NAO and AMO indices showing a strong relationship between the frequency of each class' occurrence and negative/positive variations of the indices. For example, summer classes 1 and 3 had $r = -0.29$ and $r = -0.44$ respectively. Such relationships were also found with the AMO in summer classes 1 and 3 with $r = +0.37$ and $r = -0.54$ respectively. Relationships which indicate strong reliance of the resulting clusters on synoptic circulation patterns.

For winter three classes are generated. The first class correlates positively ($r = 0.35$) with the NAO despite the closes matching class of Neal *et al.* (2016) not being one of those labelled as being typically related to the NAO. The second class highlights a strong high MSLP anomaly over Greenland and Iceland, with a low MSLP to the south, as expected this class correlated negatively with the NAO ($r = -0.23$). These first two winter classes also showed strong correlations with time which dissipated once the dependence on the NAO index was removed. The final winter class showed no significant correlation with the NAO or AMO but represented a eastwards shift in the subtropical high-pressure. Similar to summer class three, winter class 3 showed a dominance in frequency of occurrence for the North West of Great Britain.

The inclusion of temperature in the clustering mechanism presents patterns with a

dependence between the MSLP and 2AT synoptic conditions. The resulting classes also show distinguishing features in terms of frequency of occurrence across both the spatial and temporal domain with some significant relationships with the NAO and AMO. With a link found between MSLP and 2AT the next question raised in **Hypothesis 3** is whether such patterns can be used to distinguish heavy rainfall events.

Chapter 4 reports on a study which uses neural networks to distinguish between extreme and non extreme rainfall events using their concurrent synoptic MSLP patterns in answer to **Hypothesis 3**. Using the UK as a case study this chapter generated three classification models:

1. M_{NW} distinguishes between extreme and regular rainfall events in the North West of England.
2. M_{SE} distinguishes between extreme and regular rainfall events in the South East of England.
3. M_{comp} distinguishes between extreme rainfall events in the North West and those in the South East of England.

Each of the classification models is trained using a varying number of hidden nodes to ensure an optimal architecture is achieved. Across all three model variants the optimal parameter choice resulted in a testing accuracy of 62% (M_{NW}), 60% (M_{SE}) and 65% (M_{comp}). The precision and recall of extreme events in both M_{NW} and M_{SE} are higher than for regular rainfall events which indicates there are identifiable differences in the extreme events patterns which are possibly obscured in the regular rainfall patterns. Further to this a sensitivity analysis was conducted to identify the synoptic region which was important for distinguishing between extreme and regular rainfall events. For both M_{NW} and M_{SE} a strong attribution was found over Ireland and the Irish Sea whereas the mid and western Atlantic did not provide any useful indication as to whether events were extreme or regular. This indicates that the results from this study show there may not be significant differences in the synoptic patterns involved with extreme and regular rainfall events.

Following the theme of interpretable models, Chapter 5 reports the results of a study which developed seasonal to sub-seasonal rainfall forecast models using convolutional neural networks for the 13 regions of Great Britain. In comparing the resulting models with the ECMWF's SEA5 forecasting model the CNN models produced validation errors 6.89mm lower than the ECMWF model using a one month lead time and this improvement was exacerbated at the extremes with the CNN model producing errors

28.19mm lower than the ECMWF model when predicting the top 5% of extreme events for each region. Following this, an integrated gradients analysis was performed on the CNN models to identify the level and type of attribution for both the MSLP and 2AT input patterns. This revealed a strong negative MSLP anomaly to the west of the British Isles and a positive MSLP anomaly over Newfoundland provides a positive influence to the resulting rainfall forecast. Further to this, a mixture of positive and negative 2AT anomalies over southern Great Britain and north western France is another indicator of heavy rainfall values.

The findings of Chapter 5 indicate that not only are CNNs capable of forecasting seasonal and sub-seasonal rainfall to a higher standard than a modern forecasting service but also offer insight into how and why the predictions are being made. The benefits of using CNN models over traditional NWP models include the following:

1. Computational Power: The lower complexity architecture of the CNNs reduce the computational load required when running the forecasting models. While this is true when forecasting using a model it is important to note that this does not reduce the computational requirements needed to train these models in the first instance.
2. Reduced assumptions: The learning nature of CNNs allows the models to identify trends, correlative and causal relationships where they may not have been identified and implemented in traditional mathematical models. Moving the burden of identification and implementation of complex numerical systems onto the learning algorithm removes the burden of selecting and accounting for assumptions by the operator. However, this will instead require careful analysis of the trained model to ensure it has been considering appropriate combinations of inputs and has not found a non-causal correlation within the training dataset.
3. Interpretability: One remedy to the point above is the increased interpretability of the CNN models. Through sensitivity analysis one can attribute how changing the inputs influences the resulting forecast. For example, Chapter 5 shows how such models can be used to identify which areas of synoptic regions are important for rainfall forecasting and in which way they are important (i.e. do they have a positive or negative effect).

Combining these factors to answer **Hypothesis 4** reveals that the interpretation of concurrent, synoptic scale atmospheric forecasts can be used to improve both seasonal and sub-seasonal rainfall forecasts. However, a final question remains as to whether this could be expanded further to include a temporal dimension including multiple

time-steps of the atmospheric conditions.

In answer to this question Chapter 6 used an additional temporal dimension on the image input using architectures presented by Karpathy et al. (2014). In doing so, Chapter 6 highlights that video based CNNs are capable of providing accurate monthly rainfall predictions when compared to a current state of the art numerical prediction model. Specifically individual regional forecasting models presented errors close to those produced by the current state of the art model; however, all trialled CNN Architectures improved upon the current state of the art model when considering the extreme rainfall events. Further to this, by averaging the predictions made by the state of the art forecasting model with the CNN variants a new forecast was available which was able to improve on the current state of the art model by several millimeters of rainfall. Although chapter 6 only scratches the surface of the potential for video based CNNs it does highlight the applicability of these techniques to the problem domain and further highlights the ability of modern machine learning techniques to use forecasted meteorological conditions to improve the current state of the art sub-seasonal rainfall prediction models.

7.3 Future Opportunities

In Chapter 2 exploratory cluster analysis was performed to identify atmospheric trajectory systems which produce different distributions of rainfall magnitudes, this was then developed in Chapter 3 which used clustering to analyse the interdependence of two meteorological variables. Although the choice of clustering algorithm is largely a subjective choice, these chapters also highlight the importance of a subjective review of the developed clusters. Simply using numerical errors is not enough to identify a suitable number of cluster, instead the identification of new methods for empirically evaluating cluster models related to physical processes. This is especially relevant when the datasets concerned contain a large number of variables and result in models falling foul to the curse of dimensionality (Kohonen and Honkela 2007). This can be due to a large number of input features and is more prominent in datasets which contain more features than observations. Further work could be conducted on meteorological datasets to identify at what point clustering becomes no longer applicable due to this phenomenon and to what extent the datasets can reasonably be used for cluster based exploratory analysis.

Despite this, the exploratory clustering revealed interesting patterns throughout Chapter 2 and Chapter 3 indicating the applicability of clustering as a useful tool for dis-

tinguishing heavy rainfall events and it would be very interesting to explore further different combinations of atmospheric variables such as geopotential height, evaporation and dew point temperature which are all variables associated with intense rainfall events (Allan, Blenkinsop, et al. 2020). Further to this, similar exploratory analysis using clustering could focus on the identification of new meteorological variable combinations which could support forecast post-processing models such as those presented in Chapter 5 and 6.

Chapter 5 introduced a new method for forecasting regional based precipitation using forecast MSLP and 2AT synoptic conditions. Although the model presented does not greatly improve upon the current ECMWF SEA5 model it does highlight the potential in the use of CNNs for analysis of meteorological images. Conjoining this with future exploratory analysis regarding the covariance of other meteorological variables future work could create new images which can be used for prediction of both rainfall and other meteorological variables such as wind speed. Further to this, as detailed in chapter 6 CNNs can be expanded to utilise a temporal dimension cross the datasets. In doing so, higher resolution models could be developed to predict daily or even sub-daily conditions.

The opportunities presented by this thesis offer new avenues of exploration regarding the sensitivity of the methods to the inputs provided. For example, the length of trajectories clustered in Chapter 2, the meteorological variables used for clustering in Chapter 3 and forecasting in Chapters 4, 5 & 6. However, there is also the opportunity to conduct a series of analyses using a range of techniques to identify the trade-off between the data intensive methods (as used throughout this thesis), the state-of-the-art mathematical models and simpler techniques such as regression models. Through understanding the trade-offs at play more detailed recommendations can then be made to operational meteorologists. Finally, with increasing data availability and new, big-data sets becoming available there are new opportunities to further push the limits of this work. This could be done through the application of these techniques on higher spatial & temporal resolution data sets to further improve results.

In conclusion, this thesis has highlighted that the development of new state-of-the-art machine learning techniques offers bountiful opportunities to improve our understanding of extreme rainfall and to provide more accurate results from which climate resilience and understanding can be drawn.

Bibliography

- Aggarwal, Charu C., Alexander Hinneburg, and Daniel A. Keim (2001). “On the surprising behavior of distance metrics in high dimensional space”. In: *Lecture Notes in Computer Science (including subseries Lecture Notes in Artificial Intelligence and Lecture Notes in Bioinformatics)*. Vol. 1973, pp. 420–434. ISBN: 9783540414568. DOI: 10.1007/3-540-44503-x_27. URL: http://link.springer.com/10.1007/3-540-44503-x%7B%5C_%7D27.
- Allan, Richard P., Stephen Blenkinsop, et al. (June 2020). “Atmospheric precursors for intense summer rainfall over the United Kingdom”. In: *International Journal of Climatology* 40.8, pp. 3849–3867. ISSN: 10970088. DOI: 10.1002/joc.6431. URL: <https://onlinelibrary.wiley.com/doi/abs/10.1002/joc.6431>.
- Allan, Richard P., Chunlei Liu, et al. (May 2014). “Physically Consistent Responses of the Global Atmospheric Hydrological Cycle in Models and Observations”. In: *Surveys in Geophysics* 35.3, pp. 533–552. ISSN: 01693298. DOI: 10.1007/s10712-012-9213-z. URL: <http://link.springer.com/10.1007/s10712-012-9213-z>.
- American Meteorological Society (2019). *Atmospheric River*. URL: https://glossary.ametsoc.org/wiki/Atmospheric%7B%5C_%7Driver.
- Baker, L. H., L. C. Shaffrey, and A. A. Scaife (Apr. 2018). “Improved seasonal prediction of UK regional precipitation using atmospheric circulation”. In: *International Journal of Climatology* 38, e437–e453. ISSN: 10970088. DOI: 10.1002/joc.5382. URL: <http://doi.wiley.com/10.1002/joc.5382>.
- Barnes, Andrew, Nick McCullen, and Thomas Rodding Kjeldsen (2019). “Atmospheric origins of extreme rainfall in the UK”. In: *4th IMA International Conference on Flood Risk*.
- Barnes, Andrew Paul, Marcus Suassuna Santos, et al. (Mar. 2020). “Identifying the origins of extreme rainfall using storm track classification”. In: *Journal of Hydroinformatics* 22.2, pp. 296–309. ISSN: 14651734. DOI: 10.2166/hydro.2019.164. URL: <https://iwaponline.com/jh/article/22/2/296/70268/Identifying-the->

- origins-of-extreme-rainfall-using%20https://doi.org/10.2166/hydro.2019.164.
- Barnston, A. G. and R. E. Livezey (June 1987). “Classification, seasonality and persistence of low-frequency atmospheric circulation patterns”. In: *Monthly Weather Review* 115.6, pp. 1083–1126. ISSN: 00270644. DOI: 10.1175/1520-0493(1987)115<1083:CSAPOL>2.0.CO;2. URL: [http://journals.ametsoc.org/doi/10.1175/1520-0493\(1987\)115%7B%5C%%7D3C1083:CSAPOL%7B%5C%%7D3E2.0.CO;2](http://journals.ametsoc.org/doi/10.1175/1520-0493(1987)115%7B%5C%%7D3C1083:CSAPOL%7B%5C%%7D3E2.0.CO;2).
- Blamey, R. C. et al. (Jan. 2018). “The influence of atmospheric rivers over the South Atlantic on winter rainfall in South Africa”. In: *Journal of Hydrometeorology* 19.1, pp. 127–142. ISSN: 15257541. DOI: 10.1175/JHM-D-17-0111.1. URL: <http://journals.ametsoc.org/doi/10.1175/JHM-D-17-0111.1>.
- Blenkinsop, S. et al. (May 2015). “Temperature influences on intense UK hourly precipitation and dependency on large-scale circulation”. In: *Environmental Research Letters* 10.5, p. 054021. ISSN: 17489326. DOI: 10.1088/1748-9326/10/5/054021. arXiv: /doi.org/10.1088/1748-9326/10/5/054021 [https:]. URL: <https://iopscience.iop.org/article/10.1088/1748-9326/10/5/054021>.
- Blöschl, Günter et al. (Aug. 2017). “Changing climate shifts timing of European floods”. In: *Science* 357.6351, pp. 588–590. ISSN: 10959203. DOI: 10.1126/science.aan2506. URL: <http://science.sciencemag.org/content/357/6351/588.abstract>.
- Bottou, Leon (1998). *Online Algorithms and Stochastic Approximation*. DOI: doi=10.1.1.52.4918.
- Brown, Simon J. (Apr. 2018). “The drivers of variability in UK extreme rainfall”. In: *International Journal of Climatology* 38.S1, e119–e130. ISSN: 10970088. DOI: 10.1002/joc.5356. URL: <http://doi.wiley.com/10.1002/joc.5356%20https://rmets.onlinelibrary.wiley.com/doi/abs/10.1002/joc.5356>.
- Caliński, T. and J. Harabasz (1974). “A Dendrite Method For Cluster Analysis”. In: *Communications in Statistics* 3.1, pp. 1–27. ISSN: 00903272. DOI: 10.1080/03610927408827101. URL: <http://www.tandfonline.com/doi/abs/10.1080/03610927408827101>.
- Champion, Adrian J., Richard P. Allan, and David A. Lavers (July 2015). “Atmospheric rivers do not explain UK summer extreme rainfall”. In: *Journal of Geophysical Research* 120.14, pp. 6731–6741. ISSN: 21562202. DOI: 10.1002/2014JD022863. URL: <http://doi.wiley.com/10.1002/2014JD022863>.
- Champion, Adrian J., Stephen Blenkinsop, et al. (Apr. 2019). “Synoptic-Scale Precursors of Extreme U.K. Summer 3-Hourly Rainfall”. In: *Journal of Geophysical Research: Atmospheres* 124.8, pp. 4477–4489. ISSN: 21698996. DOI: 10.1029/2018JD029664. URL: <https://onlinelibrary.wiley.com/doi/abs/10.1029/2018JD029664>.

- Courville, Ian Goodfellow, Yoshua Bengio, and Aaron (2016). *Deep learning*. Vol. 29. 7553. MIT Press, pp. 1–73. ISBN: 3463353563306.
- Cumbria County Council (2018). “Flooding in Cumbria. December 2015: Impact Assessment”. PhD thesis, pp. 1–66. URL: <https://cumbria.gov.uk/elibrary/Content/Internet/536/671/4674/17217/17225/43312152830.PDF>.
- Davies, David L. and Donald W. Bouldin (Apr. 1979). “A Cluster Separation Measure”. In: *IEEE Transactions on Pattern Analysis and Machine Intelligence* PAMI-1.2, pp. 224–227. ISSN: 01628828. DOI: 10.1109/TPAMI.1979.4766909. URL: <http://ieeexplore.ieee.org/document/4766909/>.
- Donat, Markus G. et al. (May 2016). “More extreme precipitation in the world’s dry and wet regions”. In: *Nature Climate Change* 6.5, pp. 508–513. ISSN: 17586798. DOI: 10.1038/nclimate2941. URL: <http://www.nature.com/articles/nclimate2941>.
- Draxler, Roland R. and G. D. Hess (1997). *Description of the HYSPLIT 4 modeling system*.
- (Dec. 1998). “An overview of the HYSPLIT 4 modelling system for trajectories, dispersion and deposition”. In: *Australian Meteorological Magazine* 47.4, pp. 295–308. ISSN: 00049743.
- Eiras-Barca, Jorge et al. (Mar. 2021). “European West Coast atmospheric rivers: A scale to characterize strength and impacts”. In: *Weather and Climate Extremes* 31, p. 100305. ISSN: 22120947. DOI: 10.1016/j.wace.2021.100305. URL: <https://linkinghub.elsevier.com/retrieve/pii/S2212094721000037>.
- Emanuel, Kerry (May 2003). “Tropical cyclones”. In: *Annual Review of Earth and Planetary Sciences* 31.1, pp. 75–104. ISSN: 00846597. DOI: 10.1146/annurev.earth.31.100901.141259. URL: <http://www.annualreviews.org/doi/10.1146/annurev.earth.31.100901.141259>.
- Emerton, R (2020). *A Month of Storms: Ciara, Dennis and Atmospheric Rivers*. URL: <https://hepex.inrae.fr/atm-rivers-ciara-dennis/>.
- Enfield, David B., Alberto M. Mestas-Núñez, and Paul J. Trimble (May 2001). “The Atlantic multidecadal oscillation and its relation to rainfall and river flows in the continental U.S”. In: *Geophysical Research Letters* 28.10, pp. 2077–2080. ISSN: 00948276. DOI: 10.1029/2000GL012745. URL: <http://doi.wiley.com/10.1029/2000GL012745>.
- Environment Agency (2019). *Long-term investment scenarios (LTIS) 2019*. URL: <https://www.gov.uk/government/publications/flood-and-coastal-risk-management-in-england-long-term-investment/long-term-investment-scenarios-ltis-2019> (visited on 01/27/2020).

- Fahimi, Farzad, Zaher Mundher Yaseen, and Ahmed El-shafie (2017). “Application of soft computing based hybrid models in hydrological variables modeling: a comprehensive review”. In: *Theoretical and Applied Climatology* 128.3-4, pp. 875–903. ISSN: 14344483. DOI: 10.1007/s00704-016-1735-8. URL: <https://doi.org/10.1007/s00704-016-1735-8>.
- Fan, Meizhu and Edwin K. Schneider (Jan. 2012). “Observed decadal North Atlantic tripole SST variability. Part I: Weather noise forcing and coupled response”. In: *Journal of the Atmospheric Sciences* 69.1, pp. 35–50. ISSN: 00224928. DOI: 10.1175/JAS-D-11-018.1. URL: <https://journals.ametsoc.org/doi/10.1175/JAS-D-11-018.1>.
- Finch, J (2020). *Storm Ciara expected to cost up to £200m in insurance claims*. URL: <https://www.theguardian.com/uk-news/2020/feb/14/storm-ciara-expected-to-cost-up-to-200m-in-insurance-claims-storm-dennis>.
- Gimeno, Luis, Anita Drumond, et al. (July 2010). “On the origin of continental precipitation”. In: *Geophysical Research Letters* 37.13. ISSN: 00948276. DOI: 10.1029/2010GL043712. URL: <https://doi.org/10.1029/2010GL043712>.
- Gimeno, Luis, Raquel Nieto, et al. (Apr. 2010). “Where does the Iberian Peninsula moisture come from? An answer based on a Lagrangian approach”. In: *Journal of Hydrometeorology* 11.2, pp. 421–436. ISSN: 1525755X. DOI: 10.1175/2009JHM1182.1.
- Gimeno, Luis, Marta Vázquez, et al. (Feb. 2020). “Recent progress on the sources of continental precipitation as revealed by moisture transport analysis”. In: *Earth-Science Reviews* 201, p. 103070. ISSN: 00128252. DOI: 10.1016/j.earscirev.2019.103070. URL: <https://linkinghub.elsevier.com/retrieve/pii/S0012825218303763>.
- Gustafsson, Malin, David Rayner, and Deliang Chen (Jan. 2010). “Extreme rainfall events in southern Sweden: Where does the moisture come from?” In: *Tellus, Series A: Dynamic Meteorology and Oceanography* 62.5, pp. 605–616. ISSN: 02806495. DOI: 10.1111/j.1600-0870.2010.00456.x. URL: <https://www.tandfonline.com/doi/full/10.1111/j.1600-0870.2010.00456.x>.
- Halkidi, Maria, Yannis Batistakis, and Michalis Vazirgiannis (2001). “On clustering validation techniques”. In: *Journal of Intelligent Information Systems* 17.2-3, pp. 107–145. ISSN: 09259902. DOI: 10.1023/A:1012801612483.
- Hannaford, Jamie and Terry J. Marsh (Aug. 2008). “High-flow and flood trends in a network of undisturbed catchments in the UK”. In: *International Journal of Climatology* 28.10, pp. 1325–1338. ISSN: 08998418. DOI: 10.1002/joc.1643. URL: <http://doi.wiley.com/10.1002/joc.1643>.
- Hellström, Cecilia (Apr. 2005). “Atmospheric conditions during extreme and non-extreme precipitation events in Sweden”. In: *International Journal of Climatology*

- 25.5, pp. 631–648. ISSN: 08998418. DOI: 10.1002/joc.1119. URL: <http://doi.wiley.com/10.1002/joc.1119>.
- Hirschboeck, K. K. (1986). “Hydroclimatically-defined mixed distributions in partial duration flood series.” In: *Hydrologic Frequency Modeling*. Dordrecht: Springer Netherlands, pp. 199–212. ISBN: 3804204422. DOI: 10.1007/978-94-009-3953-0_13. URL: http://link.springer.com/10.1007/978-94-009-3953-0%7B%5C_%7D13.
- Hu, Pan et al. (Dec. 2018). “Flood-induced mortality across the globe: Spatiotemporal pattern and influencing factors”. In: *Science of the Total Environment* 643, pp. 171–182. ISSN: 18791026. DOI: 10.1016/j.scitotenv.2018.06.197. URL: <https://linkinghub.elsevier.com/retrieve/pii/S0048969718322745>.
- Hudson et. al., Debra (2017). “ACCESS-S1 The new Bureau of Meteorology multi-week to seasonal prediction system”. In: *Journal of Southern Hemisphere Earth System Science* 67.3, pp. 132–159. ISSN: 2206-5865. DOI: 10.22499/3.6703.001. URL: <http://www.bom.gov.au/jshess/docs/2017/Hudson.pdf>.
- Huntingford, Chris et al. (Sept. 2014). “Potential influences on the United Kingdom’s floods of winter 2013/14”. In: *Nature Climate Change* 4.9, pp. 769–777. ISSN: 17586798. DOI: 10.1038/nclimate2314. URL: <http://www.nature.com/articles/nclimate2314>.
- Jenkinson, A. F. and F. P. Collison (1977). “An initial climatology of gales over the North Sea”. In: *Synoptic Climatology Branch Memorandum* 62, Meteorological Office: Bracknell, 18 pp.
- Johnson, Stephanie J. et al. (Mar. 2019). “SEAS5: The new ECMWF seasonal forecast system”. In: *Geoscientific Model Development* 12.3, pp. 1087–1117. ISSN: 19919603. DOI: 10.5194/gmd-12-1087-2019. URL: <https://gmd.copernicus.org/articles/12/1087/2019/>.
- Jones, Mari R., Hayley J. Fowler, et al. (Apr. 2013). “An assessment of changes in seasonal and annual extreme rainfall in the UK between 1961 and 2009”. In: *International Journal of Climatology* 33.5, pp. 1178–1194. ISSN: 08998418. DOI: 10.1002/joc.3503. URL: <http://doi.wiley.com/10.1002/joc.3503>.
- Jones, P. D., T. Jonsson, and D. Wheeler (Nov. 1997). “Extension to the North Atlantic oscillation using early instrumental pressure observations from Gibraltar and south-west Iceland”. In: *International Journal of Climatology* 17.13, pp. 1433–1450. ISSN: 08998418. DOI: 10.1002/(sici)1097-0088(19971115)17:13<1433::aid-joc203>3.0.co;2-p. URL: [https://onlinelibrary.wiley.com/doi/10.1002/\(SICI\)1097-0088\(19971115\)17:13%7B%5C_%7D3C1433::AID-JOC203%7B%5C_%7D3E3.0.CO;2-P](https://onlinelibrary.wiley.com/doi/10.1002/(SICI)1097-0088(19971115)17:13%7B%5C_%7D3C1433::AID-JOC203%7B%5C_%7D3E3.0.CO;2-P).

- Kalnay, E. et al. (Mar. 1996). "The NCEP/NCAR 40-year reanalysis project". In: *Bulletin of the American Meteorological Society* 77.3, pp. 437–471. ISSN: 00030007. DOI: 10.1175/1520-0477(1996)077<0437:TNYRP>2.0.CO;2. URL: [http://journals.ametsoc.org/doi/10.1175/1520-0477\(1996\)077%7B%5C%%7D3C0437:TNYRP%7B%5C%%7D3E2.0.CO;2](http://journals.ametsoc.org/doi/10.1175/1520-0477(1996)077%7B%5C%%7D3C0437:TNYRP%7B%5C%%7D3E2.0.CO;2).
- Kalteh, A. M., P. Hjorth, and R. Berndtsson (2008). "Review of the self-organizing map (SOM) approach in water resources: Analysis, modelling and application". In: *Environmental Modelling and Software* 23.7, pp. 835–845. ISSN: 13648152. DOI: 10.1016/j.envsoft.2007.10.001. URL: <https://www.sciencedirect.com/science/article/pii/S1364815207001879>.
- Kaplan, Alexey et al. (Aug. 1998). "Analyses of global sea surface temperature 1856–1991". In: *Journal of Geophysical Research: Oceans* 103.C9, pp. 18567–18589. ISSN: 21699291. DOI: 10.1029/97JC01736. URL: <http://doi.wiley.com/10.1029/97JC01736>.
- Karpathy, Andrej et al. (June 2014). "Large-scale video classification with convolutional neural networks". In: *Proceedings of the IEEE Computer Society Conference on Computer Vision and Pattern Recognition*. IEEE, pp. 1725–1732. ISBN: 9781479951178. DOI: 10.1109/CVPR.2014.223. URL: <https://ieeexplore.ieee.org/document/6909619>.
- Keef, Caroline, Cecilia Svensson, and Jonathan A. Tawn (Nov. 2009). "Spatial dependence in extreme river flows and precipitation for Great Britain". In: *Journal of Hydrology* 378.3-4, pp. 240–252. ISSN: 00221694. DOI: 10.1016/j.jhydrol.2009.09.026. URL: <https://linkinghub.elsevier.com/retrieve/pii/S0022169409005897>.
- Keller, V. D.J. et al. (June 2015). "CEH-GEAR: 1 Km resolution daily and monthly areal rainfall estimates for the UK for hydrological and other applications". In: *Earth System Science Data* 7.1, pp. 143–155. ISSN: 18663516. DOI: 10.5194/essd-7-143-2015. URL: <https://essd.copernicus.org/articles/7/143/2015/>.
- Khalilia, Mohammed and Mihail Popescu (2014). "Topology preservation in fuzzy self-organizing maps". In: *Studies in Fuzziness and Soft Computing*. Vol. 312, pp. 105–114. ISBN: 9783319036731. DOI: 10.1007/978-3-319-03674-8_10.
- Kingma, Diederik P. and Jimmy Lei Ba (Dec. 2015). "Adam: A method for stochastic optimization". In: *3rd International Conference on Learning Representations, ICLR 2015 - Conference Track Proceedings*. arXiv: 1412.6980. URL: <http://arxiv.org/abs/1412.6980>.
- Kjeldsen, Thomas Rodding et al. (Oct. 2018). "Mixture Gumbel models for extreme series including infrequent phenomena". In: *Hydrological Sciences Journal* 63.13-

- 14, pp. 1927–1940. ISSN: 21503435. DOI: 10.1080/02626667.2018.1546956. URL: <https://doi.org/10.1080/02626667.2018.1546956>.
- Knapp, Kenneth R. et al. (Mar. 2010). “The international best track archive for climate stewardship (IBTrACS)”. In: *Bulletin of the American Meteorological Society* 91.3, pp. 363–376. ISSN: 00030007. DOI: 10.1175/2009BAMS2755.1. URL: <https://journals.ametsoc.org/doi/10.1175/2009BAMS2755.1>.
- Kohonen, Teuvo and Timo Honkela (2007). “Kohonen network”. In: *Scholarpedia* 2.1, p. 1568. ISSN: 1941-6016. DOI: 10.4249/scholarpedia.1568. URL: http://www.scholarpedia.org/article/Kohonen%7B%5C_%7Dnetwork.
- Lamb, H. H. (1950). “Types and spells of weather around the year in the British Isles : Annual trends, seasonal structure of the year, singularities”. In: *Quarterly Journal of the Royal Meteorological Society* 76.330, pp. 393–429. ISSN: 1477870X. DOI: 10.1002/qj.49707633005. URL: <https://rmets.onlinelibrary.wiley.com/doi/abs/10.1002/qj.49707633005>.
- (1972). “British Isles weather types and a register of daily sequence of circulation patterns”. In: *Geophysical Memoir, HMSO, London* 116, HMSO, London, 85pp.
 - (Apr. 1965). “The English climate. By H. H. Lamb. London (English Universities Press). Second (rewritten) edition, 1964. Pp. ix, 212; 30 Figures; 3 Appendices. 12s. 6d paperback; 21s. cloth bound”. In: *Quarterly Journal of the Royal Meteorological Society* 91.388, pp. 252–252. ISSN: 00359009. DOI: 10.1002/qj.49709138829. URL: <http://doi.wiley.com/10.1002/qj.49709138829%20https://rmets.onlinelibrary.wiley.com/doi/abs/10.1002/qj.49709138829>.
- Lavers, David A., Richard P. Allan, et al. (Dec. 2011). “Winter floods in Britain are connected to atmospheric rivers”. In: *Geophysical Research Letters* 38.23, n/a–n/a. ISSN: 00948276. DOI: 10.1029/2011GL049783. URL: <http://doi.wiley.com/10.1029/2011GL049783%20https://agupubs.onlinelibrary.wiley.com/doi/abs/10.1029/2011GL049783>.
- Lavers, David A. and Gabriele Villarini (June 2013). “The nexus between atmospheric rivers and extreme precipitation across Europe”. In: *Geophysical Research Letters* 40.12, pp. 3259–3264. ISSN: 00948276. DOI: 10.1002/grl.50636. URL: <http://doi.wiley.com/10.1002/grl.50636>.
- (Mar. 2015). “The contribution of atmospheric rivers to precipitation in Europe and the United States”. In: *Journal of Hydrology* 522, pp. 382–390. ISSN: 00221694. DOI: 10.1016/j.jhydrol.2014.12.010. URL: <https://linkinghub.elsevier.com/retrieve/pii/S0022169414010208>.
- Lee, Jae Gil et al. (Aug. 2008). “TraClass: Trajectory classification using hierarchical region based and trajectory based clustering”. In: *Proceedings of the VLDB Endow-*

- ment 1.1, pp. 1081–1094. ISSN: 21508097. DOI: 10.14778/1453856.1453972. URL: <https://dl.acm.org/doi/10.14778/1453856.1453972>.
- Leung, Henry and Simon Haykin (1991). “The Complex Backpropagation Algorithm”. In: *IEEE Transactions on Signal Processing* 39.9, pp. 2101–2104. ISSN: 19410476. DOI: 10.1109/78.134446. URL: <http://ieeexplore.ieee.org/document/134446/>.
- Lewis, Matthew W. and Suzanne L. Gray (July 2010). “Categorisation of synoptic environments associated with mesoscale convective systems over the UK”. In: *Atmospheric Research* 97.1-2, pp. 194–213. ISSN: 01698095. DOI: 10.1016/j.atmosres.2010.04.001. URL: <https://linkinghub.elsevier.com/retrieve/pii/S0169809510000888>.
- Liberato, Margarida L.R. (Oct. 2014). “The 19 January 2013 windstorm over the North Atlantic: Large-scale dynamics and impacts on Iberia”. In: *Weather and Climate Extremes* 5.1, pp. 16–28. ISSN: 22120947. DOI: 10.1016/j.wace.2014.06.002. URL: <https://linkinghub.elsevier.com/retrieve/pii/S2212094714000620>.
- Lloyd, Stuart P. (Mar. 1982). “Least Squares Quantization in PCM”. In: *IEEE Transactions on Information Theory* 28.2, pp. 129–137. ISSN: 15579654. DOI: 10.1109/TIT.1982.1056489. URL: <http://ieeexplore.ieee.org/document/1056489/>.
- Macdonald, Neil, Ian D. Phillips, and Gareth Mayle (Mar. 2010). “Spatial and temporal variability of flood seasonality in Wales”. In: *Hydrological Processes* 24.13, pp. 1806–1820. ISSN: 08856087. DOI: 10.1002/hyp.7618. URL: <http://doi.wiley.com/10.1002/hyp.7618>.
- MacLachlan, C. et al. (Apr. 2015). “Global Seasonal forecast system version 5 (GloSea5): A high-resolution seasonal forecast system”. In: *Quarterly Journal of the Royal Meteorological Society* 141.689, pp. 1072–1084. ISSN: 1477870X. DOI: 10.1002/qj.2396. URL: <http://doi.wiley.com/10.1002/qj.2396>.
- Marimont, R. B. and M. B. Shapiro (Aug. 1979). “Nearest neighbour searches and the curse of dimensionality”. In: *IMA Journal of Applied Mathematics (Institute of Mathematics and Its Applications)* 24.1, pp. 59–70. ISSN: 02724960. DOI: 10.1093/imamat/24.1.59. URL: <https://doi.org/10.1093/imamat/24.1.59>.
- Matthews, T. et al. (Jan. 2018). “Super Storm Desmond: A process-based assessment”. In: *Environmental Research Letters* 13.1, p. 014024. ISSN: 17489326. DOI: 10.1088/1748-9326/aa98c8. URL: <https://iopscience.iop.org/article/10.1088/1748-9326/aa98c8>.
- Mayes, Julian and Dennis Wheeler (Jan. 2013). “Regional weather and climates of the British Isles - Part 1: Introduction”. In: *Weather* 68.1, pp. 3–8. ISSN: 00431656. DOI: 10.1002/wea.2041. URL: <http://doi.wiley.com/10.1002/wea.2041>.
- McIntosh, D. H. (Apr. 1978). “Atmospheric science: An introductory survey. By J. M. Wallace and P. V. Hobbs. Academic Press (New York), 1977. Pp. xvii, 467, 229

- figs., 15 tables. £12.80". In: *Quarterly Journal of the Royal Meteorological Society* 104.440, pp. 534–534. ISSN: 00359009. DOI: 10.1002/qj.49710444024. URL: <https://doi.org/10.1002/qj.49710444024>.
- Murphy, Conor et al. (Jan. 2020). "Multi-century trends to wetter winters and drier summers in the England and Wales precipitation series explained by observational and sampling bias in early records". In: *International Journal of Climatology* 40.1, pp. 610–619. ISSN: 10970088. DOI: 10.1002/joc.6208. URL: <https://onlinelibrary.wiley.com/doi/abs/10.1002/joc.6208>.
- Nalley, D. et al. (July 2019). "A multiscale and multivariate analysis of precipitation and streamflow variability in relation to ENSO, NAO and PDO". In: *Journal of Hydrology* 574, pp. 288–307. ISSN: 00221694. DOI: 10.1016/j.jhydrol.2019.04.024. URL: <https://linkinghub.elsevier.com/retrieve/pii/S0022169419303579>.
- Neal, Robert et al. (July 2016). "A flexible approach to defining weather patterns and their application in weather forecasting over Europe". In: *Meteorological Applications* 23.3, pp. 389–400. ISSN: 14698080. DOI: 10.1002/met.1563. URL: <http://doi.wiley.com/10.1002/met.1563%20https://rmets.onlinelibrary.wiley.com/doi/abs/10.1002/met.1563>.
- NOAA (2003). *NCEP/NCAR Global Reanalysis Data Archive Information*. URL: https://www.ready.noaa.gov/gbl%7B%5C_%7Dreanalysis.php (visited on 09/11/2019).
- O'Hare, G. and J. Sweeney (1993). "Lamb's circulation types and British weather: an evaluation". In: *Geography* 78.1, pp. 43–60. ISSN: 00167487.
- Onogi, Kazutoshi et al. (2007). "The JRA-25 reanalysis". In: *Journal of the Meteorological Society of Japan* 85.3, pp. 369–432. ISSN: 00261165. DOI: 10.2151/jmsj.85.369. URL: https://www.jstage.jst.go.jp/article/jmsj/85/3/85%7B%5C_%7D3%7B%5C_%7D369/%7B%5C_%7Darticle.
- Owens, J. and A. Hunter (2000). "Application of the self-organising map to trajectory classification". In: *Proceedings - 3rd IEEE International Workshop on Visual Surveillance, VS 2000*. IEEE Comput. Soc, pp. 77–83. ISBN: 0769506984. DOI: 10.1109/VIS.2000.856860. URL: <http://ieeexplore.ieee.org/document/856860/>.
- Pfahl, Stephan and Heini Wernli (Oct. 2012). "Quantifying the relevance of cyclones for precipitation extremes". In: *Journal of Climate* 25.19, pp. 6770–6780. ISSN: 08948755. DOI: 10.1175/JCLI-D-11-00705.1. URL: <http://journals.ametsoc.org/doi/10.1175/JCLI-D-11-00705.1>.
- Prosdocimi, Ilaria et al. (Nov. 2019). "Areal Models for Spatially Coherent Trend Detection: The Case of British Peak River Flows". In: *Geophysical Research Letters* 46.22, pp. 13054–13061. ISSN: 19448007. DOI: 10.1029/2019GL085142. URL: <https://onlinelibrary.wiley.com/doi/10.1029/2019GL085142>.

- Richardson, Doug, Hayley J. Fowler, Christopher G. Kilsby, Robert Neal, and Rutger Dankers (Jan. 2020). “Improving sub-seasonal forecast skill of meteorological drought: A weather pattern approach”. In: *Natural Hazards and Earth System Sciences* 20.1, pp. 107–124. ISSN: 16849981. DOI: 10.5194/nhess-20-107-2020. URL: <https://nhess.copernicus.org/articles/20/107/2020/>.
- Richardson, Douglas, Hayley J. Fowler, Christopher G. Kilsby, and Robert Neal (Feb. 2018). “A new precipitation and drought climatology based on weather patterns”. In: *International Journal of Climatology* 38.2, pp. 630–648. ISSN: 10970088. DOI: 10.1002/joc.5199. URL: <http://doi.wiley.com/10.1002/joc.5199>.
- Robson, Alice J. (July 2002). “Evidence for trends in UK flooding”. In: *Philosophical Transactions of the Royal Society A: Mathematical, Physical and Engineering Sciences* 360.1796. Ed. by David Cox et al., pp. 1327–1343. ISSN: 1364503X. DOI: 10.1098/rsta.2002.1003. URL: <https://royalsocietypublishing.org/doi/10.1098/rsta.2002.1003>.
- Rumelhart, David E., Geoffrey E. Hinton, and Ronald J. Williams (Oct. 1986). “Learning representations by back-propagating errors”. In: *Nature* 323.6088, pp. 533–536. ISSN: 00280836. DOI: 10.1038/323533a0. URL: <http://www.nature.com/articles/323533a0>.
- Santos, Marcus Suassuna et al. (Dec. 2018). “Links between different classes of storm tracks and the flood trends in Spain”. In: *Journal of Hydrology* 567, pp. 71–85. ISSN: 00221694. DOI: 10.1016/j.jhydrol.2018.10.003. URL: <https://linkinghub.elsevier.com/retrieve/pii/S0022169418307649>.
- Sarkar, Sudipta, Ramesh P. Singh, and Akshansha Chauhan (May 2018). “Anomalous changes in meteorological parameters along the track of 2017 Hurricane Harvey”. In: *Remote Sensing Letters* 9.5, pp. 487–496. ISSN: 21507058. DOI: 10.1080/2150704X.2018.1441562. URL: <https://www.tandfonline.com/doi/full/10.1080/2150704X.2018.1441562>.
- Scoccimarro, Enrico, Silvio Gualdi, and Simon O. Krichak (Aug. 2018). ““Extreme precipitation events over north-western Europe: Getting water from the tropics””. In: *Annals of Geophysics* 61.4. ISSN: 2037416x. DOI: 10.4401/ag-7772.
- Simonyan, Karen, Andrea Vedaldi, and Andrew Zisserman (Dec. 2014). “Deep inside convolutional networks: Visualising image classification models and saliency maps”. In: *2nd International Conference on Learning Representations, ICLR 2014 - Workshop Track Proceedings*. arXiv: 1312.6034. URL: <http://arxiv.org/abs/1312.6034>.
- Stein, A. F. et al. (2015). “Noaa’s hysplit atmospheric transport and dispersion modeling system”. English. In: *Bulletin of the American Meteorological Society* 96.12,

- pp. 2059–2077. ISSN: 00030007. DOI: 10.1175/BAMS-D-14-00110.1. URL: <https://journals.ametsoc.org/view/journals/bams/96/12/bams-d-14-00110.1.xml>.
- Stohl, Andreas and Paul James (2004). “A Lagrangian analysis of the atmospheric branch of the global water cycle: Part 1: Method description, validation, and demonstration for the August 2002 flooding in central Europe”. English. In: *Journal of Hydrometeorology* 5.4, pp. 656–678. ISSN: 1525755X. DOI: 10.1175/1525-7541(2004)005<0656:ALAOTA>2.0.CO;2. URL: https://journals.ametsoc.org/view/journals/hydr/5/4/1525-7541%7B%5C_%7D2004%7B%5C_%7D005%7B%5C_%7D0656%7B%5C_%7Dalaota%7B%5C_%7D2%7B%5C_%7D0%7B%5C_%7Dco%7B%5C_%7D2.xml.
- Sundararajan, Mukund, Ankur Taly, and Qiqi Yan (2017). “Axiomatic attribution for deep networks”. In: *34th International Conference on Machine Learning, ICML 2017*. Vol. 7, pp. 5109–5118. ISBN: 9781510855144. DOI: <https://doi.org/10.5555/3305890.3306024>. arXiv: 1703.01365.
- Svensson, Cecilia and Jamie Hannaford (Sept. 2019). “Oceanic conditions associated with euro-atlantic high pressure and uk drought”. In: *Environmental Research Communications* 1.10, p. 101001. ISSN: 25157620. DOI: 10.1088/2515-7620/ab42f7. URL: https://iopscience.iop.org/article/10.1088/2515-7620/ab42f7%20https://doi.org/10.1088%7B%5C_%7D2F2515-7620%7B%5C_%7D2Fab42f7.
- Tan, Xuezhi., Thian Yew. Gan, and Yongqin David. Chen (Jan. 2018). “Moisture sources and pathways associated with the spatial variability of seasonal extreme precipitation over Canada”. In: *Climate Dynamics* 50.1-2, pp. 629–640. ISSN: 14320894. DOI: 10.1007/s00382-017-3630-0. URL: <http://link.springer.com/10.1007/s00382-017-3630-0>.
- Tanguy, M. et al. (2015). *Gridded estimates of daily and monthly areal rainfall for the United Kingdom (1890-2014) [CEH-GEAR]. NERC Environmental Information Data Centre*. DOI: <https://doi.org/10.5285/ee9ab43d-a4fe-4e73-afd5-cd4fc4c82556>. URL: <https://doi.org/10.5285/ee9ab43d-a4fe-4e73-afd5-cd4fc4c82556>.
- Tsukijihara, Takumi, Ryuichi Kawamura, and Tetsuya Kawano (Mar. 2019). “Influential role of inter-decadal explosive cyclone activity on the increased frequency of winter storm events in Hokkaido, the northernmost island of Japan”. In: *International Journal of Climatology* 39.3, pp. 1700–1715. ISSN: 10970088. DOI: 10.1002/joc.5910. URL: <http://doi.wiley.com/10.1002/joc.5910>.
- Ummenhofer, Caroline C. et al. (Aug. 2017). “Emerging European winter precipitation pattern linked to atmospheric circulation changes over the North Atlantic region in recent decades”. In: *Geophysical Research Letters* 44.16, pp. 8557–8566. ISSN:

19448007. DOI: 10.1002/2017GL074188. URL: <http://doi.wiley.com/10.1002/2017GL074188>.
- Utsumi, Nobuyuki, Hyungjun Kim, et al. (Jan. 2017). “Relative contributions of weather systems to mean and extreme global precipitation”. In: *Journal of Geophysical Research* 122.1, pp. 152–167. ISSN: 21562202. DOI: 10.1002/2016JD025222. URL: <http://doi.wiley.com/10.1002/2016JD025222>.
- Utsumi, Nobuyuki, Shinta Seto, et al. (Aug. 2011). “Does higher surface temperature intensify extreme precipitation?” In: *Geophysical Research Letters* 38.16, n/a–n/a. ISSN: 00948276. DOI: 10.1029/2011GL048426. URL: <http://doi.wiley.com/10.1029/2011GL048426>.
- Wainwright, Caroline M. et al. (Jan. 2020). “Extreme rainfall in East Africa, October 2019–January 2020 and context under future climate change”. In: *Weather* 76.1, pp. 26–31. ISSN: 14778696. DOI: 10.1002/wea.3824. URL: <https://onlinelibrary.wiley.com/doi/10.1002/wea.3824>.
- Westra, S., H. J. Fowler, et al. (Sept. 2014). “Future changes to the intensity and frequency of short-duration extreme rainfall”. In: *Reviews of Geophysics* 52.3, pp. 522–555. ISSN: 19449208. DOI: 10.1002/2014RG000464. URL: <http://doi.wiley.com/10.1002/2014RG000464>.
- Westra, Seth, Lisa V. Alexander, and Francis W. Zwiers (June 2013). “Global increasing trends in annual maximum daily precipitation”. In: *Journal of Climate* 26.11, pp. 3904–3918. ISSN: 08948755. DOI: 10.1175/JCLI-D-12-00502.1. URL: <http://journals.ametsoc.org/doi/10.1175/JCLI-D-12-00502.1>.
- Wheeler, Dennis (July 2013). “Regional weather and climates of the British Isles - Part 4: North East England and Yorkshire”. In: *Weather* 68.7, pp. 184–190. ISSN: 00431656. DOI: 10.1002/wea.2081. URL: <http://doi.wiley.com/10.1002/wea.2081>.
- Wilby, R. L., D. Conway, and P. D. Jones (2002). “Prospects for downscaling seasonal precipitation variability using conditioned weather generator parameters”. In: *Hydrological Processes* 16.6, pp. 1215–1234. DOI: <https://doi.org/10.1002/hyp.1058>. eprint: <https://onlinelibrary.wiley.com/doi/pdf/10.1002/hyp.1058>. URL: <https://onlinelibrary.wiley.com/doi/abs/10.1002/hyp.1058>.
- World Meteorological Organisation (2021). *State of the Global Climate 2020*. Tech. rep. 1264. World Meteorological Organisation, p. 56. URL: https://library.wmo.int/index.php?lvl=notice%7B%5C_%7Ddisplay%7B%5C%7D&Did=21880%7B%5C%7D.YJfRi3VKiHt.
- Yang, Aimin, Xiaolei Yang, et al. (2019). “Research on feature extraction of tumor image based on convolutional neural network”. In: *IEEE Access* 7, pp. 24204–24213.

ISSN: 21693536. DOI: 10.1109/ACCESS.2019.2897131. URL: <https://ieeexplore.ieee.org/document/8633831/>.

Yang, Xiaobing, Fansheng Kong, and Bihong Liu (2004). “A Revision for Gaussian Mixture Density Decomposition Algorithm”. In: *Lecture Notes in Computer Science (including subseries Lecture Notes in Artificial Intelligence and Lecture Notes in Bioinformatics)*. Ed. by Jun Zhang, Ji-Huan He, and Yuxi Fu. Vol. 3314. Berlin, Heidelberg: Springer Berlin Heidelberg, pp. 1014–1019. ISBN: 978-3-540-30497-5. DOI: 10.1007/978-3-540-30497-5_156.

Appendices

Supplementary Information

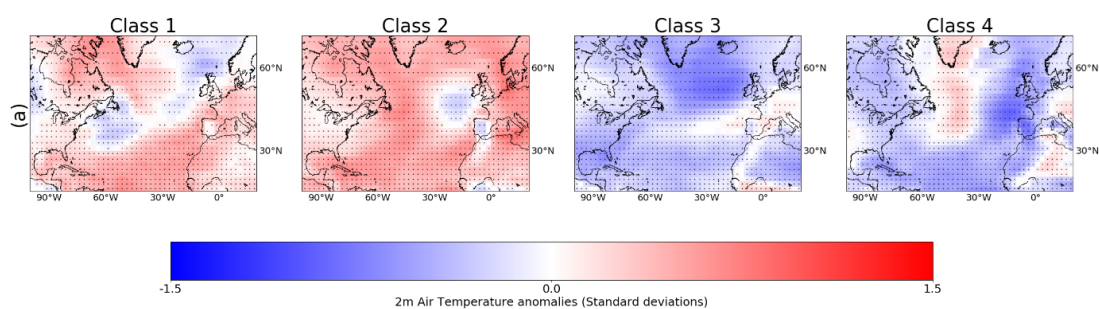


Figure S1: Air temperature anomaly patterns for the four summer classes. Cells marked with a dot denote that the anomaly is significantly different from zero at the 2% significance level based on a two-sided Student's t-test.

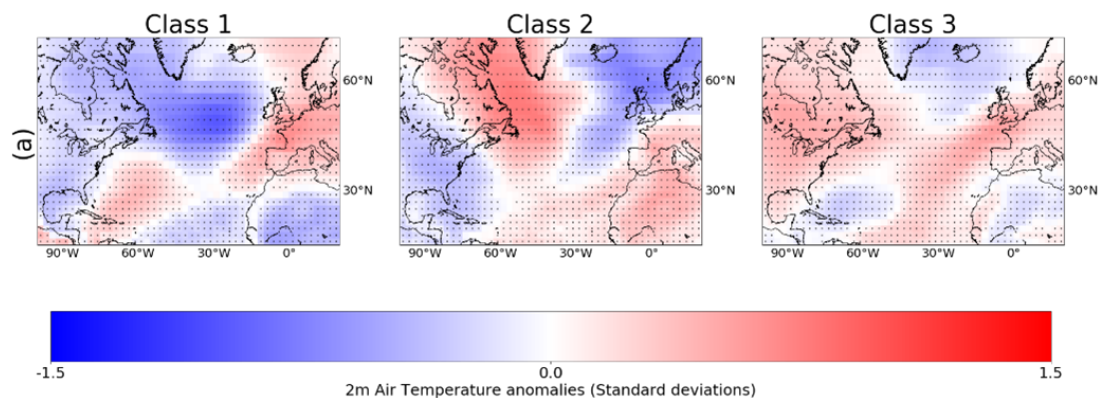


Figure S2: Air temperature anomaly patterns for the three winter classes. Cells marked with a dot denote that the anomaly is significantly different from zero at the 2% significance level based on a two-sided Student's t-test.

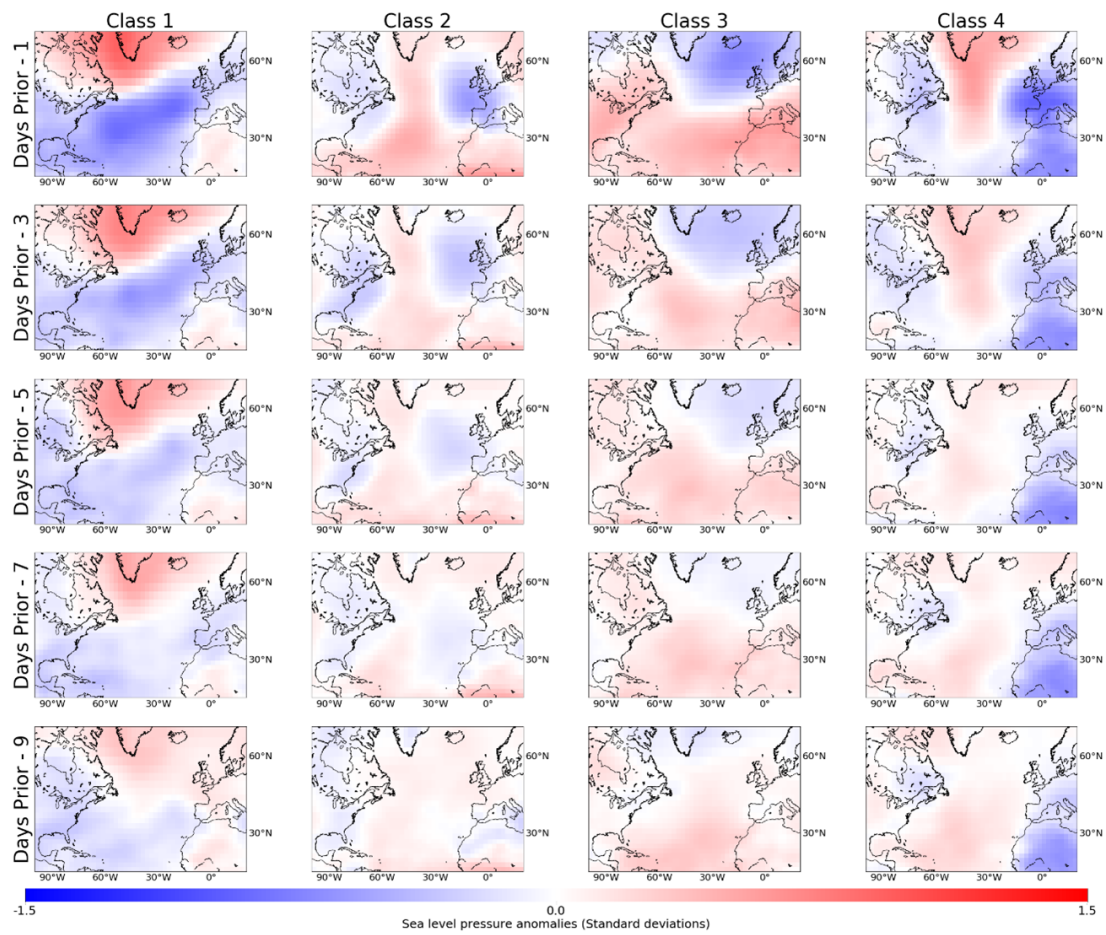


Figure S3: Sea-level pressure in the North Atlantic region in the 1, 3, 5, 7 and 9 days prior to the extreme rainfall event occurring, for the four summer classes.

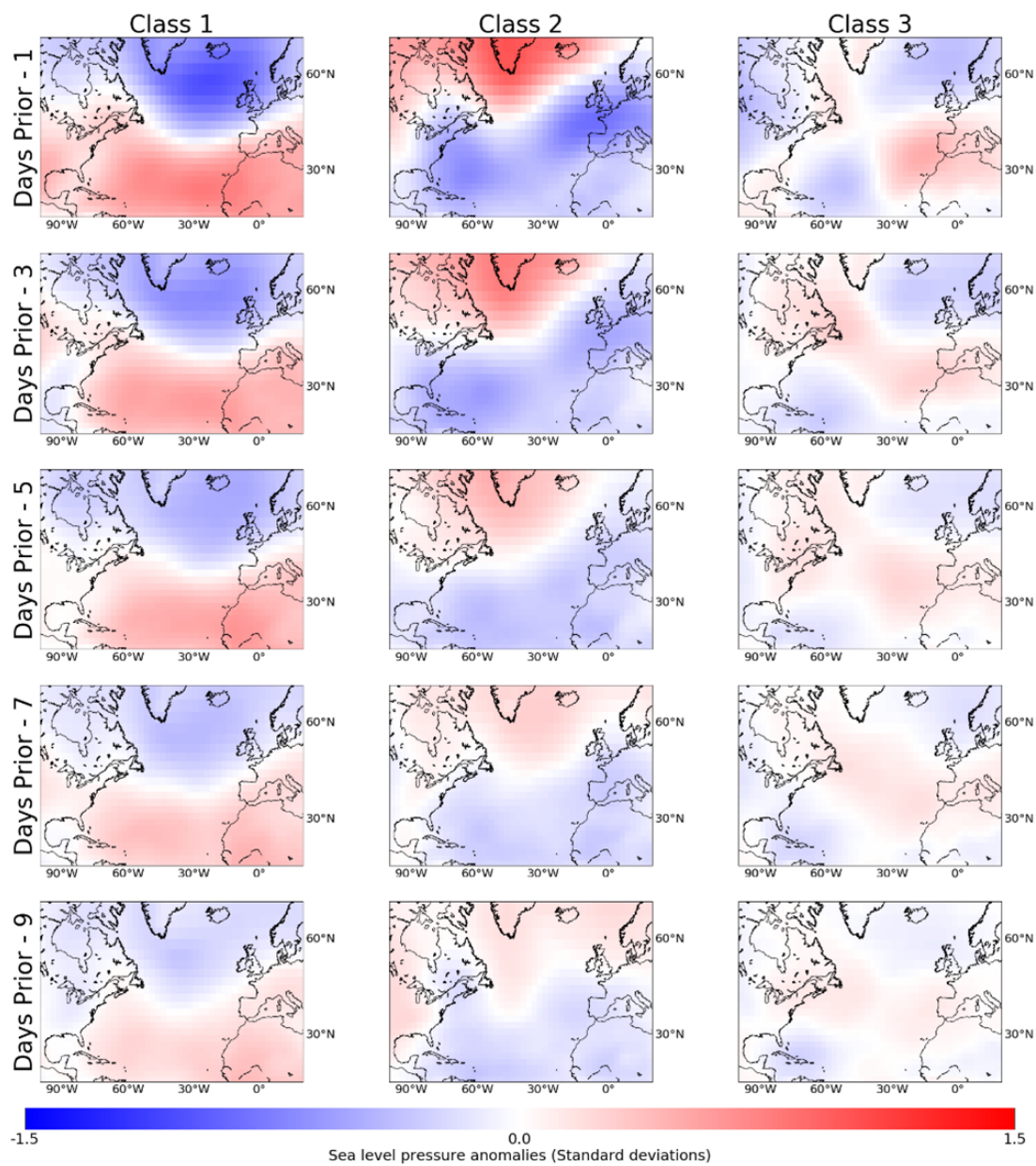


Figure S4: Sea-level pressure in the North Atlantic region in the 1, 3, 5, 7 and 9 days prior to the extreme rainfall event occurring, for the three winter classes.

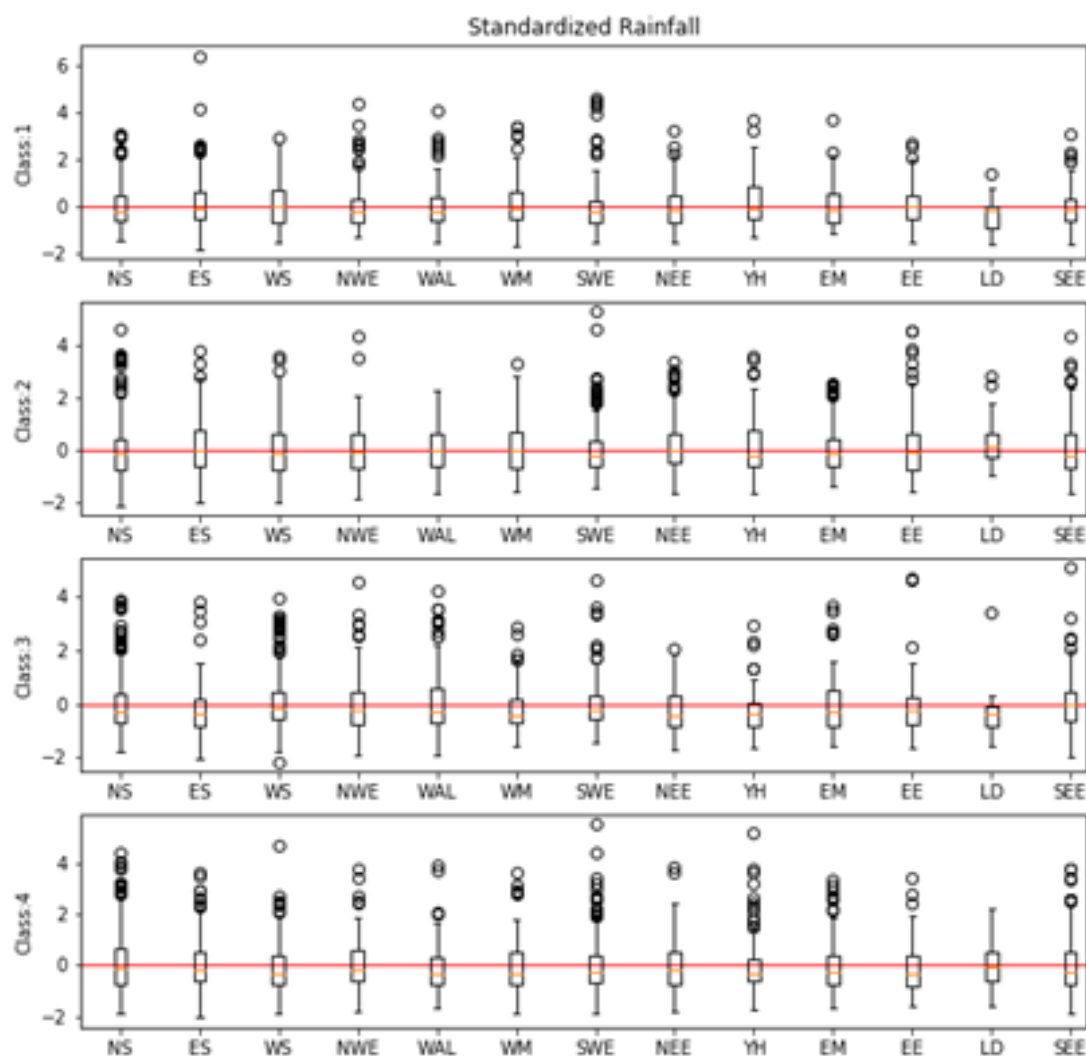


Figure S5: Box-and-whisker plots of standardized summer rainfall maxima for all study regions, for each class. The box outlines the upper and lower quartiles with the median as a red line, and the upper (lower) whisker shows the observation that is furthest away from the upper (lower) quartile, but still within 1.5 times the interquartile range.

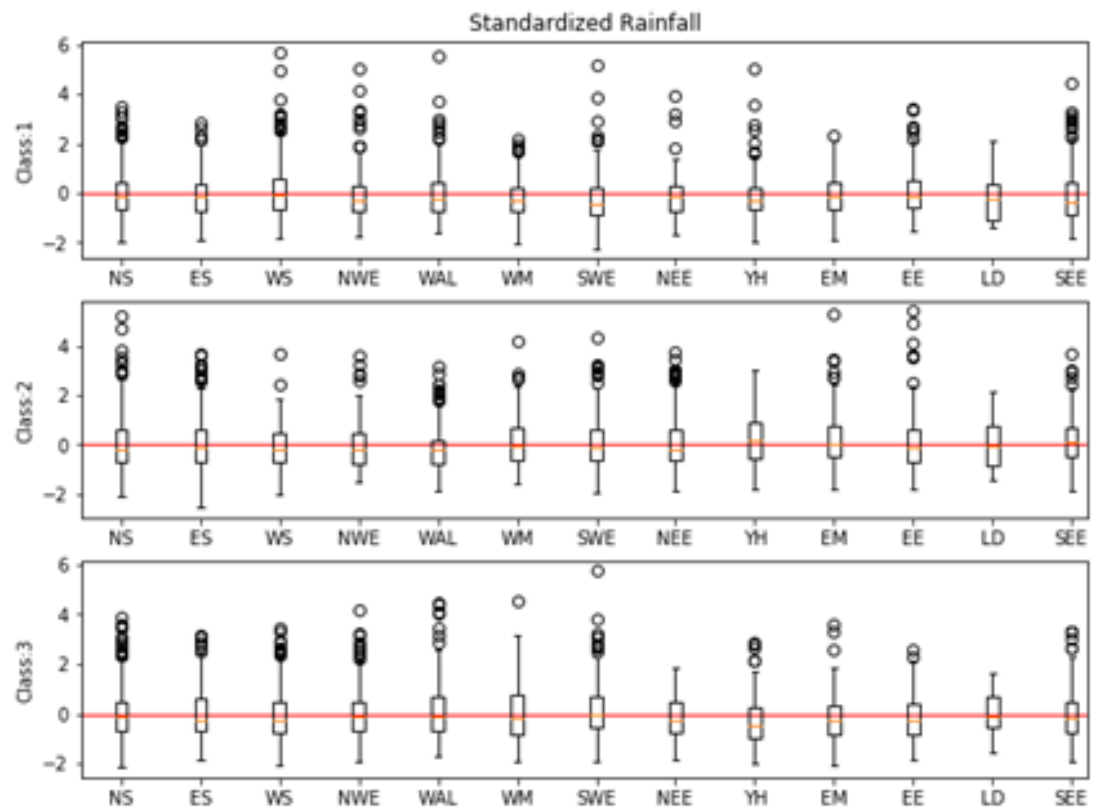


Figure S6: Same as S5, but for winter.